Properties of Hadronic Matter Near the Phase Transition

Dissertation
zur Erlangung des Doktorgrades
der Naturwissenschaften

vorgelegt beim Fachbereich Physik
der Johann Wolfgang Goethe-Universität
in Frankfurt am Main

von
Jacquelyn Noronha-Hostler
aus San Diego, CA USA

Frankfurt am Main, 2010
(D 30)

vom Fachbereich Physik der Johann Wolfgang Goethe–Universität
als Dissertation angenommen.

Dekan: Prof. Dr. Dirk-Hermann Rischke

Gutachter: Prof. Dr. Carsten Greiner

Gutachter: Prof. Dr. Horst Stoecker

Datum der Disputation: 8. Dezember 2010

Abstract

In order to fully understand the new state of matter formed in heavy ion collisions, it is vital to isolate the always present final state hadronic contributions within the primary Quark-Gluon Plasma (QGP) experimental signatures. Previously, the hadronic contributions were determined using the properties of the known mesons and baryons. However, according to Hagedorn, hadrons should follow an exponential mass spectrum, which the known hadrons follow only up to masses of $M \approx 2$ GeV. Beyond this point the mass spectrum is flat, which indicates that there are "missing" hadrons, that could potentially contribute significantly to experimental observables. In this thesis I investigate the influence of these "missing" Hagedorn states on various experimental signatures of QGP.

Strangeness enhancement is considered a signal for QGP because hadronic interactions (even including multi-mesonic reactions) underpredict the hadronic yields (especially for strange particles) at the Relativistic Heavy Ion Collider, RHIC. One can conclude that the time scales to produce the required amount of hadronic yields are too long to allow for the hadrons to reach chemical equilibrium within the lifetime of a cooling hadronic fireball. Because gluon fusion can quickly produce strange quarks, it has been suggested that the hadrons are born into chemical equilibrium following the Quantum Chromodynamics (QCD) phase transition. However, we show here that the missing Hagedorn states provide extra degrees of freedom that can contribute to fast chemical equilibration times for a hadron gas. We develop a dynamical scheme in which possible Hagedorn states contribute to fast chemical equilibration times of $X\bar{X}$ pairs (where $X = p$, K, Λ, or Ω) inside a hadron gas and just below the critical temperature. Within this scheme, we use master equations and derive various analytical estimates for the chemical equilibration times. Applying a Bjorken picture to the expanding fireball, the hadrons can, indeed, quickly chemically equilibrate for both an initial overpopulation or underpopulation of Hagedorn resonances. We compare the thermodynamic properties of our model to recent lattice results and find that for both critical temperatures, $T_c = 176$ MeV and $T_c = 196$ MeV, the hadrons can reach chemical equilibrium on very short time scales. Furthermore the ratios p/π, K/π , Λ/π, and Ω/π match experimental values well in our dynamical scenario.

The effects of the "missing" Hagedorn states are not limited to the chemical equilibration time. Many believe that the new state of matter formed at RHIC is the closet to a perfect fluid found in nature, which implies that it has a small shear viscosity to entropy density ratio close to the bound derived using the uncertainty principle. Our hadron resonance gas model, including the additional Hagedorn states, is used to obtain an upper bound on the shear viscosity to entropy density ratio, η/s, of hadronic matter near T_c that is close to $1/(4\pi)$. Furthermore, the large trace anomaly and the small speed of sound near T_c computed within this model agree

well with recent lattice calculations. We also comment on the behavior of the bulk viscosity to entropy density ratio of hadronic matter close to the phase transition, which qualitatively has a different behavior close to T_c than a hadron gas model with only the known resonances.

We show how the measured particle ratios can be used to provide non-trivial information about T_c of the QCD phase transition. This is obtained by including the effects of highly massive Hagedorn resonances on statistical models, which are generally used to describe hadronic yields. The inclusion of the "missing" Hagedorn states creates a dependence of the thermal fits on the Hagedorn temperature, T_H, and leads to a slight overall improvement of thermal fits. We find that for Au+Au collisions at RHIC at $\sqrt{s_{NN}} = 200$ GeV the best square fit measure, χ^2, occurs at $T_H \sim T_c = 176$ MeV and produces a chemical freeze-out temperature of 172.6 MeV and a baryon chemical potential of 39.7 MeV.

Übersicht

Um ein Versändnis der in Schwerionenkollisionen gebildeten Materie zu erhalten, ist es unerläßlich, die Beiträge des hadronischen Endzustandes aus den verschiedenen experimentellen Nachweismöglichkeiten eines während einer solchen Kollision gebildeten Quark-Gluon Plasmas (QGP) zu isolieren. Dabei wurden bisher alle hadronischen Beiträge aus den Eigenschaften der bekannten Mesonen und Baryonen abgeleitet. Nach Arbeiten von Rolf Hagedorn sollten jedoch alle Hadronen einem exponentiellen Massenspektrum folgen. Ein solcher exponentieller Abfall tritt allerdings nur bis zu einer Hadronmasse von $M \approx 2$ GeV auf, für schwerere Hadronen flacht das Massenspektrum ab. Dies könnte darauf hinweisen, dass bislang noch Hadronen "fehlen", die einen möglicherweise bedeutsamen Beitrag auf den experimentellen Nachweis des QGP haben. Dieser Einfluss wird in der vorliegenden Arbeit untersucht.

Allgemein wird der Anstieg sog. seltsamer (s-) Teilchen als ein möglicher Nachweis des QGP angesehen, da die anhand hadronischer Wechselwirkungen berechnete Anzahl hadronischer Teilchen am Relativistic Heavy Ion Collider (RHIC, zu Deutsch "Beschleunigerring für relativistische Schwerionen") selbst unter Hinzunahme multi-mesonischer Zerfälle zu gering ist. Daraus kann man folgern, dass die Zeitskala, innerhalb der die benötigte Anzahl hadronischer Teilchen gebildet werden kann, zu groß ist, damit die Hadronen noch während der Abkühlungsphase des expandierenden Feuerballs ein chemisches Gleichgewicht erreichen. Da Gluonfusion die Produktion vieler seltsamer (s-) Quarks bewirken kann, wurde ein Mechanismus vorgeschlagen, in dem Hadronen gewissermaßen in das nach dem Phasenübergang (zwischen dem QGP und dem sich für geringere Temperaturen anschließenden Hadrongas) auftretende chemische Gleichgewicht "geboren" werden. Die vorliegende Arbeit zeigt jedoch, dass die Hinzunahme der fehlenden Hagedornzustände mit ihren zusätzlichen Freiheitsgraden durchaus dazu führen kann, dass das chemische Gleichgewicht in einem Hadrongas auf einer sehr kurzen Zeitskale (d.h. schnell) erreicht wird. Das in dieser Arbeit vorgestellte auf Ratengleichungen basierende dynamische Modell demonstriert eine äußerst kurze Equilibrierungsphase für $X\bar{X}$ Paare direkt unterhalb der kritischen Temperatur (wobei X entweder Pionen, Kaonen, Lambda oder Omega Teilchen bezeichnen). Dabei wird das chemische Gleichgewicht sowohl für eine anfängliche Über- als auch eine Unterbevölkerung der Hagedornzustände erreicht, sofern man eine Bjorkenexpansion des während der Kollision entstehenden Feuerballs annimmt. Im Vergleich mit den neuesten Ergebnissen aus Lattice-QCD Rechnungen der beiden auf diesem Gebiet führenden Arbeitsgruppen kann gezeigt werden, dass die gebildeten Hadronen für die beiden kritischen Temperaturen von $T_c = 176$ MeV und $T_c = 196$ MeV das chemische Gleichgewicht sehr schnell erreichen können. Darüber hinaus stimmen die anhand unseres Modells bestimmten Verhältnisse von p/π, K/π , Λ/π und Ω/π sehr gut mit den experimentellen Werten überein.

Die Auswirkung der fehlenden Hagedornzustände ist allerdings nicht allein auf die Zeitskala des chemischen Gleichgewichtes beschränkt. Viele glauben, dass der neue am RHIC geformte Zustand von allen bisher entdeckten Materiezuständen am ehesten einer idealen Flüssigkeit entspricht, was sich in einem kleinen Verhältnis der Scherviskosität zu Entropiedichte, η/s, niederschlägt. In der vorliegenden Arbeit verwenden wir ein Hadron-Resonanzgas-Modell, inklusive der Hagedornzustände, um eine obere Grenze von $\eta/s \approx 1/(4\pi)$ in hadronischer Materie nahe T_c abzuleiten. Dabei stimmt die nahe der kritischen Temperatur bestimmte kleine Schallgeschwindigkeit gut mit den Berechnungen von Lattice-QCD Rechnungen überein. Darüber hinaus betrachten wir das Verhältnis von η/s in hadronischer Materie nahe des Phasenübergangs, das ein qualitativ anderes Verhalten als ein Hadrongas mit den bekannten Resonanzen aufweist.

Außerdem wird gezeigt, dass man aus den gemessenen Teilchenverhältnisse nicht-trivialen Informationen über die kritische Temperatur des QCD-Phasenübergangs ableiten kann. Dies erreichen wir durch die Hinzunahme äußerst massiver Hagedornzustände, die im Allgemeinen dazu verwendet werden, die Anzahl der gebildeten Hadronen zu beschreiben. Diese Hinzunahme der Hagedornzustände bewirkt eine Abhängigkeit der thermischen Fits von der Hagedorntemperatur T_H sowie eine Verbesserung der thermischen Fits. Eines der zentralen Ergebnisse dieser Arbeit ist, dass für Au+Au Kollisionen am RHIC mit einer Schwerpunktsenergie von $\sqrt{s_{NN}} = 200$ GeV der beste χ^2-Fit bei einer Hagedorntemperatur von $T_H \sim T_c = 176$ MeV auftritt und zu einer chemischen Ausfriertemperatur von 172.6 MeV sowie einem baryonischchemischen Potential von 39.7 MeV führt.

Contents

Chapter 1

Introduction

Albert Einstein once mused,

> "The important thing is not to stop questioning. Curiosity has its own reason for existing. One cannot help but be in awe when he [or she] contemplates the mysteries of eternity, of life, of the marvelous structure of reality. It is enough if one tries merely to comprehend a little of this mystery every day. Never lose a holy curiosity."

It is mankind's curiosity that has driven us to study the origins of our universe. The Hubble constant and cosmic microwave background radiation allude to an expanding universe, which leads to the natural question: what are we expanding away from? Our early universe was most likely an extremely hot and dense form of matter. In the first moments after the big bang this thick, scalding hadronic soup consisted of the basic building blocks of matter: quarks and gluons. The asymptotic freedom [1] property of Quantum Chromodynamics (QCD) predicts that such a phase of deconfined quarks and gluons, known as the Quark-Gluon Plasma (QGP), exists [2].

Unlike the early universe, visible mater, which is what planets and stars are composed of and accounts for 5% of the universe's mass [3], consists of hadrons. Below the critical temperature (region) quarks and gluons are confined within hadrons. Since quarks are each given an individual color, every hadron must be color neutral. Excluding exotic, hypothetical particles, hadrons are either mesons (a quark and anti-quark where the two colors cancel such as blue and anti-blue) or baryons (three quarks where a red, green, and blue color quarks combine to create a "white", color neutral hadron).

Because our visible world is limited to confined matter, we cannot directly measure the properties of quarks and gluons. Thus, we are forced to look for signals in the later stages of a man made cooled fireball following its hadronization. Comparisons must be made between what could be experimentally measured from a pure hadronic phase e.g. in p+p collisions versus an initial QGP phase that has cooled into a hadron gas, e.g., Au+Au or CuCu collisions at RHIC. Some of the common signals for QGP are jet quenching, strangeness enhancement, charm suppression, and collective flow.

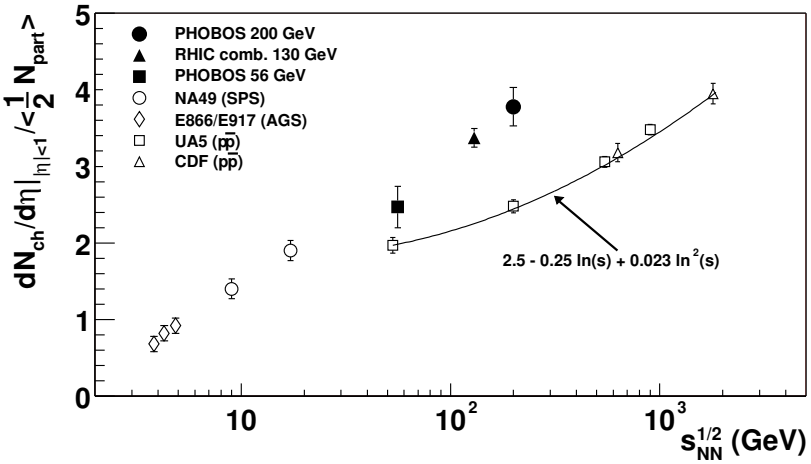

Figure 1.1: Observed energy dependence of the midrapidity particle densities from AGS, SPS, and RHIC. Figure taken from [7].

1.0.1 Experiments

Over the past 30 years heavy ion collisions have probed the extremes of hadronic matter. Bevalac, SIS, and AGS were the precursors to SPS [4] and RHIC [5], which have provided possible experimental evidence for QGP. The current generation of physicists now away impatiently for the data from LHC [6], which will push our experimental search to even further energies. Relevant specifically to this is SPS at CERN, which explored collision energies up to $\sqrt{s} \leq 20$ GeV with the experiments NA49/35, NA50/38, CERES/NA45, WA98/80, and NA57/WA97. RHIC at BNL, which collided p+p, d+Au, Au+Au, and Cu+Cu for the energy range $\sqrt{s} = 20 - 200$ AGeV, and LHC, which plans to reach collisions with energies above $\sqrt{s} > 1$ TeV.

In Fig. 1.1 a graph of the measured multiplicities of the various experiments and their dependence on collision energy is shown. It is rather surprising that heavy ion collisions follow such a linear behaviour in their relationship of particle densities as functions of the energy. Morever, it is striking that $p + \bar{p}$ data differs significantly from this linear behavior because of the difference of a possible QGP medium [7].

1.0.2 The Deconfinement Phase Transition in QCD

In order to find the deconfining phase transition one looks for a rapid change in the thermodynamic quantities such as the energy density, pressure, and entropy. This rapid change occurs because the number of degrees of freedom changes significantly at the phase transition. Below the critical temperature, T_c, there are roughly three degrees of freedom, which correspond to the 3 charge states of pions. However, above T_c, there are eight gluons with two helicity degrees of freedom each and for the quarks there are roughly three active light flavors at T just above T_c with a corresponding quark and anti-quark, two spin states, and three colors each, which gives a total of 16 degrees of freedom for the gluons and 36 degrees of freedom for the quarks. QGP

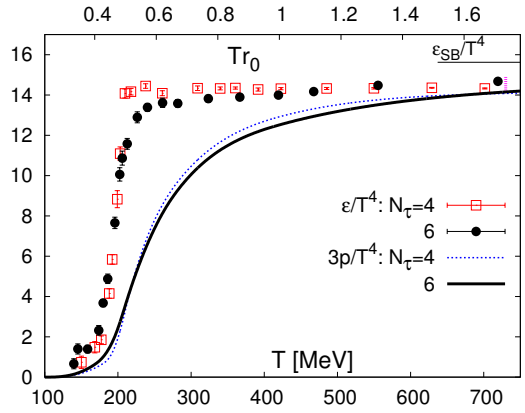

Figure 1.2: Energy and pressure from the RBC-Bielefeld collaboration calculated on the lattice [8].

as a whole has a total of 52 degrees of freedom, which differs significantly from the three in the hadron gas phase. Therefore, because the thermodynamic properties are proportional to the degrees of freedom, a rapid increase in the energy density, pressure, and entropy over a small change in the temperature signifies a phase transition from the hadron gas phase to QGP.

The order of the phase transition can be determined by the presence of discontinuities in the derivatives of the free energy. A first order phase transition occurs when there is a discontinuity in the first order of the free energy and these systems involve latent heat, whereas a second order phase occurs when there is a discontinuity in the second derivative of the free energy (the first derivative is continuous) and the system has no latent heat but does has a divergent susceptibility. A crossover occurs when both the first and second order derivatives are continuous but a rapid change still occurs.

Recent lattice results reveal sharp increases in the energy density (and the pressure and entropy) over very short temperature ranges as seen in Fig. 1.2 and Fig. 1.3. The RBC-Bielefeld collaboration has a higher critical temperature region that ranges from about $T = 180 - 200$ MeV [8] whereas the BMW collaboration has a lower critical temperature region centered at $T = 176$ MeV [9]. However, a crossover is most likely with dynamical quarks (see [10] and the references therein), which means there is a critical temperature region rather than a specific critical temperature. Thus, depending on what variables are observed in lattice QCD, a different critical "temperature" is found. In Fig. 1.4 one can see the cross-over at low baryon chemical potential and high temperatures, which is the region we are interested in. In the scenario of a rapid crossover, the bulk properties of the system emulate those of a first order phase transition.

1.1 Signals of Quark Gluon Plasma

Some of the primary signs of QGP are jet quenching, strangeness enhancement, charm suppression, and collective flow effects. The most integral ones to this thesis are strangeness enhancement and collective flow effects, both of which can be discussed in the context of Hagedorn

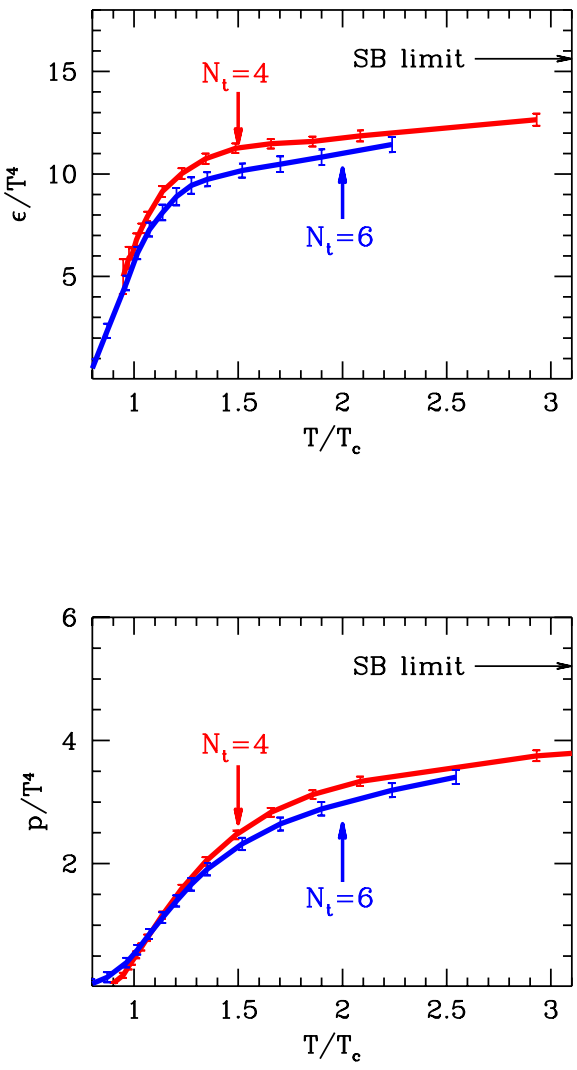

Figure 1.3: Energy and pressure from the BMW collaboration calculated on the lattice [9] .

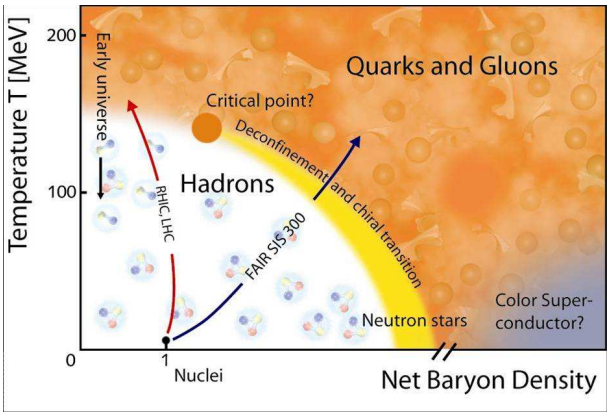

Figure 1.4: Schematic QCD phase diagram.

states. Thus far, the effects of Hagedorn states on jet quenching and charm suppression have not been studied so we leave this as an interesting problem for the future.

Charm suppression (the most famous example is J/Ψ melting [11]) was thought to be a signal of QGP. The idea was that at the onset of the deconfined phase the screening radius would be less than the binding radius of the quark system for J/Ψ, which consists of a $c\bar{c}$ pair. Then the quarks can no longer interact and J/Ψ would no longer exist. Instead, c and $\bar{c}$ will combine with other flavored quarks and produce open charm pairs e.g. $c\bar{u}$. Within the hadron gas phase it is possible to produce J/Ψ's through multiple interaction channels. Thus, while J/Ψ's are not produced within the QGP phase, they are mostly produced within the hadron gas phase.

1.1.1 Jet Quenching

Immediately following the collisions before QGP reaches equilibrium, jet pairs of quarks can be formed. If a pair of jets are formed near to the surface, then one jet immediately leaves the QGP while only minimally being affected by the medium (known as the near-side jet) whereas the other jet (known as the away-side jet) must pass through the medium meanwhile undergoing Bremsstrahlung and multiple elastic collisions. The basic idea of jet quenching is that high p_T jets can be seen as "external" probes that can be uniquely used to probe the QGP medium.

In collisions where no QGP medium is present (such as ordinary p+p collisions) both jets can be observed as seen in Fig. 1.5 for both p+p and d+Au collisions where there is clearly a peak at 0 (the near-side jet) and π (the away-side jet). However, for the central Au+Au collisions, the away-side jet is quenched, which can be seen by the lack of a hump between $\Delta\phi = 2 - 4$ radians in Fig. 1.5.

Moreover, jets can be used as a tomographic tool to determine the initial densities of partons within QGP. For instance, looking at PHENIX π^0 data [13] using GLV opacity formalism [14, 15] it can be shown that initial gluon density must be $dN_g/dy \approx 1000 \pm 200$. Additionally, this initial dN_g/dy agrees well with other measurements from: the initial entropy derived from the Bjorken formula [16] for the the measured multiplicity, the initial conditions of QGP in hydrodynamics

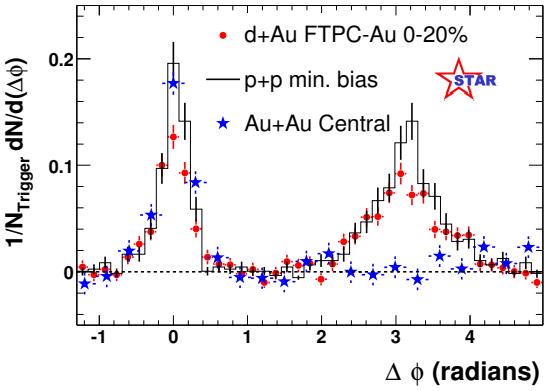

Figure 1.5: Di-jet fragment azimuthal correlations from STAR in d+Au and p+p collisions are unquenced relative to the mono-jet correlation in central Au+Au collisions [12].

needed to reproduce the elliptic flow found in experiments, and the estimate for the maximum gluon rapidity density from CGC gluon saturated initial conditions (see [17] and references therein).

However, there still remains a problem to be understood within the context of energy loss. A comparison between the energy loss in p+p and Au+Au can be made in order to compare the effects of the medium on the energy loss of the jet. The nuclear suppression factor, R_{AA} provides just such a tool and it is defined as

$$R_{AA} = \frac{dN^{AA}/dp_T dy}{T_{AA}(b) d\sigma^{NN}/dp_T dy} \tag{1.1}$$

where $T_{AA}(b)$ is the nuclear thickness function and σ^{NN} is the cross-section. It was thought that the energy loss for the jets should be strongly mass dependent because at RHIC heavier quarks would not be able to reach speeds as close to the speed of light as lighter quarks would be able to. Thus, it was thought that lighter quarks should undergo a more significant energy loss and, therefore, have a smaller R_{AA} than heavier quarks. However, in the experiment it appears that the measured R_{AA} is equivalent to that of light quarks [13], which still remains a puzzle [15].

Looking at non-photonic single electron data, which is an indirect probe of heavy quark energy loss, a larger suppression of electrons than predicted was found in the range $p_T = 4 - 8$ GeV. In Fig. 1.7 a comparison of the calculated R_{AA} from STAR [18] and PHENIX [19] data in central Au+Au reactions at 200 AGeV to the calculated R_{AA} from charm and bottom quarks using the opacity formalism DGLV [20, 21]. When only radiative energy loss is considered the amount the jet suppression is underpredicted. Including other energy loss mechanisms such as elastic energy loss does help but also still underpredicts the energy loss because the fluctuations of the jet path length in general increase R_{AA} [15].

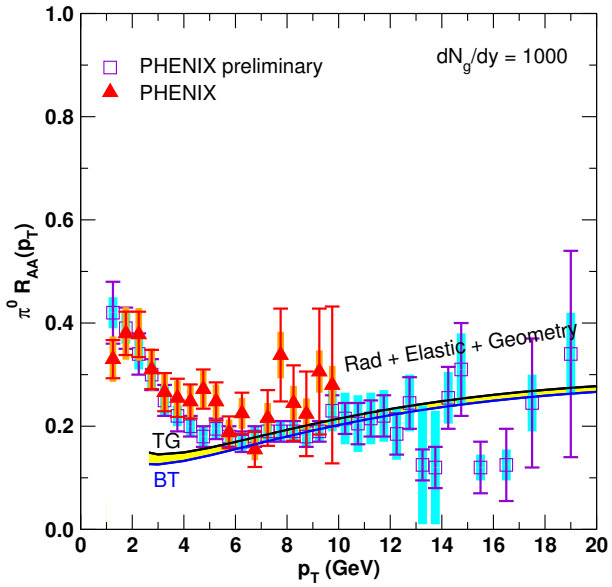

Figure 1.6: Comparison of the PHENIX data [13] to the calculated R_{AA} for light quark jets. Figure taken from [15].

1.1.2 Collective Flow

In order to produce QGP within the lab two heavy nuclei are accelerated and then collided at ultrarelativistic energies. Following the collision thousands of hadrons are produced and their flow behavior can be used to determine how strong the interactions are. The stronger the coupling the larger the flow, which means that in a plasma composed of non-interacting quarks and gluons the flow would be zero.

Originally, it was thought that the QGP should be weakly intereacting, which would indicate that the elliptic flow (also known as "v_2", see below) should be large. However, as shown in [22] the binary parton cross sections required reproduce elliptic flow data, which is larger than was expected, are an order of magnitude larger than the usual perturbative estimates, which suggests that the partons in the medium are strongly interacting. However, it has been shown that the inclusion of inelastic $2-3$ gluon reactions can considerably increase the flow and lead to an overall agreement with the large v_2 seen in $Au+Au$ collisions at $\sqrt{s} = 200A$GeV at RHIC [23] as seen in Fig. 1.8.

The collective flow components are determined from the azimuthal dependence of the multiplicity

$$\frac{dN_h(N_p)}{dydp_T^2d\phi} = \frac{dN_h(N_p)}{dydp_T^2}\frac{1}{2\pi}\left[1 + 2v_1(y, p_T, N_p, h)\cos\phi + 2v_2(y, p_T, N_p, h)\cos 2\phi + ...\right] \quad (1.2)$$

where v_1 is the directed flow, v_2 is the elliptic flow, h is the distribution of hadrons (such as π's, K's, p's, etc.), N_p is the average number of participating nucleons. The azimuthal angle is the

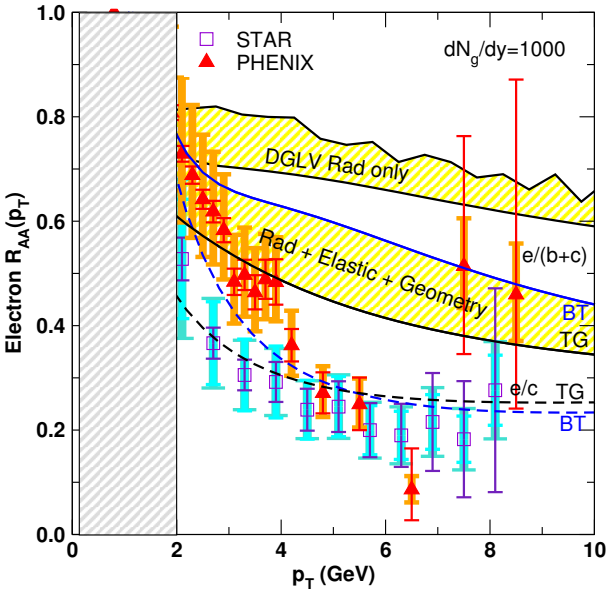

Figure 1.7: Comparison of R_{AA} derived from non-photonic electrons from the decay of quenched heavy quark (c+b) jets at RHIC from the STAR [18] and PHENIX [19] data in central Au+Au reactions at 200 AGeV to the calculated energy loss using DGLV [20, 21]. Shaded bars indicate systematic errors, while thin error lines indicate statistical ones. The upper yellow band from [21] takes into account radiative energy loss only, using a fixed L = 6 fm; the lower yellow band includes both elastic and inelastic energy losses as well as jet path length fluctuations. The bands provide a rough estimate of uncertainties from the leading log approximation for elastic energy loss. The dashed curves illustrate the lower extreme of the uncertainty from production, by showing the electron suppression after both inelastic and elastic energy loss with bottom quark jets neglected. Figure taken from [15].

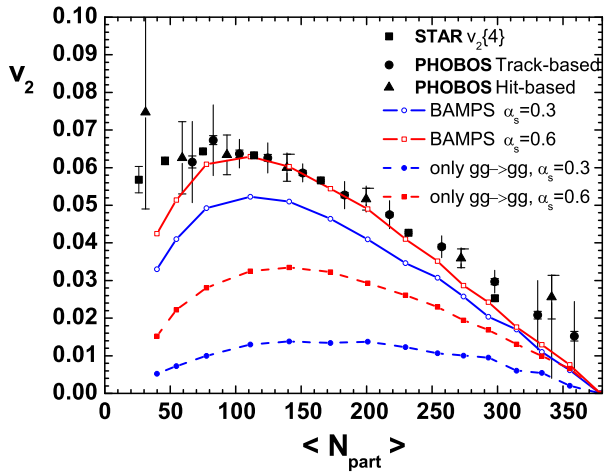

Figure 1.8: Elliptic flow $v_2(|y| < 1)$ from BAMPS using $\alpha_s = 0.3$ and 0.6, compared with the RHIC data [5]. Figure taken from [23].

angle around the beam axis for the collision and it is measured relative to a globally determined estimate for the collision reaction plane angle.

Collective flow should provide insight into how far away the system is from local equilibrium. Hydrodynamics can only be applied after the QGP has reached local equilibrium and this defines a plasma thermalization time (say 1 fm/c), which is taken as an initial parameter in hydrodynamics simulations. Ideal hydrodynamics is only applicable when local thermal equilibrium can be maintained. Viscous corrections can be neglected if the typical scattering mean free path is much smaller than the length scale defined by the spatial gradients of the flow field. Otherwise, viscous corrections may be included via an expansion in powers of the gradient of the flow.

The degree of thermalization is then checked by using various initial conditions in hydrodynamic simulations and comparing the results to experimental data. Currently, the most popular models for the initial conditions are the color glass condensate (CGC) [24, 25, 26, 27] and the Glauber model [28]. The initial eccentricity plays an important role in final v_2 coefficient computed within hydrodynamics. Since CGC models have a large initial eccentricity than the Glauber model, it may not be surprising that when the two initial conditions are compared v_2 for CGC initial conditions is roughly a factor of 2 larger than for Glauber initial conditions for the same shear viscosity to entropy density ratio, η/s, [29].

Because hydrodynamics requires having the equation of state as an input parameter, the validity of the equation of state itself can be tested. For instance, the flow pattern at RHIC energies is consistent with the numerical equation of state from Lattice QCD. Initially, the equation of state used for hydrodynamics was that for an ideal gas of quarks and gluons, $\epsilon = 3p$. However, it is now possible to use more complicated equations of states such as a combination of a hadron gas with Hagedorn states and lattice data [30], which is analyzed in [31]. A more thorough discussion can be found in [32].

Recent results at BNL at RHIC have been interpreted as providing evidence that the most perfect fluid in nature appears in Au+Au collisions. This is striking and completely unprecedented. Apparently, one has to use gold to strike gold (note that SPS used lead). The indication of near perfect fluid behavior arises from the fact that hydrodynamic simulations using a very small ratio of viscosity to entropy density can fit the RHIC data. The idea from hydrodynamic simulations is that given a set of initial conditions the transport properties of the QGP can be found by fitting the numerical predictions to experimental data. For Glauber-type initial conditions a small η/s (somewhere between $\eta/s = 0.03 - 0.16$) is seen when v_2 is fitted to experimental data from PHOBOS [33] and STAR [34] as shown in Fig. 1.9 taken from [29] whereas CGC allows for a larger η/s. Recall, though, that in [23] it was shown that including inelastic $2 - 3$ gluon reactions can also explain the v_2 seen in the datat (see Fig. 1.8).

1.1.3 Strangeness Enhancement

(Anti-)strangeness enhancement was first observed, primarily in anti-hyperons and multi-strange baryons, however, also in kaons, at CERN-SPS energies in comparison to p+p data. Originally, it was considered a signature for QGP because using binary strangeness production reactions such as

$$\pi + \bar{p} \leftrightarrow \bar{K} + \bar{\Lambda} \tag{1.3}$$

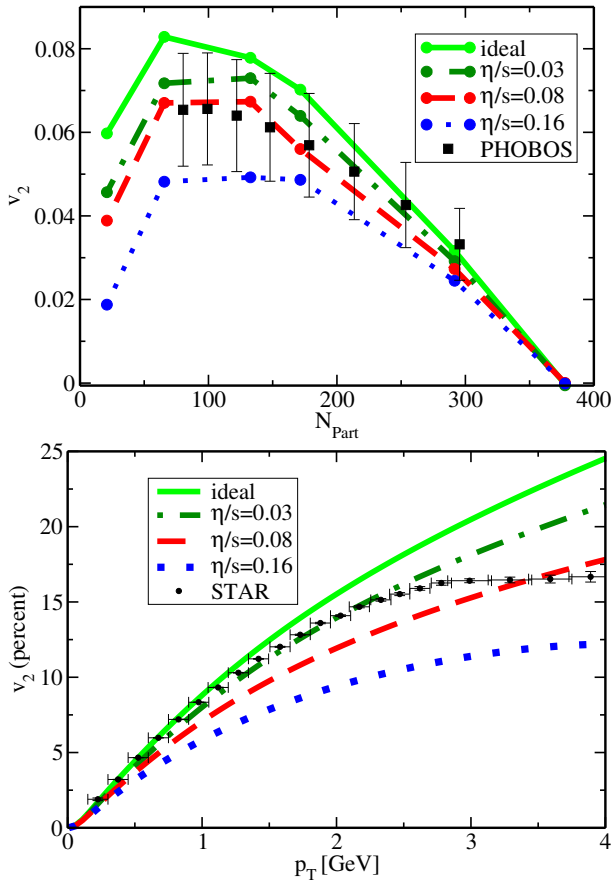

Figure 1.9: PHOBOS [33] data on p_T integrated v_2 and STAR [34] data on minimum bias v_2, for charged particles in Au+Au collisions at $\sqrt{s} = 200$ GeV, compared to a hydrodynamic model for various viscosity ratios η/s. Error bars for PHOBOS data show 90% confidence level systematic errors while for STAR only statistical errors are shown. Figures taken from [29].

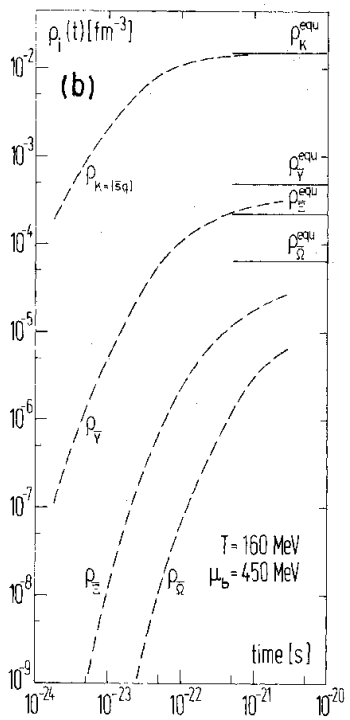

Figure 1.10: Production of hadrons through binary collisions. Graph taken from [40].

and binary strangeness exchange reactions

$$K + \bar{p} \leftrightarrow \pi + \bar{\Lambda} \tag{1.4}$$

chemical equilibrium could not be reached within the hadron gas phase [35]. The estimated time scale of chemical equilibration for binary reactions within a hadron gas model was $\tau \approx 1000$ fm/c [35] (see Fig. 1.10), which is significantly longer than the estimated lifetime of a hadronic fireball of about 10 fm/c (see later discussion in Chapter 3 about the expansion of an hadronic fireball). In [35] rate equations were employed to estimate the time scale of the strange particles. Moreover, the abundancies after a typical hadron lifetime where somewhere between 20-100 times lower than the calculated chemical equilibrium values [35].

However, looking into the quark gluon plasma phase, the quarks and gluons can efficiently produce strange particles. The production of $s\bar{s}$ quarks at the lowest order of perturbation QCD is through the collision of 2 gluons or the annihilation of a light anti-light quark pair, as seen in Fig. 1.11. From the diagrams shown in Fig. 1.11, the invariant matrix elements can be calculated, which leads to the corresponding cross-sections. Including the cross sections in rate equations it was found that reactions involving gluons in the deconfined phase could more quickly produce strange quarks. Therefore, it was conjectured that strangeness enhancement was a signal for deconfinement because gluon fusion would be the primary contributor to the abundance of strange particles following hadronization and rescattering of strange quarks [35].

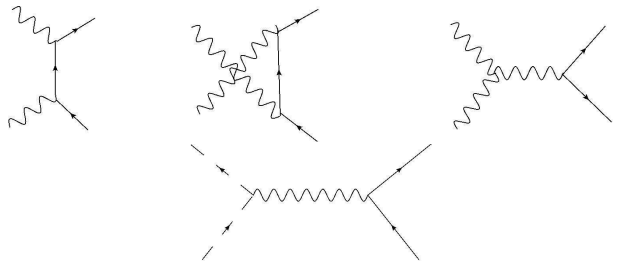

Figure 1.11: Feynman diagrams showing the production of strange quarks. The dashed lines represent light quark flavors, the solid lines strange quarks while the wavy lines are the gluons.

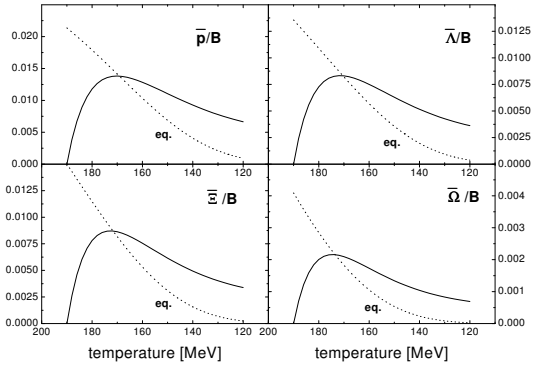

Figure 1.12: Production of anti-hyperons at SPS using multi-mesonic reactions. Graph taken from [37].

At the time it was assumed that multi-mesonic collisions would not play a significant role in strangeness production because their cross section would be too small. However, Rapp and Shuryak showed in [36] that for SPS energies it is possible for multi-pions to interact and form anti-baryons, for example,

$$\bar{p} + N \leftrightarrow n\pi, \tag{1.5}$$

which has a cross-section of $\sigma_{\rho_{\bar{p}}} \approx 50$ mb. Using a rate equations, one finds that the chemical equilibration time is proportional to the inverse of the thermal reaction rate (see Chapter 3 and Appendix C)

$$\tau_{\bar{p}} = \frac{1}{\langle\langle \sigma_{\bar{p}+N\leftrightarrow n\pi} v_{\bar{p}N} \rangle\rangle \rho_N} \approx 1 - 3 \; fm/c. \tag{1.6}$$

There the baryonic density is $\rho_B \approx \rho_0$ to $2\rho_0$, which is typical for SPS.

Furthermore, Greiner and Leupold extended this idea to anti-hyperons, which could have the following reactions:

$$\begin{aligned} \bar{\Sigma}, \bar{\Lambda} + N &\leftrightarrow n\pi + K \\ \bar{\Xi} + N &\leftrightarrow n\pi + 2K \\ \bar{\Omega} + N &\leftrightarrow n\pi + 3K, \end{aligned} \tag{1.7}$$

in Ref. [37]. The anti-hyperons (as shown in Fig. 1.12) can also be rewritten into the general equation

$$\bar{Y} + N \leftrightarrow n\pi + n_Y K, \tag{1.8}$$

which also gives time scales on the order of Eq. (1.6). Therefore, due to multi-mesonic collisions, the chemical equilibration time scales are short enough to account for chemical equilibration within a cooling hadronic fireball at SPS energies.

A problem arises if we use the same multi-mesonic reactions in the hadron gas phase at RHIC temperatures where experiments show that the particle abundances reach chemical equilibration close to the phase transition [38]. At RHIC, assuming $T = 170$ MeV, we use Eq. (1.6) where $\sigma \approx 30$ mb and $\rho_B^{eq} = \rho_{\bar{B}}^{eq} \approx 0.04$ fm^{-3} (Note that at RHIC there is approximately and equal number of baryons and anti-baryons [5]. Additionally, the density can be calculated with the context of a grand canonical model.), and find that the equilibrium rate of Ω is $\tau_\Omega \approx 10$ $\frac{\text{fm}}{\text{c}}$, which is considerably longer than the fireball's lifetime of $\tau < 4$ $\frac{\text{fm}}{\text{c}}$ in the hadronic stage. Moreover, $\tau_\Omega \approx 10$ $\frac{\text{fm}}{\text{c}}$ was also obtained in Ref. [39] using the fluctuation-dissipation theorem and Ref. [40] found thrice lower populations than experiments for various anti-hyperons in the 5% most central Au+Au collisions as shown in Fig. 1.13 (also see [41]). These discrepancies led

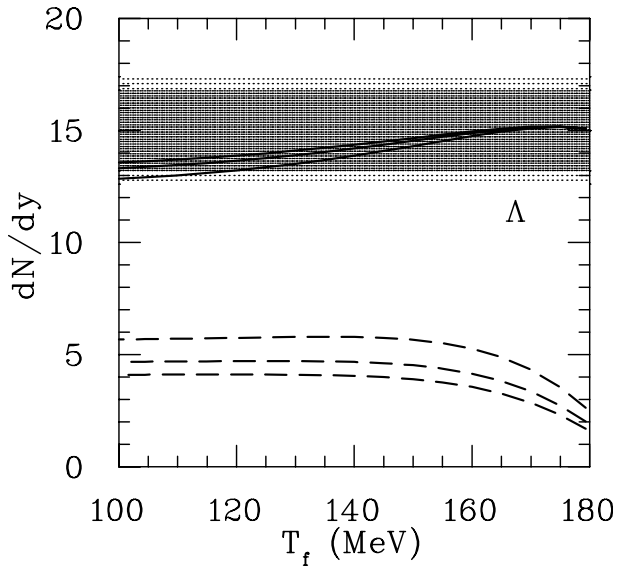

Figure 1.13: Anti-lambda production in the most central collisions at RHIC. The bottom three dashed lines start with no anti-lambdas at $T = 180$ MeV whereas the solid lines assume that the anti-lambdas begin in equilibrium. The shaded area shows the experimental results. The set of lines shows the difference for varying coupling coefficients. Graph taken from [40].

to the suggestion that the hadrons are "born" into equilibrium i.e. the system is already in a chemically frozen out state at the end of the phase transition [42, 43].

Overpopulated Mesons

It was suggested in [41] that it may be be possible to overpopulate the mesons (specifically, pions and kaons) in order to rapidly produce anti-baryons close to T_c. However, in [41] only the gain in anti-baryons is considered, which ignores the importance of detailed balance. According to detailed balance, the rate for the loss terms must be the same as that of the gain terms. Therefore, loss terms are of vital importance and cannot be ignored. Moreover, because the loss term is not included the anti-baryons are drastically overpopulated [44]. To understand this consider a stand multi-mesonic reaction

$$\bar{Y} + \Omega \leftrightarrow n_1\pi + n_2 K \tag{1.9}$$

where $\bar{Y}$ is an anti-baryon, n_1 is the number of pions in the reaction and n_2 is the number of kaons. Because strangeness needs to be conserved this would then be dependent on the number of strange quarks in $\bar{Y}$. Assuming that $\bar{Y}$ is a light baryon, we take $n_2 = 3$ and can describe the reaction through the rate equation

$$\dot{N}_\Omega = -\langle \sigma_{\Omega\bar{Y}} v_{\Omega\bar{Y}} \rangle \left[N_{\bar{Y}} N_\Omega - \frac{N^{eq}_{\bar{Y}} N^{eq}_\Omega}{\left(N^{eq}_\pi\right)^{n_1} \left(N^{eq}_K\right)^3} \sum_{n_1} B_{\bar{Y}\Omega\leftrightarrow n_1\pi 3K} \left(N_\pi\right)^{n_1} \left(N_K\right)^3 \right], \tag{1.10}$$

which we can rewrite using $\lambda = N/N^{eq}$

$$\dot{\lambda}_\Omega = -\langle \sigma_{\Omega\bar{Y}} v_{\Omega\bar{Y}} \rangle N^{eq}_{\bar{Y}} \left[\lambda_{\bar{Y}} \lambda_\Omega - \sum_{n_1} B_{\bar{Y}\Omega\leftrightarrow n_1\pi 3K} \left(\lambda_\pi\right)^{n_1} \left(\lambda_K\right)^3 \right]. \tag{1.11}$$

If one then overpopulates the pions and kaons by a factor of α while holding them constant, i.e. by ignoring back reactions, one can then substitute in $\lambda_\pi = \alpha$ and $\lambda_K = \alpha$. Additionally, for simplicity's sake we assume $n_1 = 2$,

$$\dot{\lambda}_\Omega = -\langle \sigma_{\Omega\bar{Y}} v_{\Omega\bar{Y}} \rangle N^{eq}_{\bar{Y}} \left[\lambda_{\bar{Y}} \lambda_\Omega - \alpha^5 \right]. \tag{1.12}$$

When the Ω's reach chemical equilibrium, $\lambda_\Omega = 1$

$$\dot{\lambda}_\Omega = -\langle \sigma_{\Omega\bar{Y}} v_{\Omega\bar{Y}} \rangle N^{eq}_{\bar{Y}} \alpha^5 \left[\frac{\lambda_{\bar{Y}}}{\alpha^5} - 1 \right]. \tag{1.13}$$

However, rate equations require that at chemical equilibrium at fixed point is reached, therefore,

$$\lambda_{\bar{Y}} = \alpha^5, \tag{1.14}$$

which is enormous. If $\alpha = 2$, the anti-baryons would be 32 times larger their its equilibrium value! Clearly, an overpopulation of that magnitude would be see in experiments. However, that is not the case because of results from thermal fits [45, 46], which indicate that the hadrons match chemical equilibrium extraordinarily well. Furthermore, as we will show in Chapter 3, due to Hagedorn states the initial conditions of the hadrons following the phase transition are irrelevant to the chemical equilibration.

1.2 Hagedorn States

> "One day, which I [Torleif Ericson] remember vividly, some time in 1964, I ran into you, Rolf [Hagedorn]. You were just bubbling over to a degree I have not seen you ever. Your eyes were quite bright, and you described to me all these fireballs: fireballs going into fireballs living on fireballs forever and all in a logically very consistent way. This must have been only a few days after you had invented the statistical bootstrap pictures. I really had the impression of a man who had just found the famous stone of the philosophers, and that must have been exactly how you felt about it. Clearly, you recognized at once the importance of the novel idea you introduced there. It was very interesting to observe, Rolf, how deeply you felt about it yourself from the very beginning." [47]

Indeed, Rolf Hagedorn came up with the idea that the hadron mass spectrum should follow an exponential law in the 1960's [48]. We now refer to these resonances as Hagedorn states where the very massive resonances may appear only close to the critical temperature because they are exponentially suppressed at lower temperatures. Their large masses open up the phase space for multi-particle decays. A recent analysis of the experimental evidence for the Hagedorn spectrum can be found in [49] and a graph of the mass spectrum of the known particles is shown in Fig. 1.14. Moreover, thoughts on observing Hagedorn states in experiments are given in [50] and their usage as a thermostat in [51]. Depending on the intrinsic parameters, Hagedorn states can also be used to trigger the order of the phase transition [52, 53].

Bound and resonance states are due to strong interactions and all of them (including not-yet discovered ones) must be included in order to simulate all the attractive hadronic interactions [54]. Likewise, repulsive interactions must also be included and that can be done so through volume corrections [54]. According to Hagedorn, the full spectrum is then obtained by considering clusters that are formed of clusters [48]. Thus, Hagedorn proposed [48]

$$g(M) = \int_{M_0}^{M} \frac{A}{[m^2 + (m_0)^2]^{\frac{5}{4}}} e^{\frac{m}{T_H}} dm \tag{1.15}$$

to obtain the spectra from $p-p$ and $\pi-p$ scatterings where T_H MeV is the Hagedorn temperature. At that time resonances were only known up to $\Delta(1232)$. From that he ended up with a Hagedorn temperature of $T_H \approx 160$ MeV.

Hagedorn's understanding of a strongly interacting gas was known as the statistical bootstrap model. Essentially, a strongly interacting gas is replaced with a non-interacting ideal gas of an infinite number of clusters that follow an exponential mass spectrum and where Van der Waals volume corrections are included [54].

The possibility then exists of heavier and heavier bound and resonance states that are composed of lighter ones, while at the same time these heavy states can also be a constituents of yet another still heavier resonance. These states are then described by their mass. Writing the partition function for such a system with a heat bath of temperature T and a volume of V, we have

$$Z = \exp\left[\int_0^\infty \rho(m) F(m,T)\, dm\right] \tag{1.16}$$

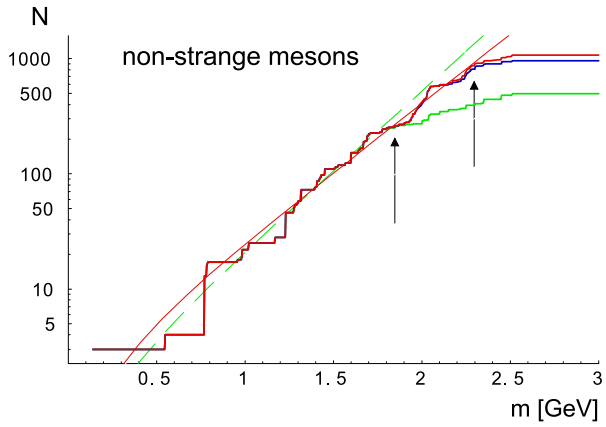

Figure 1.14: The mass spectrum of known particles is shown in the solid green line. One can see that it follows and exponentiall behavior up until a little bit below $M = 2$ GeV. Graph taken from [49].

where the calculation of Z must include the sum over all possible particles and by introducing the number of hadron states between m and $m + dm$, i.e., $\rho(m)dm$. The function $F(m, T)$ is a known function.

Alternatively, the partition can be generally expressed as

$$Z = \exp\left[\int_0^\infty \rho(m) F(m, T)\, dm\right] \tag{1.17}$$

where $\sigma(E)$ is the number of states between E and $E + dE$. Because we stay in the rest frame of the fireball, $E = m$. Thus, $\sigma(m)$ is the number of states in the mass interval $\{m, dm\}$ and $\rho(M)$ is the number of hadron states in the inteval $\{m, dm\}$. If fireballs truly are consisting of other fireballs, than

$$\frac{\ln \rho(m)}{\ln \sigma(m)} \overrightarrow{m\to\infty} 1, \tag{1.18}$$

which implies that for $m \to \infty$ the entropy of the fireball is the same function of its mass as is the entropy of the fireballs of which it is composed of.

In order for Eq. (1.18) to hold, the function $F(m, T)$ must fall off asymptotically e.g.

$$F(m, T) = m^{5/2} e^{-\frac{m}{T}}. \tag{1.19}$$

Equating Eq. (1.16) and Eq. (1.17),

$$Z = \exp\left[\int_0^\infty \rho(m) m^{5/2} e^{-\frac{m}{T}} dm\right] = \exp\left[\int_0^\infty \rho(m) F(m, T)\, dm\right], \tag{1.20}$$

which is only consistent if both ρ and σ grow exponentially. Therefore,

$$\rho(m) \overrightarrow{m\to\infty} \frac{const}{m^{5/2}} e^{\frac{m}{T_H}} \tag{1.21}$$

where T_H is the limiting temperature and the partition function diverges for $T > T_H$. We refer to T_H as the Hagedorn temperature. Note that Eq. (1.19) is an ansatz and other forms could be used, which would result in alternative forms for $\rho(m)$.

> "Most of the physicists are recognized rapidly after their contribution. After that quick recognition, their impact as time goes on gets disseminated and integrated, and people often notice it less and less. With Rolf [Hagedorn], the opposite happened. It is like the best of wines. It is not so palatable in the early years, but as time goes on it just gets more and more remarkable." [47]

Again, Ericson's word ring true about Hagedorn's remarkable discovery. Recently, we have found that Hagedorn states can account for quick dynamical chemical equilibration times within the hadron gas phase [55, 56, 57, 58, 59]. Also, Hagedorn states have been shown to contribute to the physical description of a hadron gas close to T_c. The inclusion of Hagedorn states leads to a low η/s in the hadron gas phase [30, 60], which nears the supergravity bound $\eta/s = 1/(4\pi)$ [61]. Calculations of the trace anomaly including Hagedorn states also fits recent lattice results well and correctly describe the minimum of the speed of sound squared, c_s^2, near the phase transition found on the lattice [30]. Estimates for the bulk viscosity including Hagedorn states in the hadron gas phase indicate that the bulk viscosity, ζ/s, increases near T_c, which agrees with the general arguments of [62]. Furthermore, it has been shown [63, 64] that Hagedorn states provide a slightly better fit within a thermal model to the hadron yield particle ratios. Additionally, Hagedorn states provide a mechanism to relate T_c and T_{chem}, which then leads to the suggestion that a lower critical region centered at $T \approx 170$ MeV could possibly be preferred by experimental data, according to the thermal fit analyses [63].

1.2.1 Hagedorn Temperature in Bosonic String Theory

The existence of an infinite number of resonances with an exponentially increasing mass spectrum is difficult to prove experimentally. Currently, resonances can be measured consistently up to about 2.5 GeV [65]. However, it is quite possible that resonances exist on extremely short time scales with a mass of 10 GeV or even higher. Recent attempts have been made to prove that the density of mesonic states in QCD follows a Hagedorn like behavior [66].

It is clear, however, that such an exponentially rising density of states should appear in the confined phase of QCD. The heuristic argument for that is the following. It is known experimentally [65] that the masses of radially excited ρ mesons increases linearly with the radial quantum number, i.e., $M^2 \sim N$. However, a highly excited meson can be roughly described as an ultrarelativistic quark-antiquark pair connected by a confining flux tube (which appears due to the linear potential between the quarks in the confined phase). Because of the linear potential, the energy of this configuration, or its mass, should be $M \sim \sigma L$, where σ is the string tension and L is the size of the meson. However, in a semi-classical approximation, one can use the Bohr-Sommerfeld quantization rule $\int p\, dx \sim N$ (which implies that $ML \sim N$) to derive that $M^2 \sim \sigma N$. This qualitative understanding of mesons as relativistic strings is especially useful because another important behavior of mesons can be obtained from this analogy: the existence of an exponentially increasing density of states associated with a Hagedorn temperature. In fact,

we shall show in the following that a system of relativistic bosonic strings possesses a Hagedorn temperature. We will take this as an indication that QCD should also display this behavior.

The following derivation is taken from [67]. In order to derive the Hagedorn temperature we use relativistic open strings that carry no spatial momentum. Additionally, we will use a microcanonical ensemble to describe the thermodynamics of the string modes. Recall from thermodynamics that a microcanonical ensemble is a composition of copies of a system, A, which is in isolation with a fixed energy E. The number of possible states of A with the energy E is $\Omega(E)$, and, thus, the entropy is defined as (we use natural units $\hbar = k_B = 1$):

$$S(E) = \ln \Omega(E) \tag{1.22}$$

where k is the Boltzmann's constant. Additionally, in the previous paragraph we heuristically justified that we should see the relationship $M^2 \sim N$. In [67] the exact mass expression is derived

$$M^2 = \frac{1}{\alpha'}\left(N^{\perp} - 1\right) \approx \frac{N^{\perp}}{\alpha'} \tag{1.23}$$

where $\alpha' = l_s^2$ and l_s is the string length. Since $E = M$,

$$\sqrt{N^{\perp}} = \sqrt{\alpha'}E. \tag{1.24}$$

Therefore, we can now talk about the total number of states in terms of a function of the square root of the number of excitations of a string, i.e.,

$$\Omega(E) \to \Omega(\sqrt{N}). \tag{1.25}$$

$\Omega(\sqrt{N})$ can be found by first looking at a quantum non-relativistic string, which has the number of partitions $p(N)$ where $p(N) = \Omega(\sqrt{N})$. In Appendix A we derive $p_{24}(N)$ for the number of partitions of large integers where the 24 is for the number of dimensions for a bosonic string such that

$$p_{24}(N) \approx \frac{1}{\sqrt{2}} N^{-27/4} \exp\left(4\pi\sqrt{N}\right). \tag{1.26}$$

Then, using Eq. (A.30), we can find the entropy within the microcanonical model

$$\begin{aligned} S(E) &= 2\pi\sqrt{\frac{24N^{\perp}}{6}} = 4\pi\sqrt{N^{\perp}} \\ &= 4\pi\sqrt{\alpha'}E. \end{aligned} \tag{1.27}$$

We can then find the temperature using standard thermodynamics

$$\begin{aligned} T_H &= \left(\frac{\partial S}{\partial E}\right)^{-1} \\ &= \frac{1}{4\pi\sqrt{\alpha'}} \end{aligned} \tag{1.28}$$

where T_H is the thermal energy associated with the Hagedorn temperature.

1.3 Outline

This thesis is organized as follows. In Chapter 2 we explain how we obtain the chemical equilibrium values for the particles (both the standard hadrons and highly massive Hagedorn states) through a grand-canonical model, which can be used to determine the thermodynamics of the fireball. Furthermore, cooling effects are included using Bjorken expansion. We solve master equations to describe out of equilibrium dynamics. In Chapter 3 the hadrons are allowed to dynamically reach chemical equilibrium via resonance decays of Hagedorn states and we find that they match experimental data well.

In Chapter 4 we derive η/s for a hadron gas that includes Hagedorn states and it is found that in this case this ratio is close to the string theory value $1/4\pi$ [61]. Furthermore, the equation state in the hadronic phase including Hagedorn states is compared to lattice and it is found that it matches almost perfectly at T_c. Finally, a comment is made on the bulk viscosity to entropy ratio within our model.

In Chapter 5 thermal fits are calculated for a hadron gas both with and without Hagedorn states with $M > 2$ GeV included. When these highly massive Hagedorn states are included the fits appear to be improved for low values of the QCD critical temperature.

I provide a discussion of my results in Chapter 6 as well as possible continuations of this work that would be relevant to future physics. Additionally, I have included further background information for the derivation of Hagedorn states in bosonic string theory in Appendix A, the derivation of the kubo formula for shear and bulk viscosities is shown in Appendix E, an explanation and derivation of master equations is given in Appendix C, and the analytical derivation of estimates for the chemical equilibration times in Appendix D.

Chapter 2

Model

Hagedorn states are massive resonances that have large decay widths, which open up the phase space to multi-particle collisions. Because they decay so quickly they can catalyse quick reactions between hadrons that would otherwise have smaller cross-sections and take longer to reach chemical equilibrium. These reactions follow the general form

$$n\pi \leftrightarrow HS \leftrightarrow n\pi + X\bar{X} \tag{2.1}$$

where $X\bar{X} = p\bar{p}$, $K\bar{K}$, $\Lambda\bar{\Lambda}$, or $\Omega\bar{\Omega}$. Our idea is that these very massive Hagedorn states exist, as pictured in Fig. 2.1, and are so large that they decay almost immediately into multiple pions and $X\bar{X}$ pairs.

2.1 Description of the Model

Hagedorn states have an exponential mass spectrum, which is described by Eq. (1.15). It is repeated here for convenience

$$g(M) = \int_{M_0}^{M} \frac{A}{[m^2 + (m_0)^2]^{\frac{5}{4}}} e^{\frac{m}{T_H}} dm. \tag{2.2}$$

We note that in this work we consider only mesonic Hagedorn states with no net strangeness. The exponential in Eq. (1.15) arises from Hagedorn's original idea that there is an exponentially growing mass spectrum. Thus, as T_H is approached, Hagedorn states become increasingly more relevant and heavier resonances "appear". The factor in front of the exponential may appear in various forms [49, 51]. While the choice in this factor can vary, it was found in [49] that the present form gives lower values of T_H, which more closely match the predicted lattice critical temperature [8, 9, 68]. Further discussion on the parameters can be found in [69].

Returning to Eq. (1.15), we assume that $T_H = T_c$, and then we consider the two different different lattice results for T_c: $T_c = 196$ MeV [8, 68], which uses an almost physical pion mass, and $T_c = 176$ MeV [9]. Furthermore, we need to take into account the repulsive interactions and, therefore, we use the following volume corrections (as also seen in [30, 70, 71]):

$$T = \frac{T^*}{1 - \frac{p_{pt}(T^*, \mu_b^*)}{4B}}$$

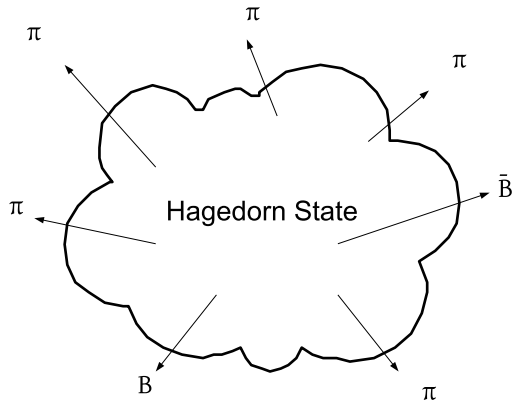

Figure 2.1: Hagedorn states decay into multiple pions and a $B\bar{B}$ pair.

$$\begin{aligned}
\mu_b &= \frac{\mu_b^*}{1-\frac{p_{pt}(T^*,\,\mu_b^*)}{4B}} \\
p_{xv} &= \frac{p_{pt}\,(T^*,\mu_b^*)}{1-\frac{p_{pt}(T^*,\,\mu_b^*)}{4B}} \\
\varepsilon_{xv} &= \frac{\varepsilon_{pt}\,(T^*,\mu_b^*)}{1+\frac{\varepsilon_{pt}(T^*,\,\mu_b^*)}{4B}} \\
n_{xv} &= \frac{n_{pt}\,(T^*,\mu_b^*)}{1+\frac{\varepsilon_{pt}(T^*,\,\mu_b^*)}{4B}}, \\
s_{xv} &= \frac{s_{pt}\,(T^*,\mu_b^*)}{1+\frac{\varepsilon_{pt}(T^*,\,\mu_b^*)}{4B}},
\end{aligned} \tag{2.3}$$

which ensure that the our model is thermodynamically consistent. In the equations above, the subscript "pt" denotes the value of the given quantity computed without the volume corrections. Note that B is a free parameter that is based upon the idea of the MIT bag constant. The derivation of Eq. (2.3) is shown in Appendix B.

In order to find the maximum Hagedorn state mass M and the "degeneracy" A, we fit our model to the thermodynamic properties of the lattice. In the RBC-Bielefeld collaboration the thermodynamical properties are derived from the quantity $\varepsilon - 3p$, the so-called interaction measure, which is what we fit in order to obtain the parameters for the Hagedorn states. Thus, we obtain $T_H = 196$ MeV, $A = 0.5\text{GeV}^{3/2}$, $M = 12$ GeV, and $B = (340\text{MeV})^4$. The fit for the trace anomaly Θ/T^4 is shown in Fig. 2.2. We also show the fit for the entropy density in Fig. 2.3. Both fits are within the error of lattice and mimic the behavior of the lattice results. As discussed in [30], a hadron resonance gas model with Hagedorn states uniquely fits the lattice data whereas a hadron resonance gas without Hagedorn states (but with excluded volume corrections) completely misses the general behavior displayed by the lattice data. Here

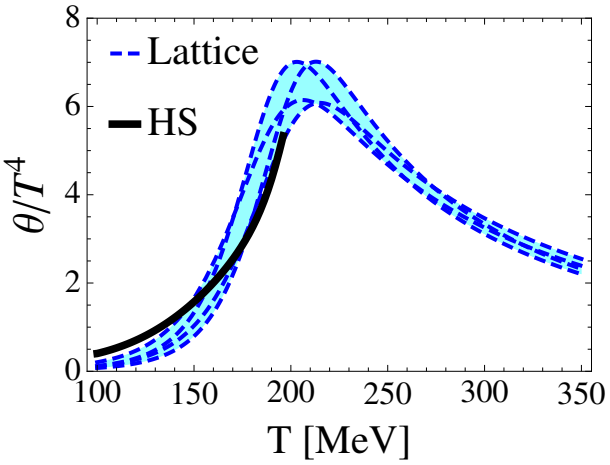

Figure 2.2: Comparison between the trace anomaly $\theta(T)/T^4 = (\epsilon - 3P)/T^4$ computed using a hadron resonance gas model that includes Hagedorn states with $2 < M < 12$ GeV [55] (solid black line) and a hadronic gas model where only the known hadrons with $M < 2$ GeV are included (black dashed line) [72]. The blue band between the curves is used to emphasize the effects of HS. Repulsive interactions between the hadrons are included via an excluded volume approach [70] with $B^{1/4} = 0.34$ GeV. Lattice data points for the $p4$ action with $N_\tau = 6$ [8] are also shown.

we follow Hagedorn's idea [54] and do not neglect the repulsive interactions between the hadrons.

BMW obtains the thermodynamical properties differently than RBC-Bielefeld and, therefore, we fit only the energy density as shown in Fig. 2.4. From that we obtain $T_H = 176$ MeV, $A = 0.1\text{GeV}^{3/2}$, $M = 12$ GeV, and $B = (300\text{MeV})^4$. We also show a comparison to the entropy density in Fig. 2.5 Our results with the inclusion of Hagedorn states are able to match lattice data near the critical temperature but do not match as well at lower temperatures in Fig. 2.2 and Fig. 2.3.

Note that lattice data does not include physical quark masses, which can affect the thermodynamic properties of the lattice at lower temperatures (see [32]). If physical quark masses are used, then the thermodynamic properties should improve, however they are not yet included in the current lattice models.

The maximum mass $M = 12$ GeV is used in both cases because it is a limit on the precision of the master equations. A maximum mass of greater than 12 GeV could be used but then the reactions would have to be fundamentally changed. For instance, one could include decays where multiple $X\bar{X}$ pairs were produced at a time, i.e., $HS \leftrightarrow n_1\pi + n_2 X\bar{X}$

2.1.1 Master Equations

In order to describe the dynamics of Eq. (2.1) we use master equations. They are practical because they give us a method to describe both the forward and back reactions, which ensures that detailed balance is mantained. Moreover, the state of chemical equilibrium is a fixed point of the rate equations. Additionally, master equations are naturally suited to describe multi-particle reactions whereas the transport equations used in UrQMD [73], for example, are better

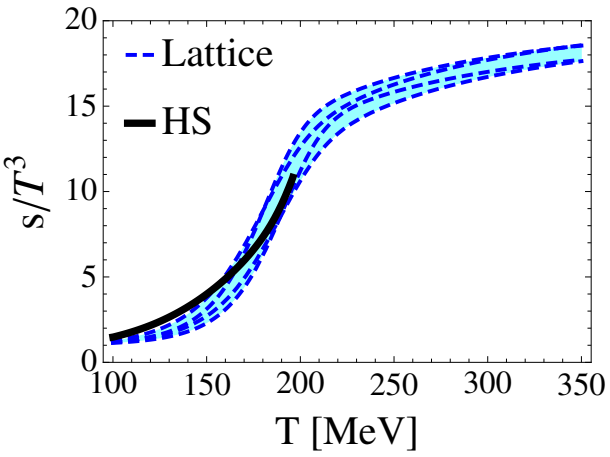

Figure 2.3: Comparison of entropy density to lattice QCD results from [8, 68] where $T_c = 196$ MeV. HS is in reference to our model including Hagedorn states.

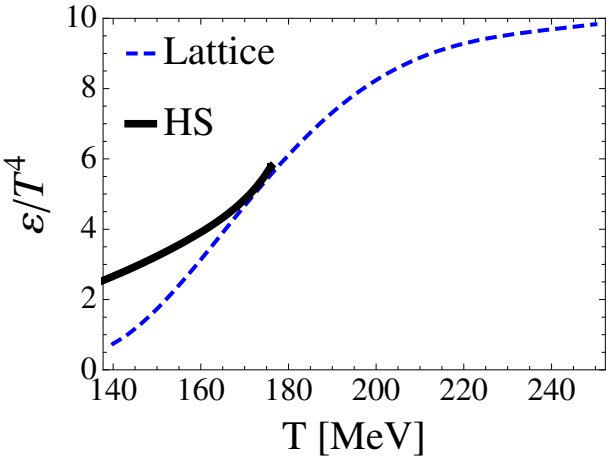

Figure 2.4: Comparison of energy density to lattice QCD results from [9] where $T_c = 176$ MeV. HS is in reference to our model including Hagedorn states.

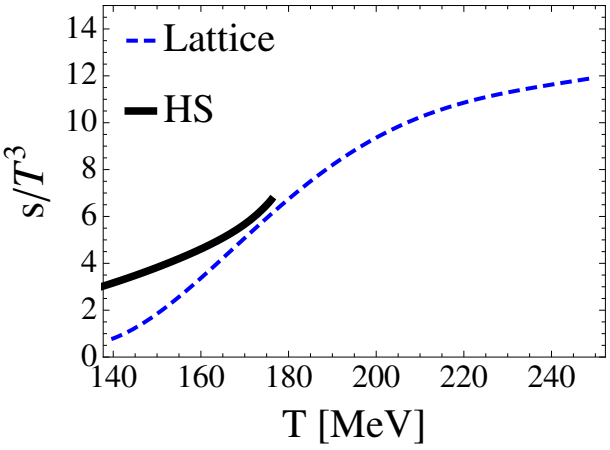

Figure 2.5: Comparison of entropy density to lattice QCD results from [9] where $T_c = 176$ MeV. HS is in reference to our model including Hagedorn states.

suited to describe the dynamics of binary collisions. A further discussion of master equations can be found in Appendix C. Additionally, a discrete spectrum of Hagedorn states is considered, which is separated into mass bins of 100 MeV. Each bin is described by its own rate equation.

The rate equations for the Hagedorn resonances N_i, pions N_π, and the $X\bar{X}$ pair $N_{X\bar{X}}$, respectively, in Eq. (2.1) are given by

$$\begin{aligned}
\dot{N}_i &= \Gamma_{i,\pi}\left[N_i^{eq}\sum_n B_{i,n}\left(\frac{N_\pi}{N_\pi^{eq}}\right)^n - N_i\right] + \Gamma_{i,X\bar{X}}\left[N_i^{eq}\left(\frac{N_\pi}{N_\pi^{eq}}\right)^{\langle n_{i,x}\rangle}\left(\frac{N_{X\bar{X}}}{N_{X\bar{X}}^{eq}}\right)^2 - N_i\right] \\
\dot{N}_\pi &= \sum_i \Gamma_{i,\pi}\left[N_i\langle n_i\rangle - N_i^{eq}\sum_n B_{i,n} n\left(\frac{N_\pi}{N_\pi^{eq}}\right)^n\right] + \sum_i \Gamma_{i,X\bar{X}}\langle n_{i,x}\rangle\left[N_i - N_i^{eq}\left(\frac{N_\pi}{N_\pi^{eq}}\right)^{\langle n_{i,x}\rangle}\left(\frac{N_{X\bar{X}}}{N_{X\bar{X}}^{eq}}\right)^2\right] \\
\dot{N}_{X\bar{X}} &= \sum_i \Gamma_{i,X\bar{X}}\left[N_i - N_i^{eq}\left(\frac{N_\pi}{N_\pi^{eq}}\right)^{\langle n_{i,x}\rangle}\left(\frac{N_{X\bar{X}}}{N_{X\bar{X}}^{eq}}\right)^2\right].
\end{aligned} \tag{2.4}$$

The decay widths for the i^{th} resonance are $\Gamma_{i,\pi}$ (for the decay into multiple pions) and $\Gamma_{i,X\bar{X}}$ (for the decay into multiple pions and a $X\bar{X}$ pair), the branching ratio is $B_{i,n}$ (clearly $\sum_n B_{i,n} = 1$), and the average number of pions that each resonance will decay into is $\langle n_i\rangle$. The equilibrium values N^{eq} are both temperature and chemical potential dependent. However, here we set $\mu_b = 0$, which is a good approximation for collisions at large $\sqrt{s}$.

In the rate equation for the Hagedorn states in Eq. (2.4), $\dot{N}_i$, the first term describes the reaction $HS \leftrightarrow n\pi$. Thus, the decay with for only the pions is used, $\Gamma_{i,\pi}$. The loss term, hence the minus sign, is N_i for when a Hagedorn state decays into $n\pi$ and the gain term is $N_i^{eq}\sum_n B_{i,n}\left(\frac{N_\pi}{N_\pi^{eq}}\right)^n$ for the case when $n\pi$ combine together to form a Hagedorn state. The branching ratio enters the loss term because one needs to calculate the probability that the Hagedorn state will decay into $n\pi$ and must also include all possible n's. The second term describes the decay $HS \leftrightarrow n\pi + X\bar{X}$. The decay width, $\Gamma_{i,X\bar{X}}$, is specifically for decays with

an $X\bar{X}$ pair is included and, once again, the loss term is described by N_i. The gain term is described by $N_i^{eq}\left(\frac{N_\pi}{N_\pi^{eq}}\right)^{\langle n_{i,x}\rangle}\left(\frac{N_{X\bar{X}}}{N_{X\bar{X}}^{eq}}\right)^2$, which is similar to the gain term for $HS \leftrightarrow n\pi$. However, we do not include a branching ratio in it and isntead just include the average number of pions a Hagedorn state could decay into. Furthemore, the $X\bar{X}$ pairs are also included in the term.

The pion rate equation, $\dot{N}_\pi$, is similar to that of the Hagedorn states. The primary differences are that the terms are multiplied by n to include the number of pions that a Hagedorn state can decay into. Additionally the loss and gain terms are reversed because in this case the gain occurs when the Hagedorn states decay, which is the opposite of the first master equation. The final master equation for the $X\bar{X}$ pairs only includes terms for the reaction $HS \leftrightarrow n\pi + X\bar{X}$ because the reaction $HS \leftrightarrow n\pi$ does not directly contribute to the total number of $X\bar{X}$ pairs in the system. As with the pions N_i is used as the gain term and $N_i^{eq}\left(\frac{N_\pi}{N_\pi^{eq}}\right)^{\langle n_{i,x}\rangle}\left(\frac{N_{X\bar{X}}}{N_{X\bar{X}}^{eq}}\right)^2$ is the loss term. Only one pair is produced at a time so the equation is not multiplied by any factor.

Eq. (2.4) can also be represented by the respective fugacities (λ_i, λ_π, and $\lambda_{X\bar{X}}$), which are found by dividing each total number by its respective equilibrium value, for example, $\lambda_i = \frac{N_i}{N_i^{eq}}$

$$\begin{aligned}
\dot{\lambda}_i &= \Gamma_{i,\pi}\left(\sum_{n=2}^{\infty} B_{i,n}\lambda_\pi^n - \lambda_i\right) + \Gamma_{i,X\bar{X}}\left(\lambda_\pi^{\langle n_{i,x}\rangle}\lambda_{X\bar{X}}^2 - \lambda_i\right), \\
\dot{\lambda}_\pi &= \sum_i \Gamma_{i,\pi}\frac{N_i^{eq}}{N_\pi^{eq}}\left(\lambda_i\langle n_i\rangle - \sum_{n=2}^{\infty} B_{i,n}n\lambda_\pi^n\right) + \sum_i \Gamma_{i,X\bar{X}}\langle n_{i,x}\rangle\frac{N_i^{eq}}{N_\pi^{eq}}\left(\lambda_i - \lambda_\pi^{\langle n_{i,x}\rangle}\lambda_{X\bar{X}}^2\right), \\
\dot{\lambda}_{X\bar{X}} &= \sum_i \Gamma_{i,X\bar{X}}\frac{N_i^{eq}}{N_{X\bar{X}}^{eq}}\left(\lambda_i - \lambda_\pi^{\langle n_{i,x}\rangle}\lambda_{X\bar{X}}^2\right),
\end{aligned} \tag{2.5}$$

In Eq. (2.5) one can easily see that at chemical equilibrium, i.e. when $\lambda = 1$, the right-hand side of the rate equations approach zero.

While it can be argued that Hagedorn states are more likely to decay into a pair of particles (e.g., a lighter Hagedorn state and another particle), these reactions are so quick that here we consider only the end results, which are the multiple particles (mostly pions). This could, however, be later checked by putting binary collisions of Hagedorn states into a hadronic transport code such as UrQMD. Then the cross-section could be described similarly to what is shown in [74]. We leave this as a challenge for the future.

2.1.2 Branching Ratios

The branching ratio, $B_{i,n}$, is the probability that the i^{th} Hagedorn state will decay into n pions. Since we are dealing with probabilities, then $\sum_n B_{i,n} = 1$ must always hold. We have the condition that each Hagedorn resonance must decay into at least 2 pions. Thus, our average number of pions must be normalized to ensure that $n \geq 2$ and $\sum_n B_{i,n} = 1$. The branching ratios for the reaction $HS \leftrightarrow n\pi$ are described by a Gaussian distribution

$$B_{i,n} \approx \frac{1}{\sigma_i\sqrt{2\pi}}e^{-\frac{(n-\langle n_i\rangle)^2}{2\sigma_i^2}}, \tag{2.6}$$

which has its peak centered at $\langle n_i \rangle$ and the width of the distribution is σ^2.

Because the Hagedorn states that we consider here have not been measured experimentally we cannot know their branching ratios. Future measurements of high exotic hadronic resonances can be used to obtain these ratios in the future. In the meantime, we can, however, look at statistical ensembles in order to estimate the branching ratios of the Hagedorn states. Following the principle of (maximum) missing information, we assume here that the branching ratios can be obtained from a microcanonical calculation. Such a description is, for instance, also appropriate for describing the annihilation of p and anti-p.

Assuming a statistical, microcanonical branching for the decay of Hagedorn states, we can take a linear fit to the average number of pions in Fig. 1 in Ref. [44] (multiplying π^+ by three to include all pions) to find $\langle n_\pi \rangle$ such that

$$\langle n_i \rangle = 0.9 + 1.2\frac{m_i}{m_p} \tag{2.7}$$

is the average pion number that each Hagedorn state decays intowhere m_p is the mass of the proton. In the microcanonical model the volume is

$$V = M_i/\varepsilon \tag{2.8}$$

where ε is the mean energy density of a Hagedorn state (taken as $\varepsilon = 0.5\frac{GeV}{fm^3}$). Further discussions regarding this can be found in [44, 75]. The width of the distrubtion is $\sigma_i^2 = (0.5\frac{m_i}{m_p})^2$. Both our choice in $\langle n \rangle$ and σ^2 roughly match the canonical description in [76].

Furthermore, we have the condition that each Hagedorn resonance must decay into at least 2 pions. Because of the nature of a Gaussian distribution there is a non-zero probability that a Hagedorn state can decay into less than 2 pions. Therefore, we calculate the percentage of the distribution that falls below 2 pions and redistribute that over $n \geq 2$ so that $\sum_n B_{i,n} = 1$. This in turn leads to a new $\langle n_i \rangle$ and σ_i^2, which we find by calculating

$$\langle n_i \rangle = \sum_n n B_{i,n} \tag{2.9}$$

and

$$\sigma_i^2 = \langle n_i^2 \rangle - \langle n_i \rangle^2 \tag{2.10}$$

Thus, after we normalize for the cutoff $n \geq 2$, we have $\langle n_i \rangle \approx 3 - 34$ and $\sigma_i^2 \approx 0.8 - 510$. Examples of the branching ratios can be seen in Fig. 2.6.

For the average number of pions when a $X\bar{X}$ pair is present, we again refer to the microcanonical model in [44, 75] and see also Fig. 2.7. We use $\langle n_\pi \rangle$ but then readjust it to the average pion number according to Fig. 2 in Ref. [44] for when a baryon anti-baryon pair is present (there the distribution is for a resonance of mass $m = 4$ GeV). Thus,

$$\langle n_{i,x} \rangle = \left(\frac{2.7}{1.9}\right)(0.3 + 0.4m_i) \approx 2 - 7. \tag{2.11}$$

where m_i is in GeV. In this paper we do not consider a distribution but rather only the average number of pions when a $X\bar{X}$ pair is present. We assume that $\langle n_{i,x} \rangle = \langle n_{i,p} \rangle = \langle n_{i,k} \rangle = \langle n_{i,\Lambda} \rangle = \langle n_{i,\Omega} \rangle$ for when a proton anti-proton pair, kaon anti-kaon pair, $\Lambda\bar{\Lambda}$, or $\Omega\bar{\Omega}$ pair is present. Ideally, $\langle n_{i,k} \rangle$, $\langle n_{i,\Lambda} \rangle$, and $\langle n_{i,\Omega} \rangle$ should be derived separately and that may possibly be done in a future study using a canonical model.

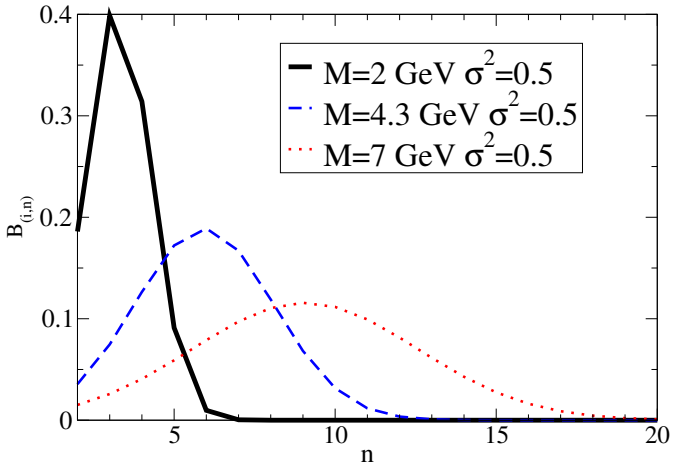

Figure 2.6: The average n, $\langle n_i \rangle$, and the standard deviation σ_i^2 for the branching ratios are shown.

2.1.3 Decay Width

We used a linear fit for the decay width similar to that used in Ref. [77] without considering different isospins. To do so we find a linear fit to the light, non-strange, mesonic resonances given in [65]. The error in the decay widths varies significantly for each resonance so much so that it is impractical to use a χ^2 fit because all the resonances but 3 would be ignored, which would result in completely missing the rising behavior of the data see in Fig. 2.8. Additionally, we do not consider the $f_0(600)$ because it is an extreme outlier with very wide error bars that do not even come close to the same range as the other particles (see Fig. 2.8). For the fits we only use resonances up to $M = 2$ GeV, which is reasonable considering that we make the assumption that they are missing resonances above $M > 2$ GeV and, therefore, it's only up to $M = 2$ GeV that we can reasonable fit the decay widths. However in Fig. 2.8 we show all the light, non-strange mesons to show that even above $M > 2$ GeV they still follow and increasing behavior.

Because a χ^2 fit is impractical, we do three different fits (one using the upper bound of the error of the decay widths, one at the given decay width and one at the lower bound of the error)to the data to see the dependence on Γ_i, the results of which are shown in section 3.2.1. Throughout the rest of this work we use the given decay width value, which is

$$\Gamma_i[GeV] = 0.15 m_i[GeV] - 0.03, \tag{2.12}$$

which ranges from $\Gamma_i = 250$ MeV to 1800 MeV. Fitting the lower end of the error bars one finds

$$\Gamma_i^{lo}[GeV] = 0.15 m_i[GeV] - 0.06, \tag{2.13}$$

and fitting the higher end of the errors one finds

$$\Gamma_i^{hi}[GeV] = 0.15 m_i[GeV]. \tag{2.14}$$

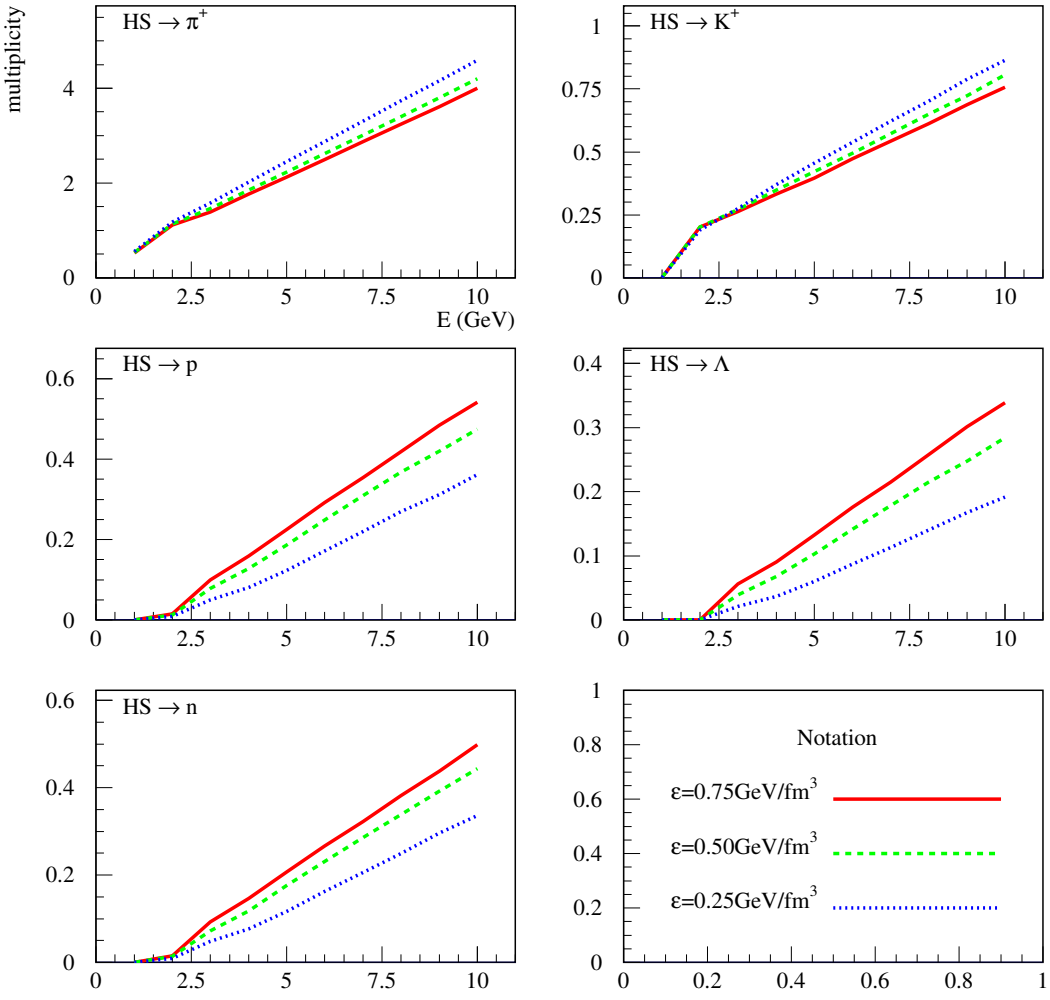

Figure 2.7: Multiplicities of pions, kaons, protons, and lambdas taken from Fig. 2 in Ref. [44].

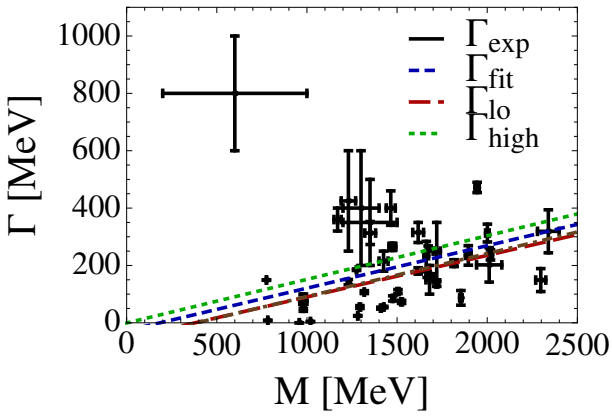

Figure 2.8: Linear fit for the decay width for the light (non-strange), mesonic resonances.

The total decay width has been separated into two parts in Eq. (2.4): one for the reactions $HS \leftrightarrow n\pi$, $\Gamma_{i,\pi}$, and one for the reaction in Eq. (2.1), $\Gamma_{i,X\bar{X}}$, whereby

$$\Gamma_i = \Gamma_{i,\pi} + \Gamma_{i,X\bar{X}}, \tag{2.15}$$

which ensures that Eqs. (2.4, 2.5) are zero at equilibrium. Then, the relative decay width $\Gamma_{i,X\bar{X}}$ modeled after the decay width in reference Ref. [44] is the average number of $X\bar{X}$ in the system $\langle X \rangle$ multiplied by the total decay width Γ_i,

$$\Gamma_{i,X\bar{X}} = \langle X \rangle \, \Gamma_i. \tag{2.16}$$

Essentially, a fraction of the decay of the i^{th} Hagedorn state goes into $X\bar{X}$ (set by the number of $X\bar{X}$ the i^{th} Hagedorn state on average decays into) and the remainder goes into pions. That means that $\Gamma_{i,\pi}$ is then

$$\begin{aligned} \Gamma_{i,\pi} &= \Gamma_i - \Gamma_{i,X\bar{X}} \\ &= (1 - \langle X \rangle)\Gamma_i. \end{aligned} \tag{2.17}$$

We find $\langle p \rangle$ by linearly fitting the proton in Fig. 2 in Ref. [44] (see Fig. 2.7) so that

$$p = 0.058 \, m_i - 0.10 \tag{2.18}$$

where m_i is in GeV and $\langle p \rangle \approx 0.01 - 0.6$. Thus, $\Gamma_{i,p\bar{p}}$ is between 3 and 1000 MeV. Clearly, $\Gamma_{i,\pi}$ is then $\Gamma_{i,\pi} = \Gamma_i - \langle p \rangle \Gamma_{i,\pi}$. Analogously for the kaons, the decay width is $\Gamma_{i,K\bar{K}} = \langle K \rangle \Gamma_i$ where

$$K^+ = 0.075 \, m_i + 0.047 \tag{2.19}$$

where m_i is in GeV, which is also taken from Fig. 2 in Ref. [44] (see Fig. 2.7). We find that $\langle K \rangle = 0.2$ to 0.95 [75, 44]. Thus, $\Gamma_{i,K\bar{K}}$ is between 50 and 1700 MeV.

For Λ we use a canonical model assuming that the baryon number $B = 0$, the strangeness $S = 0$, and the electrical charge $Q = 0$ in order to calculate the average number of Λ's. The

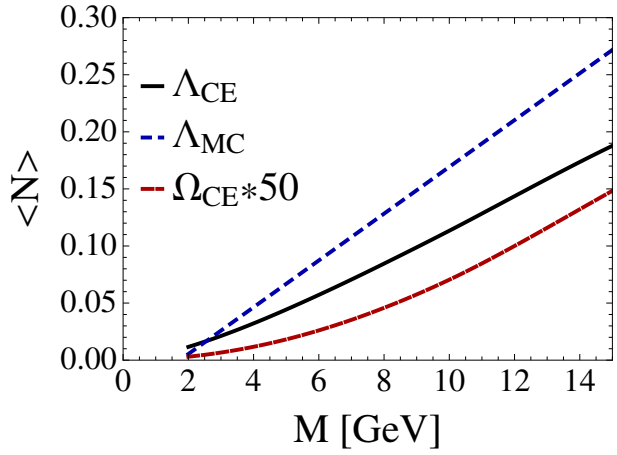

Figure 2.9: Average number of Λ's and Ω's (multiplied by 50). The Ω's are calculated within our canonical ensemble and the Λ's are calculated both in our canonical ensemble and a micro-canonical ensemble.

results are shown in Fig. 2.9. We find that our $\langle\Lambda\rangle$ is lower than that from the micro-canonical ensemble in [44] (see Fig. 2.7), which is also shown in Fig. 2.9. This corresponds to a decay width of $\Gamma_{i,\Lambda\bar{\Lambda}} = 3 - 250$ MeV.

Furthermore, the average number of Ω's is also shown in Fig. 2.9 from our canonical model again assuming that the baryon number $B = 0$, the strangeness $S = 0$, and the electrical charge $Q = 0$. In Fig. 2.9 we multiple $\langle\Omega\rangle$ by 50 in order to better view the results. The resulting decay width is $\Gamma_{i,\Omega\bar{\Omega}} = 0.01 - 4$ MeV.

2.1.4 Initial Conditions

The equilibrium values are found using a statistical model [72], which includes 104 particles from the the PDG [65] (only light and strange particles). As in [72], we also consider the effects of feeding (the contributions of higher lying resonances such as the ρ or ω resonances on the number of "pions" in our system, i.e., N_π^{eq} includes "all" the pions from resonances from the PDG [65]). Feeding is also considered for the protons, kaons, and lambdas (Ω's have no resonances). Additionally, throughout this work our initial conditions are the various fugacities at t_0 (at the point of the phase transition into the hadron gas phase)

$$\alpha \equiv \lambda_\pi(t_0)\,,\ \beta_i \equiv \lambda_i(t_0)\,,\text{and}\,\phi \equiv \lambda_{X\bar{X}}(t_0)\ , \tag{2.20}$$

which are chosen by holding the contribution to the total entropy from the Hagedorn states and pions constant, i.e.,

$$s_{Had}(T_0,\alpha)V(t_0) + s_{HS}(T_0,\beta_i)V(t_0) = s_{Had+HS}(T_0)V(t_0) = const. \tag{2.21}$$

and the corresponding initial condition configurations we choose later can be seen in Tab. 3.2 in the next chapter. $s_{Had}(T_0,\alpha)$ is the entropy density at the initial temperature, i.e., the critical temperature multiplied by our choice in α. Because the hadron resonance is dominated by

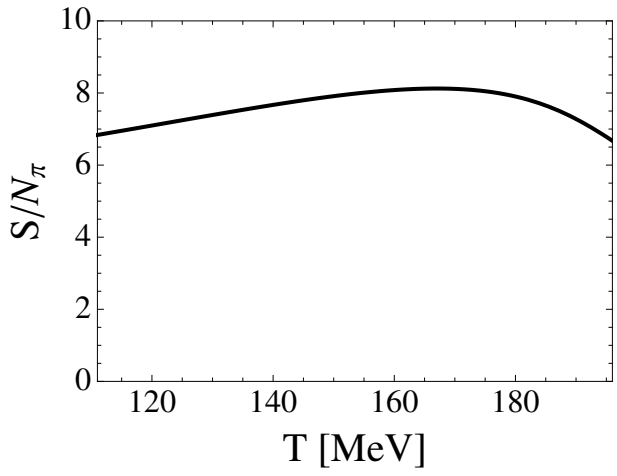

Figure 2.10: Entropy per pion for a hadron gas in chemical equilibrium within the fireball ansatz.

pions we can assume that α represents the initial fraction of pions in equilibrium. $s_{HS}(T_0, \beta_i)$ represents the entropy contribution from the Hagedorn states at T_c multiplied by the initial fraction of Hagedorn states in equilibrium. We hold α as a constant and then find the appropriate β_i.

2.1.5 Expansion

In order to include the cooling of the fireball we need to find a relationship between the temperature and the time, i.e., $T(t)$. To do this we apply a Bjorken expansion for which the total entropy is held constant

$$\text{const.} = s(T)V(t) \sim \frac{S_\pi}{N_\pi} \int \frac{dN_\pi}{dy} dy. \tag{2.22}$$

where $s(T)$ is the entropy density of the hadron gas with volume corrections.

The total number of pions in the 5% most central collisions, $\frac{dN_\pi}{dy}$, can be found from experimental results in [78]. There they found the phase-space yields for the pions π^+ (292.0) and π^- (290.9) using a Gaussian fit for yields as a function of the rapidity $\frac{dN_\pi}{dy}$ where we used the rapidity range $y = \pm 0.5$. We then assumed that the number of π^0's were also in that same range and took the average of the two to find 291.5. Thus, our total pion number is $\sum_i N_{\pi^i} = \int_{-0.5}^{0.5} \frac{dN_\pi}{dy} dy = 874$. While for a non-interacting Bose gas of massless pions $S_\pi/N_\pi = 3.6$, we do have a mass for our pions, so we must adjust S_π/N_π accordingly. In [79] it was shown that when the pions have a mass the ratio changes and, therefore, the entropy per pion is close to $S_\pi/N_\pi \approx 5.5$. The actual S_π/N_π in our model is shown in Fig. 2.10 where $S_\pi/N_\pi \approx 6$, which is only slightly higher.

The effective volume at mid-rapidity can be parametrized as a function of time. We do this by using a Bjorken expansion and including accelerating radial flow. The volume term is then

$$V(t) = \pi\, ct \left(r_0 + v_0(t - t_0) + \frac{1}{2} a_0 (t - t_0)^2 \right)^2 \tag{2.23}$$

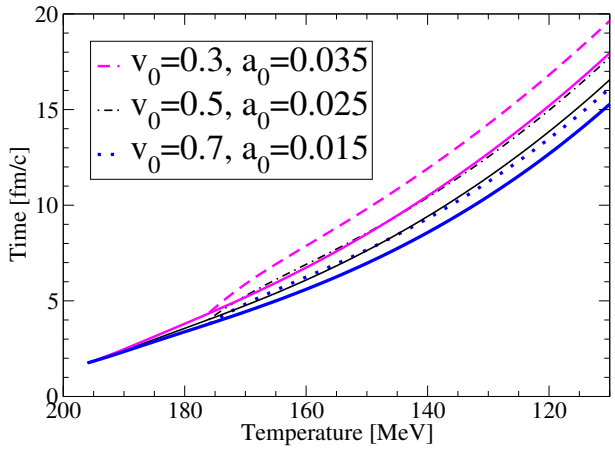

Figure 2.11: The temperature-time relationship is directly linked to the average transversel velocity chosen in Eq. (2.23) within the fireball model ansatz.

where the initial radius is $r_0(t_0) = 7.1$ fm, which is the radius of a gold nucleus, for $T_H = 196$ and the corresponding $t_0^{(196)} \approx 2fm/c$. For $T_H = 176$ we allow for a longer expansion before the hadron gas phase is reached and, thus, calculate the appropriate $t_0^{(176)}$ from the expansion starting at $T_H = 196$, which is $t_0^{(176)} \approx 4fm/c$ (there is a slightly variation dependent on the choice of v_0 and a_0). The $T(t)$ relation is shown in Fig. 2.11, which has almost no effect on the results as seen later on in Fig. 3.7 and Fig. 3.8. Therefore, we choose $v_0 = 0.5$ and $a_0 = 0.025$ for the remainder of this work. The relation depicted allows to translate the later shown figures labeled by the effective global temperature of the evolving system directly into the evolving system time.

2.1.6 Effective Numbers

Because the volume expansion depends on the entropy according to Eq. (2.22) and the Hagedorn resonances contribute strongly to the entropy only close to the critical temperature (see Fig. 2.12), the equilibrium values actually decrease with increasing temperature close to T_c for the hadrons as seen in Fig. 2.13 and Fig. 2.14. One can clearly see from Fig. 2.12 that the Hagedorn states contribute strongly close to T_c down to about 80% of T_c.

Therefore, one has to include the potential contribution of the Hagedorn resonances to the pions as in the case of standard hadronic resonances, e.g. a ρ-meson decays dominantly into two pions and, thus, accounts for them by a factor two. This is similar to what was done in Appendix D in Eq. (D.18). Including the Hagedorn state contribution, we arrive at our effective number of pions

$$\tilde{N}_{\pi,X\bar{X}} \quad = \quad N_\pi + \sum_i N_i \left[(1 - \langle X_i \rangle) \langle n_i \rangle + \langle X_i \rangle \langle n_{i,x} \rangle \right] \tag{2.24}$$

which are shown in Fig. 2.13. In Fig. 2.13 we see that after the inclusion of the effective pion numbers that the number of pions only decreases with decreasing temperature. Furthermore,

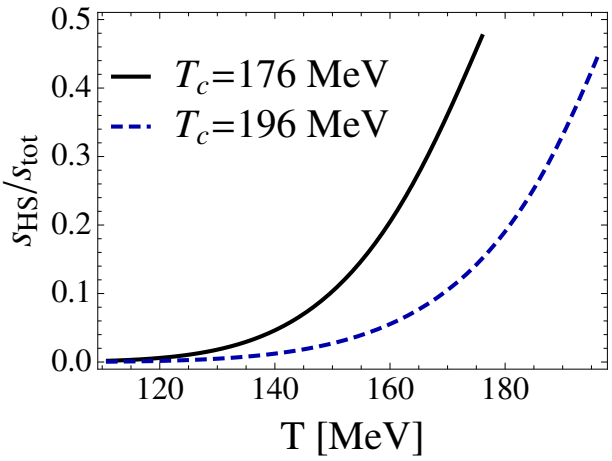

Figure 2.12: Ratio of the entropy of the Hagedorn states to the total entropy.

in Fig. 2.13 the total number of Hagedorn states, $\sum_i N_i^{eq}$ is also shown. While there are by far fewer Hagedorn states present than pions, we see that they are important because of their large contribution to the entropy density as shown in Fig. 2.12. The reason that the effective number of pions increase close to T_c is due to the large number of pions that the heavy Hagedorn states decay into. If $\langle n_i \rangle$ was smaller or no longer linear than it could be possible that the effective number of pions would remain constant.

Moreover, it is useful to consider the effective number of $X\bar{X}$ pairs

$$\tilde{N}_{X\bar{X}} = N_{X\bar{X}} + \sum_i N_i \langle X_i \rangle \tag{2.25}$$

because Hagedorn states also contribute strongly to the $X\bar{X}$ pairs close to T_c as seen in Fig. 2.14. Again we see that only the effective number of $X\bar{X}$ pairs have consistent decreasing behaviour with decreasing temperature whereas without the Hagedorn state contributions we see a decrease close to T_c.

2.1.7 Numerical Solutions of Rate Equations

Along with the expansion we also must solve these rate equations, Eq. (2.4), numerically [1]. We start with various initial conditions, as mentioned previously, that are described by α, β_i, and ϕ (see table 3.2). The initial temperature is the respective critical temperature and we end the expansion at $T = 110$ MeV, which is taken to be a global kinetic freezeout temperature.

[1] We solve our coupled non-linear differential equations using NDSolve in Mathematica.

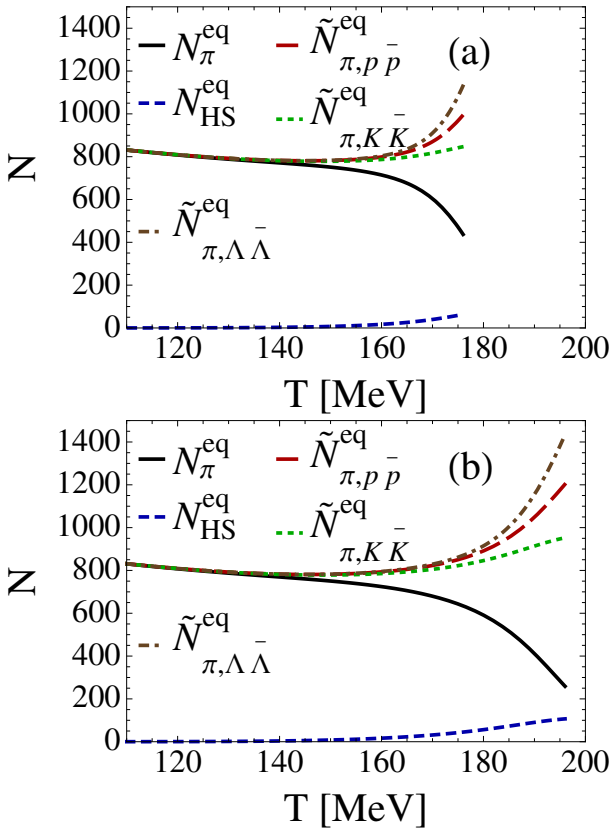

Figure 2.13: Comparison of the effective pion numbers when (a) $T_H = 176$ MeV or (b) $T_H = 196$ MeV.

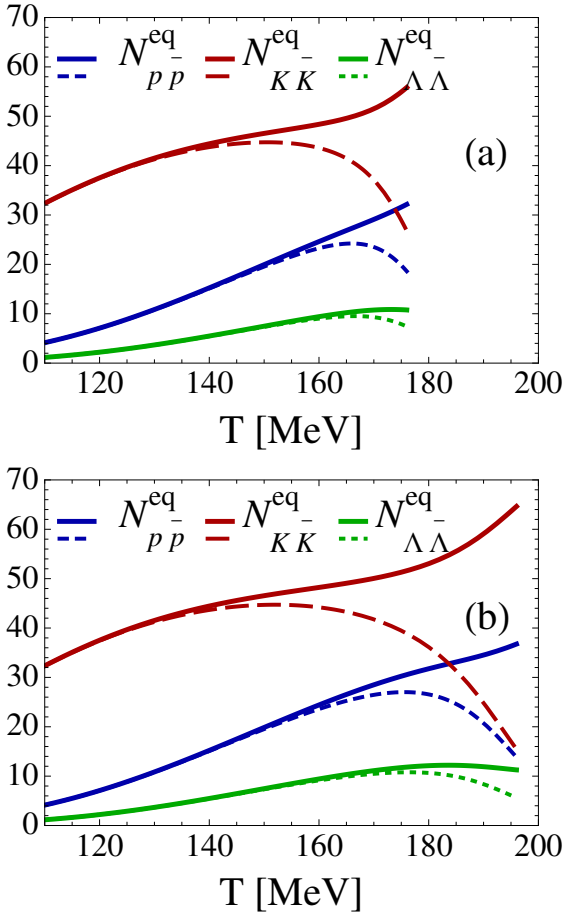

Figure 2.14: Comparison of the total number of $X\bar{X}$ and their effective numbers when (a) $T_H = 176$ MeV or (b) $T_H = 196$ MeV.

Chapter 3

Dynamical Chemical Equilibration of Hadrons

It has been suggested that particle ratios observed in heavy ion collisions such as SPS or RHIC can be indicative of the properties of the phase of nuclear matter before the phase transition into the hadron gas phase. In other words, particle ratios (specifically strangeness enhancement to light hadrons) can be used as a signal for QGP. This assumption is based on the idea that the particles are "born" in chemical equilibrium, i.e., that following the QGP stage the particles are already in chemical equilibrium when they enter the hadron gas phase.

Initial lattice results appeared to give a critical temperature close to the chemical freeze-out temperature found from thermal fits somewhere between $T = 160 - 170$ MeV [46]. However, recent lattice results with almost physical quark masses have established critical temperatures as high as 35 MeV above the stand thermal fit temperature of ~ 160 MeV. These discrepancies can be understood within a dynamical chemical freeze-out scenario where the hadrons are born out of chemical equilibrium following the QGP phase. While binary collisions and multi-mesonic reactions cannot reach chemical equilibrium at ~ 160 MeV (as discussed in Section 1.1.3), we will demonstrate in this chapter that reactions involving Hagedorn states can account for the particle abundances observed at RHIC and also account for the discrepancy between the critical temperature and the chemical freeze-out temperature.

In this chapter rate equations are used to describe Hagedorn resonances, which drive multi-pions and $X\bar{X}$ pairs into chemical equilibrium. The model used here was described in its entirety in the previous chapter. We find analytical results for the chemical equilibration time when the pions and Hagedorn resonances are out of equilibrium, which can be extrapolated to the protons, kaons, lambdas, and omegas. Moreover, we include a Bjorken expansion in order to describe the change of temperature over time in an expanding fireball. Our results show that (anti-)protons, (anti-)kaons, (anti-)lambdas, and (anti-)omegas do not need to be "born" into chemical equilibrium, but rather they have sufficient time within the hadron gas phase to equilibrate. Thus, the effectiveness of strangeness enhancement as a signal for QGP is brought into question because strangeness enhancement can be sufficiently explained within a hadron gas model.

3.1 Chemical Equilibration Time Scales at Constant Temperatures

Due to the complexity of the rate equations given in Eq. (2.4), it is not a trivial problem to solve them analytically. In order to gain a grasp on their solutions we first look at only the reaction $HS \leftrightarrow n\pi$ in section 3.1.1, which has a significantly easier solution, while holding the temperature constant. For the reaction $HS \leftrightarrow n\pi$ we are able to solve its rate equations analytically (see Appendix D for the derivation). Our solution shows that there are a number of non-linear effects, which slows down the chemical equilibration time. However, they only appear when the species are already very close to their respective chemical equilibrium values.

Using the same methods, we are able to look at the reaction in Eq. (2.1). However, the inclusion of an $X\bar{X}$ pair significantly complicates the matter. Only when either the pions or Hagedorn states are held constant, have we been able to determine an analytical solution. A discussion of which can be found in section 3.1.2. For simplicity's sake we use only the Hagedorn temperature $T_H = 176$ MeV and observe only $K\bar{K}$. Other parameters have similar results to those shown here.

3.1.1 A Simplified System: Pions and Hagedorn States

To understand the dynamics in more detail, we consider the simplified case when the Hagedorn resonances decay only into pions $HS \leftrightarrow n\pi$, which gives

$$\begin{aligned} \dot{N}_i &= \Gamma_i \left[N_i^{eq} \sum_{n=2} B_{i,n} \left(\frac{N_\pi}{N_\pi^{eq}} \right)^n - N_i \right] \\ \dot{N}_\pi &= \sum_i \Gamma_i \left[N_i \langle n_i \rangle - N_i^{eq} \sum_{n=2} B_{i,n} n \left(\frac{N_\pi}{N_\pi^{eq}} \right)^n \right]. \end{aligned} \tag{3.1}$$

Assuming that the pions and the Hagedorn states described above are then allowed to equilibrate near T_c in a static system, we are able to derive analytical solutions, the derivation of which is shown in detail in Appendix D. The simplest case involves holding the pions constant while the Hagedorn states are free to equilibrate. The resonance then reaches chemical equilibrium with the time scale

$$\tau_i = \frac{1}{\Gamma_i}. \tag{3.2}$$

A graph of the Hagedorn states while the pions are held in chemical equilibrium at a constant temperature is shown in Fig. D.1, although the results are temperature independent as seen in Eq. (3.2). We then hold the Hagedorn states while the pions equilibrate. Again, we are able to find an analytical solution. However, we must divide the equilibration into two different stages. The first of which is when $\lambda_\pi(t) \approx 0$, which has a time scale of

$$\tau_\pi^0 = \frac{N_\pi^{eq}}{\sum_i \Gamma_i N_i^{eq} \langle n \rangle \beta_i} \, . \tag{3.3}$$

Then the second is when $\lambda_\pi(t) \approx 1$, and has the time scale

$$\tau_\pi = \frac{N_\pi^{eq}}{\sum_i \Gamma_i N_i^{eq} \langle n^2 \rangle} \, . \tag{3.4}$$

		M_{2GeV}	M_{12GeV}
HS	$\tau_i = 1/\Gamma_i$	$0.8\frac{\text{fm}}{c}$	$0.1\ \frac{\text{fm}}{c}$
		$0.95T_c^B$	$0.95T_c^R$
$\lambda_\pi \approx 0$	$\tau_\pi^0 \equiv \frac{N_\pi^{eq}}{\sum_i \Gamma_i N_i^{eq} \langle n_i \rangle \beta_i}$	$0.5\frac{\text{fm}}{c}$	$0.1\frac{\text{fm}}{c}$
$\lambda_\pi \approx 1$	$\tau_\pi \equiv \frac{N_\pi^{eq}}{\sum_i \Gamma_i N_i^{eq} \langle n_i^2 \rangle}$	$0.01\frac{\text{fm}}{c}$	$0.003\frac{\text{fm}}{c}$
QE	$\tau_\pi^{QE} \equiv \frac{N_\pi^{eq}}{\sum_i \Gamma_i N_i^{eq} \sigma_i^2} + \frac{\sum_{QE} N_i^{eq} \langle n_i^2 \rangle}{\sum_i \Gamma_i N_i^{eq} \sigma_i^2}$	$1.7\frac{\text{fm}}{c}$	$1.6\frac{\text{fm}}{c}$

Table 3.1: Chemical equilibration times from analytical estimates where QE is quasi-equilibrium at 95% of each respective T_H. Here $T_c^B = 176$ MeV and $T_c^R = 196$ MeV.

The results for the Hagedorn states is shown in Fig. D.2.

Finally, for the analytical solutions of the case when both the pions and Hagedorn states are allowed to reach chemical equilibrium we divide the chemical equilibration into three stages, the chemical equilibration times of which are shown in Tab. 3.1. The first stage (described by τ_π^0 in Tab. 3.1) of the evolution is dominated by the chemical equilibration of the pions when the pions are still far away from their chemical equilibrium values. After the pions are close to chemical equilibrium, new dynamics take over, which are described by τ_π in Tab. 3.1 and Fig. 3.1.

In both Stage 1 and 2 the equilibration of the Hagedorn states is set by the dynamics of the pions. Finally, in Stage 3 the pions, which are already almost in chemical equilibrium, reach a quasi-equilibrium state with the Hagedorn states. Quasi-equilibrium is reached when at least one species of Hagedorn states has succeeded it's chemical equilibrium time scale determined from the inverse of its decay width, i.e., $\tau_i = 1/\Gamma_i$ (same as Eq. (3.2)). Since the heaviest Hagedorn states have the shortest τ_i's, then quasi-equilibrium is reached when τ_i of the heaviest Hagedorn state is surpassed. During this stage non-linear affects take over and, thus, a longer time scale, τ_π^{QE}, is seen. While this time scale may appear long, both the pions and Hagedorn states are so close to chemical equilibrium that they are within roughly 10% (depending on the initial conditions) or less of their chemical equilibrium values before quasi-equilibrium is even reached. The detailed calculations are shown in the Appendix D.

Therefore, the most important chemical equilibration time is then that from the pions in Stage 1, i.e., τ_π^0. The time scale from Stage 2 is so short that it is not of much importance. Additionally, by the time that Stage 3 is reached both the pions and Hagedorn states are essentially in chemical equilibrium and, therefore, the non-linear affects do not play a large role in the overall chemical equilibration time. One can see this more clearly in Fig. D.3a in Appendix D where the pions and heavier Hagedorn states are extremely close to chemical equilibrium, while the lighter Hagedorn states are still only moderately close to their chemical equilibrium values. Therefore, the Hagedorn states and pions are able to be roughly in chemical equilibrium on the order of $< 1\frac{fm}{c}$ according to our analytical solution when held at a constant temperature.

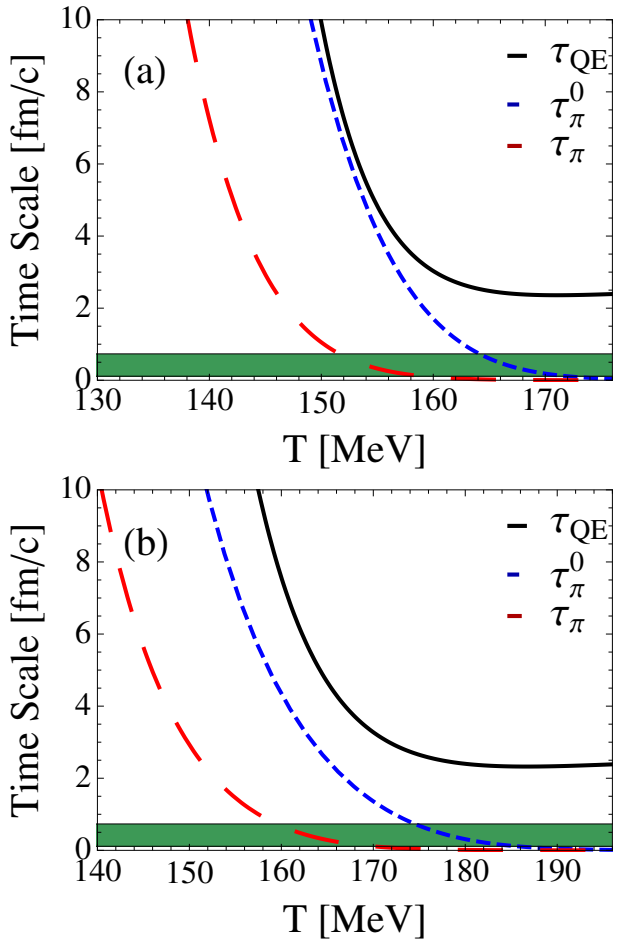

Figure 3.1: Comparison of the chemical equilibration times of the pions to the total chemical equilibration time for (a) $T_H = 176$ MeV and (b) $T_H = 196$ MeV.

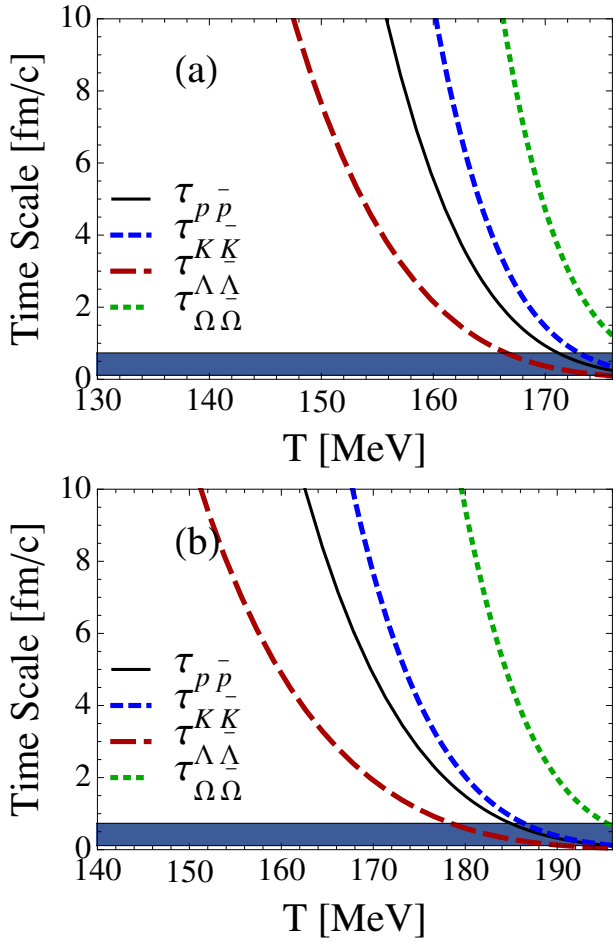

Figure 3.2: Comparison of the chemical equilibrium times for p's, K's, Λ's, and Ω's when $\alpha = 1$ and $\beta_i = 1$ where (a) $T_H = 176$ MeV and (b) $T_H = 196$ MeV. The gray band is the range of chemical equilibrium times for the Hagedorn states (see Tab. 3.1).

3.1.2 Hagedorn States, Pions, and $X\bar{X}$ Pairs

We first estimate the chemical equilibration time of the $X\bar{X}$ by looking at the $X\bar{X}$ rate equation in Eq. (2.5), when both the pions and Hagedorn states are held constant. Then we will hold the pions constant and allow all the $X\bar{X}$ pairs and Hagedorn states to equilibrate. Finally, we hold the Hagedorn states constant and allow all the $X\bar{X}$ pairs and pions to equilibrate.

Hagedorn States and Pions held Constant

Returning to Eq. (2.4), we first hold both the Hageodorn states and pions constant at β_i and α, respectively. That means that we set $N_i = \beta_i$ and $N_\pi = \alpha$ in Eq. (2.4) and solve for $N_{X\bar{X}}$. We must also assume that $\alpha \neq 0$ because we will need to divide by α. The $X\bar{X}$ rate equation then

becomes

$$\dot{\lambda}_{X\bar{X}} = \sum_i \Gamma_{i,X\bar{X}} \frac{N_i^{eq}}{N_{X\bar{X}}^{eq}} \left(\beta_i - \alpha^{\langle n_x \rangle} \lambda_{X\bar{X}}^2\right), \tag{3.5}$$

which we can integrate

$$\lambda_{X\bar{X}} = \zeta \left[\frac{\left(\frac{\phi+\zeta}{\phi-\zeta}\right) e^{\frac{2t}{\tau_{X\bar{X}}}} + 1}{\left(\frac{\phi+\zeta}{\phi-\zeta}\right) e^{\frac{2t}{\tau_{X\bar{X}}}} - 1} \right] \tag{3.6}$$

where

$$\tau_{X\bar{X}} \equiv \frac{N_{X\bar{X}}^{eq}}{\sqrt{\sum_i \Gamma_{i,X\bar{X}} N_i^{eq} \beta_i} \sqrt{\sum_i \Gamma_{i,X\bar{X}} N_i^{eq} \alpha^{\langle n_x \rangle}}}, \tag{3.7}$$

$\zeta \equiv \sqrt{\frac{\sum_i \Gamma_{i,X\bar{X}} N_i^{eq} \beta_i}{\sum_i \Gamma_{i,X\bar{X}} N_i^{eq} \alpha^{\langle n_x \rangle}}}$, and $\lambda_{X\bar{X}}(0) \equiv \phi$. Substituting in $\alpha = 1$ and $\beta_i = 1$ when the pions and Hagedorn states are in chemical equilibrium, we rederive Eq. (7) in Ref. [58]

$$\tau_{X\bar{X}} = \frac{N_{X\bar{X}}^{eq}}{\sum_i \Gamma_{i,X\bar{X}} N_i^{eq}}, \tag{3.8}$$

which is shown in Fig. 3.2. From Eq. (3.8) we see that the time scale has an indirect dependence on the decay width. Since the decay width has a linear dependence on the mass, the time scale decreases when more Hagedorn states are included. However, N_i^{eq} also decreases with increasing mass so above a certain point very many Hagedorn states need to be included in order to see an effect in the time scale. Furthermore, the chemical equilibrium values have a dependence on the temperature, which makes the time scale shortest for the highest temperatures.

In Fig. 3.3 and Fig. 3.4 we hold the Hagedorn states and pions and let the $X\bar{X}$ pairs reach chemical equilibrium. That means that in Eq. (2.4) we set $N_\pi = N_\pi^{eq}$ and $N_i = N_i^{eq}$ in the $\dot{N}_{X\bar{X}}$ equation. Fig. 3.3 shows the results for $p\bar{p}$, $K\bar{K}$, and $\Lambda\bar{\Lambda}$, respectively, for $T_H = 176$ MeV and Fig. 3.4 shows the same for $T_H = 196$ MeV. In all cases the temperature is held constant while the rate equations are solved over time. At $T = T_c$ all $X\bar{X}$ reach chemical equilibrium almost immediately (on the order of $t < 0.2 fm/c$). As T is decreased the chemical equilibrium time obviously increases, which is clear from Fig. 3.2.

Even as the temperature is lowered we still see quick chemical equilibrium times. For the $p\bar{p}$ and $\Lambda\bar{\Lambda}$ pairs at $T = 0.9T_c$ the chemical equilibrium time is still about $t < 1 fm/c$. The $K\bar{K}$ pairs do have a slower chemical equilibrium time due to their larger chemical equilibrium abundances, which is directly related to the chemical equilibration time through Eq. (2.4). This again represents the main idea, which is the importance of potential Hagedorn states in understanding fast chemical equilibration of hadrons close and below T_c. The Hagedorn states increase dramatically in number close to the critical temperature and, thus, by its subsequent decay and re-population they will quickly produce the various hadronic particles.

The equilibration of $X\bar{X}$ pairs then shown in Fig. 3.3 and Fig. 3.4 where the analytical result in Eq. (3.6) matches the numerical result exactly. From Fig. 3.3 and Fig. 3.4 it can be seen that all $X\bar{X}$ pairs equilibrate quickly close to the critical temperature $\tau < 1\frac{fm}{c}$. Clearly, though, as the temperature decreases the chemical equilibration time lengthens. However, at $T_H = 196$ MeV chemical equilibrium is still reached quickly, $\tau < 1\frac{fm}{c}$.

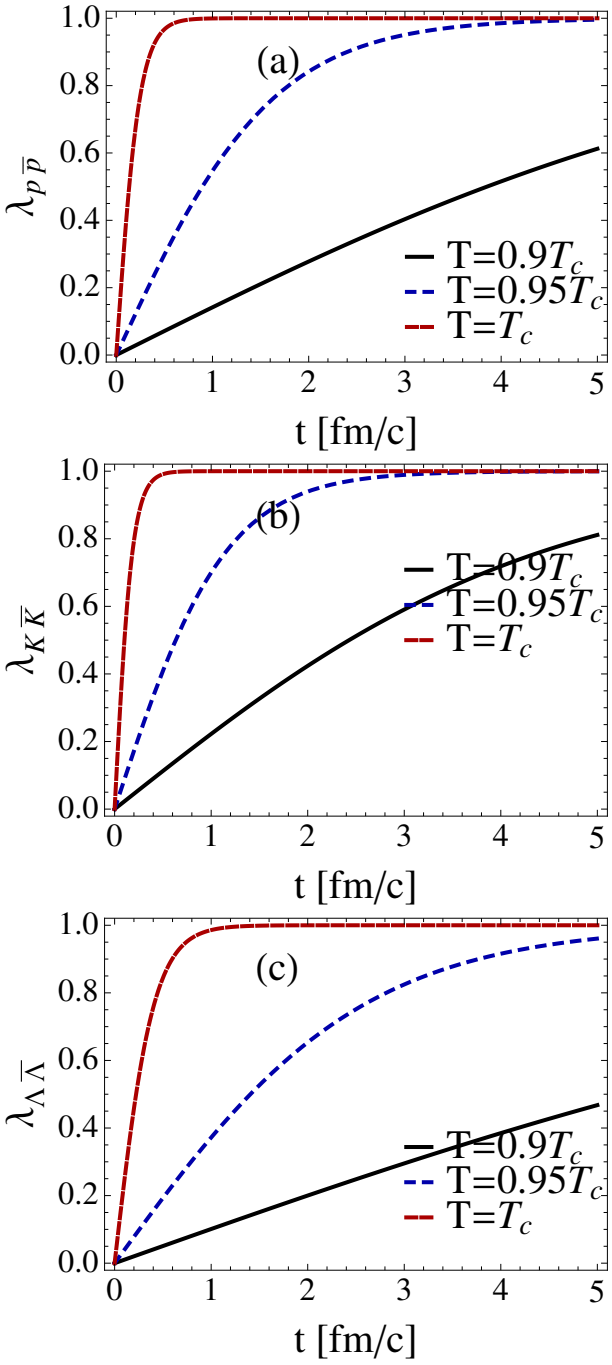

Figure 3.3: Graph of the number of proton anti-proton pairs, kaon anti-kaon pairs, and lambda anti-lambda pairs when both the resonances and pions are held in equilibrium for $T_H = 176$ MeV.

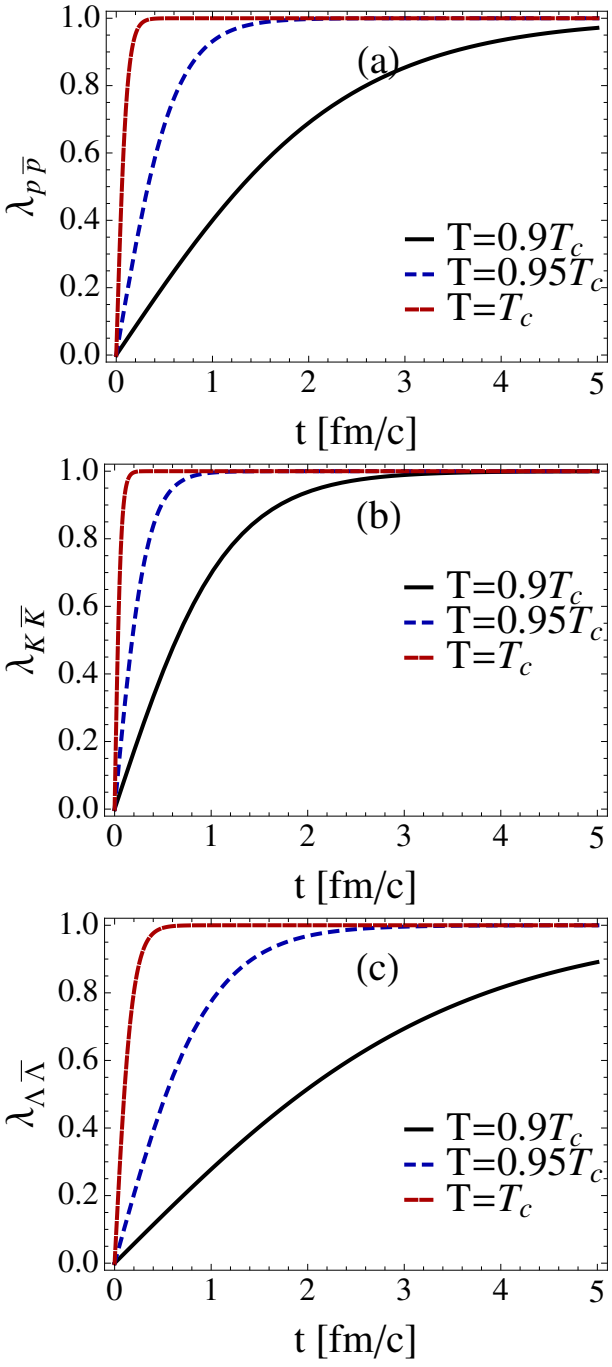

Figure 3.4: Graph of the number of proton anti-proton pairs, kaon anti-kaon pairs, and lambda anti-lambda when both the resonances and pions are held in equilibrium for $T_H = 196$ MeV.

If $\alpha = 0$ Eq. (3.6) is no longer valid because $\tau_{X\bar{X}}$ requires dividing by α. Instead we return to Eq. (3.5) and substitute in $\alpha = 0$

$$\dot{\lambda}_{X\bar{X}} = \sum_i \Gamma_{i,X\bar{X}} \frac{N_i^{eq}}{N_{X\bar{X}}^{eq}} \beta_i, \tag{3.9}$$

which has practically the same form as Eq. (D.6). After integration

$$\lambda_{X\bar{X}} = \left(\frac{t}{\tau_{X\bar{X}}^{\beta}} + \phi \right) \tag{3.10}$$

where

$$\tau_{X\bar{X}}^{\beta} = \frac{N_{X\bar{X}}^{eq}}{\sum_i \Gamma_{i,X\bar{X}} N_i^{eq} \beta_i} \, . \tag{3.11}$$

Pions held constant

When the pions are held constant at α

$$\begin{aligned} \dot{\lambda}_{X\bar{X}} &= \sum_i \Gamma_{i,X\bar{X}} \frac{N_i^{eq}}{N_{X\bar{X}}^{eq}} \left(\lambda_i - \alpha^{\langle n_x \rangle} \lambda_{X\bar{X}}^2 \right) \\ \dot{\lambda}_i &= \Gamma_{i,\pi} \left(\langle \alpha^n \rangle - \lambda_i \right) + \Gamma_{i,X\bar{X}} \left(\alpha^{\langle n_x \rangle} \lambda_{X\bar{X}}^2 - \lambda_i \right). \end{aligned} \tag{3.12}$$

Assuming that the resonances start at $\beta_i \approx 0$ the $X\bar{X}$ equation becomes

$$\begin{aligned} \dot{\lambda}_{X\bar{X}} &= -\sum_i \Gamma_{i,X\bar{X}} \frac{N_i^{eq}}{N_{X\bar{X}}^{eq}} \alpha^{\langle n_x \rangle} \lambda_{X\bar{X}}^2 \\ \lambda_{X\bar{X}} &= \frac{\phi}{\frac{\phi t}{\tau_{X\bar{X}}^{\alpha}} + 1} \end{aligned} \tag{3.13}$$

where

$$\tau_{X\bar{X}}^{\alpha} = \frac{N_{X\bar{X}}^{eq}}{\sum_i \Gamma_{i,X\bar{X}} N_i^{eq} \alpha^{\langle n_x \rangle}} \, . \tag{3.14}$$

Then the resonance equations becomes

$$\begin{aligned} \dot{\lambda}_i &= \Gamma_{i,\pi} \langle \alpha^n \rangle + \Gamma_{i,X\bar{X}} \alpha^{\langle n_x \rangle} \left(\frac{\phi}{\frac{\phi t}{\tau_{X\bar{X}}^{\alpha}} + 1} \right)^2 \\ \lambda_i &= \frac{t}{\tau_i^{\alpha}} + \Gamma_{i,X\bar{X}} \alpha^{\langle n_x \rangle} \phi \tau_{X\bar{X}}^{\alpha} \left(1 - \frac{1}{\frac{\phi t}{\tau_{X\bar{X}}^{\alpha}} + 1} \right) + \beta_i \end{aligned} \tag{3.15}$$

where $\tau_i^{\alpha} = \frac{1}{\Gamma_{i,\pi} \langle \alpha^n \rangle}$, which explains the longer time scales we see with the addition of $X\bar{X}$ pairs. The results for the pions held constant for $p\bar{p}$ pairs for $T_H = 196$ MeV can be seen in Fig. 3.5.

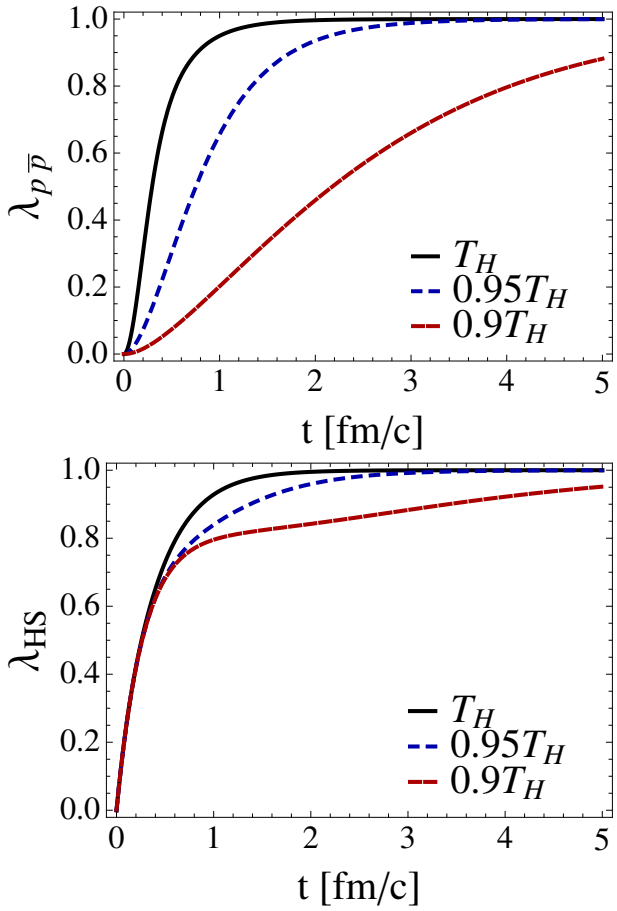

Figure 3.5: $p\bar{p}$ pair results for $\alpha = 1$, $\beta_i = 0$, and $\phi = 0$ when the pions are held in equilibrium.

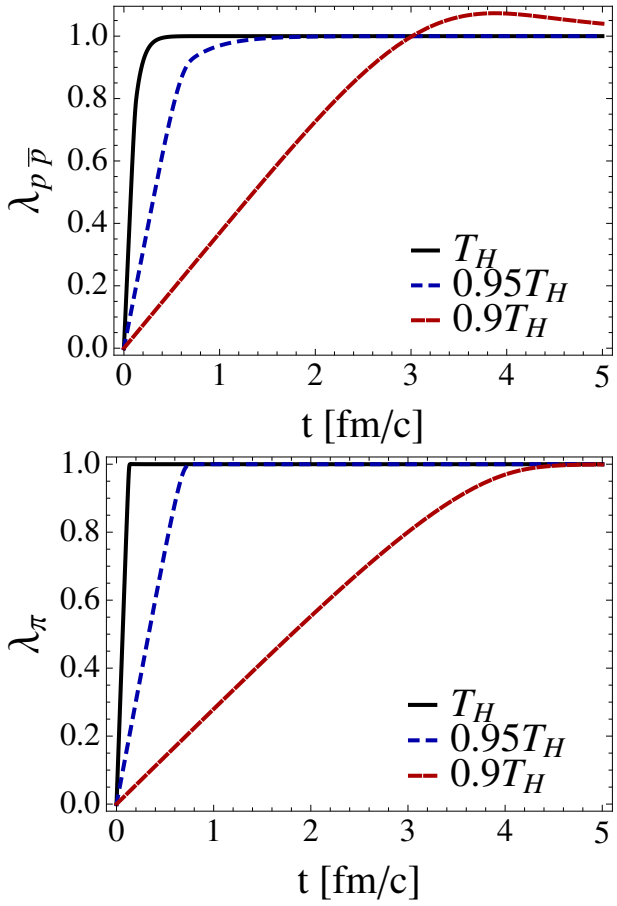

Figure 3.6: $p\bar{p}$ pair results for $\alpha = 0$, $\beta_i = 1$, and $\phi = 0$ when the Hagedorn resonances are held in equilibrium.

Hagedorn states held constant

When the resonances are held constant at β_i

$$\begin{aligned}\dot{\lambda}_\pi &= \sum_i \Gamma_{i,\pi}\frac{N_i^{eq}}{N_\pi^{eq}}\left(\beta_i\langle n\rangle - \sum_n B_{i,n} n \lambda_\pi^n\right) + \sum_i \Gamma_{i,X\bar{X}}\langle n_x\rangle \frac{N_i^{eq}}{N_\pi^{eq}}\left(\beta_i - \lambda_\pi^{\langle n_x\rangle}\lambda_{X\bar{X}}^2\right)\\ \dot{\lambda}_{X\bar{X}} &= \sum_i \Gamma_{i,X\bar{X}}\frac{N_i^{eq}}{N_{X\bar{X}}^{eq}}\left(\beta_i - \lambda_\pi^{\langle n_x\rangle}\lambda_{X\bar{X}}^2\right). \end{aligned} \tag{3.16}$$

To solve Eq. (3.16) analytically we need to consider first the case when both the $X\bar{X}$ and pions start roughly at zero. Then we can rewrite Eq. (3.16) as

$$\begin{aligned}\dot{\lambda}_\pi &= \sum_i \Gamma_{i,\pi}\frac{N_i^{eq}}{N_\pi^{eq}}\beta_i\langle n\rangle + \sum_i \Gamma_{i,X\bar{X}}\langle n_x\rangle \frac{N_i^{eq}}{N_\pi^{eq}}\beta_i\\ \dot{\lambda}_{X\bar{X}} &= \sum_i \Gamma_{i,X\bar{X}}\frac{N_i^{eq}}{N_{X\bar{X}}^{eq}}\beta_i, \end{aligned} \tag{3.17}$$

which after integration gives

$$\begin{aligned}\lambda_\pi &= \frac{t}{\tau_{\pi,b}^0} + \alpha\\ \lambda_{X\bar{X}} &= \frac{t}{\tau_{X\bar{X}}^\beta} + \phi \end{aligned} \tag{3.18}$$

where

$$\tau_{\pi,x}^0 = \frac{N_\pi^{eq}}{\sum_i \Gamma_{i,\pi} N_i^{eq}\beta_i\langle n\rangle + \sum_i \Gamma_{i,X\bar{X}} N_i^{eq}\beta_i\langle n_x\rangle}. \tag{3.19}$$

Incidentally, Eq. (3.18) for the $X\bar{X}$ pairs is identical to Eq. (3.10). This is because the pions and resonances do not affect each other in the earliest stage of their equilibration.

Once the pions and $X\bar{X}$ pairs near equilibrium we need to rewrite our rate equations. Unlike before where we said that the pions treated the resonances as if they were constant and then later we substituted in the pion equation into the resonance equation, here both the pions and $X\bar{X}$ pairs see each other as constant. Thus, in order to solve the pion and $X\bar{X}$ pair rate equations we hold the other constant and solve it analytically. Since the pions are near their equilibrium value we can once again use $\lambda_\pi = 1 - \epsilon$, which gives the pion rate equation

$$\begin{aligned}\epsilon &= -\sum_i \Gamma_{i,\pi}\frac{N_i^{eq}}{N_\pi^{eq}}\langle n\rangle\left(\beta_i - 1\right) - \sum_i \Gamma_{i,X\bar{X}}\langle n_x\rangle\frac{N_i^{eq}}{N_\pi^{eq}}\left(\beta_i - 1\right)\\ &- \left[\sum_i \Gamma_{i,\pi}\frac{N_i^{eq}}{N_\pi^{eq}}\langle n^2\rangle - \sum_i \Gamma_{i,X\bar{X}}\frac{N_i^{eq}}{N_\pi^{eq}}\langle n_x\rangle^2\lambda_{X\bar{X}}^2(t_o)\right]\epsilon\,. \end{aligned} \tag{3.20}$$

Following integration

$$\lambda_\pi = 1 + \gamma_x + (\eta - 1 - \gamma_x)\, e^{-\frac{t-t_0}{\tau_{\pi,b}}} \tag{3.21}$$

where

$$\begin{aligned}\tau_{\pi,b} &= \frac{N_\pi^{eq}}{\sum_i \Gamma_{i,\pi} N_i^{eq}\langle n^2\rangle - \sum_i \Gamma_{i,X\bar{X}} N_i^{eq}\langle n_x\rangle^2 \lambda_{X\bar{X}}^2(t_o)} \\ \gamma_x &= \frac{\sum_i \Gamma_{i,\pi} N_i^{eq}\langle n\rangle\,(\beta_i - 1) - \sum_i \Gamma_{i,X\bar{X}}\langle n_x\rangle N_i^{eq}\,(\beta_i - 1)}{\sum_i \Gamma_{i,\pi} N_i^{eq}\langle n^2\rangle - \sum_i \Gamma_{i,X\bar{X}} N_i^{eq}\langle n_x\rangle^2 \lambda_{X\bar{X}}^2(t_o)}\,. \end{aligned} \tag{3.22}$$

The $X\bar{X}$ pair equation is almost the same as in Eq. (3.6) except that we substitute in $\lambda_{X\bar{X}}(t_o)$ for ϕ and we assume that $\zeta = 1$ even though the pions are near equilibrium and not actually in equilibrium. If we do not take $\zeta = 1$ then the $X\bar{X}$ pairs can never reach equilibrium, thus, the assumption is necessary. The $X\bar{X}$ pair rate equation then becomes

$$\lambda_{X\bar{X}} = \left[\frac{\left(\frac{\lambda_{X\bar{X}}(t_o)+1}{\lambda_{X\bar{X}}(t_o)-1}\right) e^{\frac{2(t-t_0)}{\tau_{X\bar{X}}}} + 1}{\left(\frac{\lambda_{X\bar{X}}(t_o)+1}{\lambda_{X\bar{X}}(t_o)-1}\right) e^{\frac{2(t-t_0)}{\tau_{X\bar{X}}}} - 1}\right]\,. \tag{3.23}$$

The results for the Hagedorn states held constant for $p\bar{p}$ pairs for $T_H = 196$ MeV can be seen in Fig. 3.6.

At high temperatures i.e. $T > 170$ MeV are results change little from Figs. 3.3-3.4 for the $X\bar{X}$ pairs and Fig. 3.6 for the pions. It is only at low temperatures that we see a significant deviation from our original results in Fig. 3.3-3.4 and Fig. 3.6. This implies that if the resonances are in equilibrium that the pions and $X\bar{X}$ pairs treat each other as if they were in equilibrium. It is only at low temperatures that they affect each other, however, only indirectly.

3.1.3 All Particles Out of Equilibrium

When we allow the pions, Hagedorn resonances, and $X\bar{X}$ pairs to all equilibrate simultaneously we find results similar to that in Section 3.1.1. However, the individual time scales are slightly longer due to the addition of the $X\bar{X}$ pairs as shown in Fig. D.3b in Appendix D for a $p\bar{p}$ pair. The time scale for the pions and Hagedorn states are slightly longer when the $p\bar{p}$ pairs are present. The same goes for the estimated chemical equilibration time of the $p\bar{p}$ pairs in the previous section, $\tau_{p\bar{p}}$. We still have yet to find an analytical solution when the $X\bar{X}$ pairs are included. The addition of a $X\bar{X}$ pair complicates this task quite a bit compared to what we were previously able to do. Thus, we leave this as a problem for the future.

	$\alpha = \lambda_\pi(t_0)$	$\beta_i = \lambda_i(t_0)$	$\phi = \lambda_{X\bar{X}}(t_0)$
IC_1	1	1	0
IC_2	1	1	0.5
IC_3	1.1	0.5	0
IC_4	0.95	1.2	0

Table 3.2: Initial condition configurations, recalling Eq. (2.20)

3.2 Expanding Fireball

The details of our Bjorken expansion are already outlined in Sec. 2.1.5. Here we no longer use the fugacities, but rather we look at the total number of pions, Hagedorn states, and $X\bar{X}$ pairs as seen in Eq. (2.4). For the remainder of this work we include only results for an expanding fireball, which are solved numerically. As an initial test we hold both the pions and Hagedorn states in chemical equilibrium and allow just $X\bar{X}$ to equilibrate as seen in Fig. 3.7 and Fig. 3.8. The black solid line in each graph is the chemical equilibrium abundances and the colored lines are the dynamical calculations for various expansions that follow the $T(t)$ shown in Fig. 2.11. We see that regardless of our volume expansion they all quickly approach equilibrium. In Fig. 3.7 and Fig. 3.8 the $X\bar{X}$ all reach chemical equilibrium almost immediately, well before $0.9T_c$ the chemnical equilibration time is $< 1\frac{fm}{c}$. The only exception is the $K\bar{K}$ pairs for $T_H = 176$ MeV. However, we see later on that the K/π ratio matches the data.

More interestingly, we consider the case when the pions, Hagedorn states, and $X\bar{X}$ all are allowed to chemical equilibrate. We then vary the initial conditions and observe their effects. The results for $p\bar{p}$ pairs are shown in Fig. 3.9 and Fig. 3.10. In Fig. 3.9 and Fig. 3.10 we show the evolution of both the $p\bar{p}$ pairs and the pions for the reaction $n\pi \leftrightarrow HS \leftrightarrow n\pi + X\bar{X}$. Note that in all the following figures the effective numbers are shown so that the contribution of the Hagedorn states is included.

One can see that the chemical equilibration time does depend slightly on our choice of β_i, i.e., a larger β_i means a quicker chemical equilibration time. For instance, if the Hagedorn states were overpopulated coming out of the QGP phase than chemical equilibrium times would be slightly shorter. However, even when the Hagedorn resonances start underpopulated the $p\bar{p}$ pairs are able to reach chemical equilibrium immediately. Additionally, when the $p\bar{p}$ pairs start at about half their chemical equilibrium values, it only helps the $p\bar{p}$ pairs to reach equilibrium at a slightly higher temperature (on the order of a couple of MeV). Additionally, we see a greater dependence on β_i for $T_H = 176$ MeV than for $T_H = 196$ MeV. Throughout the evolution we see from the pions that they remain roughly in chemical equilibrium. Thus, our initial analytical approximation appears reasonable.

In Fig. 3.11 the ratio of p/π^+'s is shown. We also compare our results to that of experimental data. We see that for $T_H = 176$ MeV that our results enter the band of experimental data before $T = 170$ MeV and remain there throughout the entire expansion regardless of the initial conditions. However, for $T_H = 176$ MeV the results are slightly different. In this case, the ratios

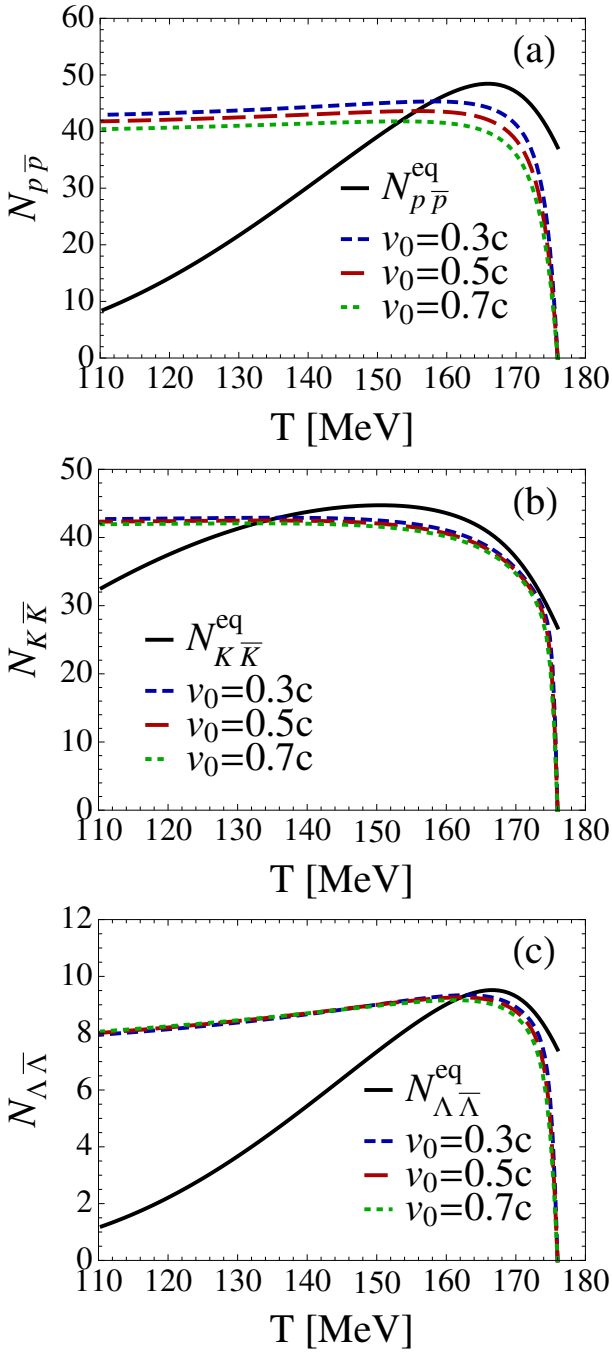

Figure 3.7: Results for the (a) $p\bar{p}$, (b) $K\bar{K}$, and (c) $\Lambda\bar{\Lambda}$ when the pions and Hagedorn resonances are held in equilibrium for $T_H = 176$ MeV.

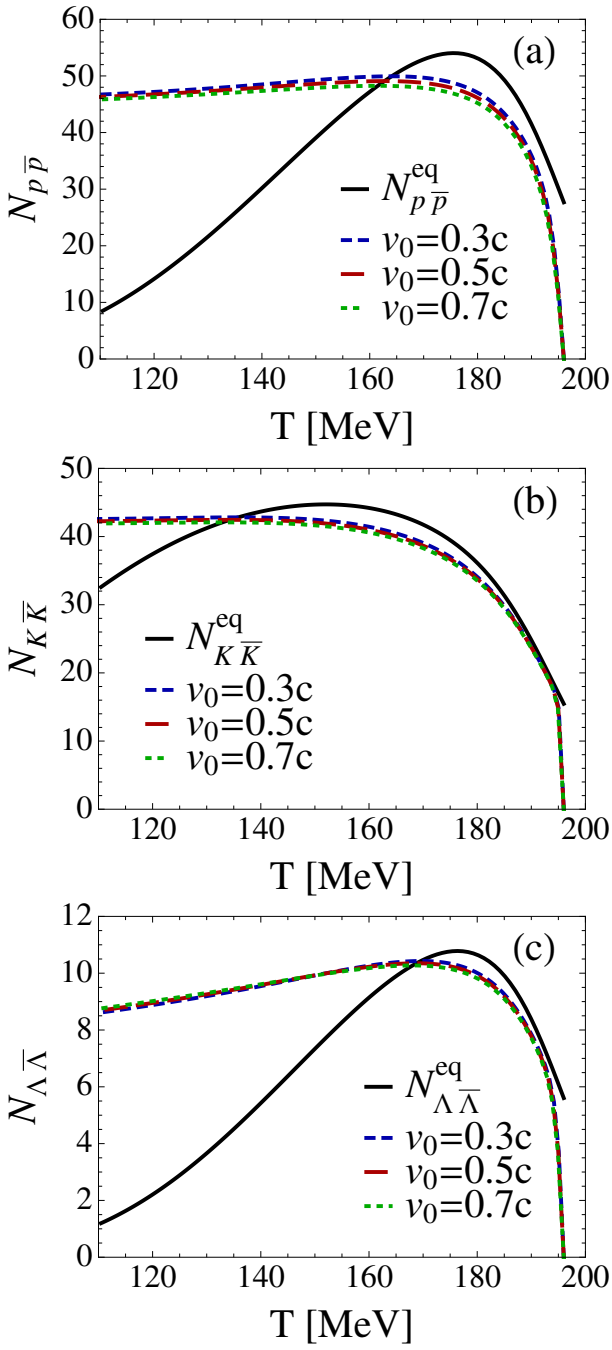

Figure 3.8: Results for the (a) $p\bar{p}$, (b) $K\bar{K}$, and (c) $\Lambda\bar{\Lambda}$ when the pions and Hagedorn resonances are held in equilibrium for $T_H = 196$ MeV.

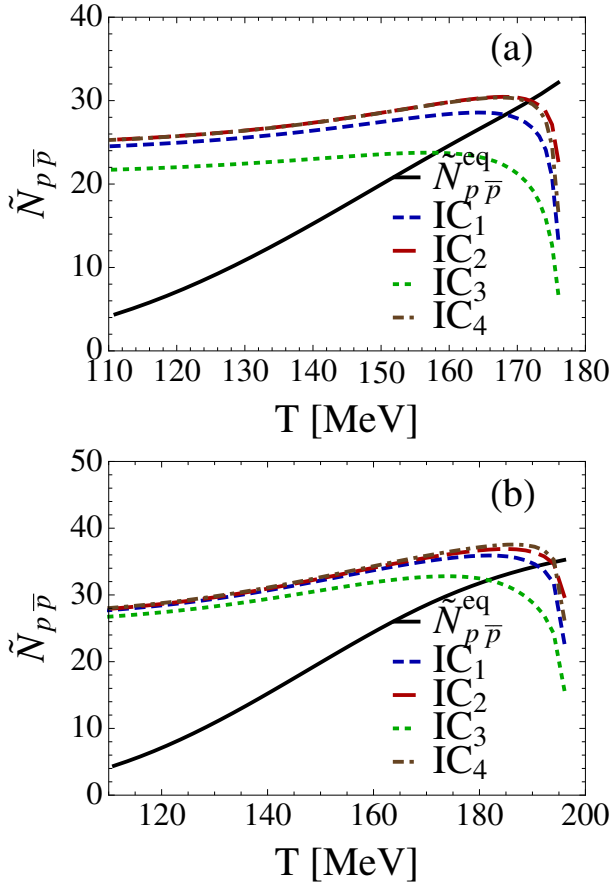

Figure 3.9: Results for the p's with various initial conditions for (a) $T_H = 176$ MeV and (b) $T_H = 196$ MeV.

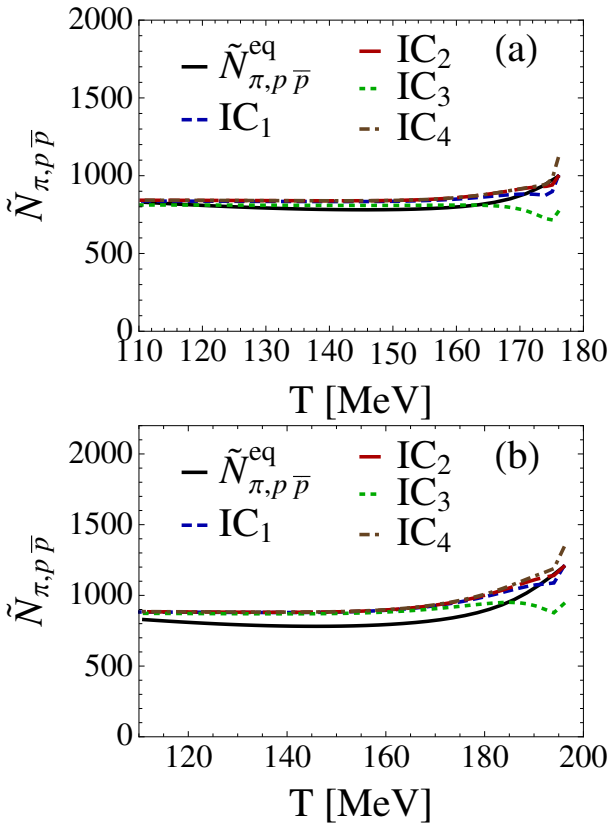

Figure 3.10: Results for the π's with various initial conditions for (a) $T_H = 176$ MeV and (b) $T_H = 196$ MeV.

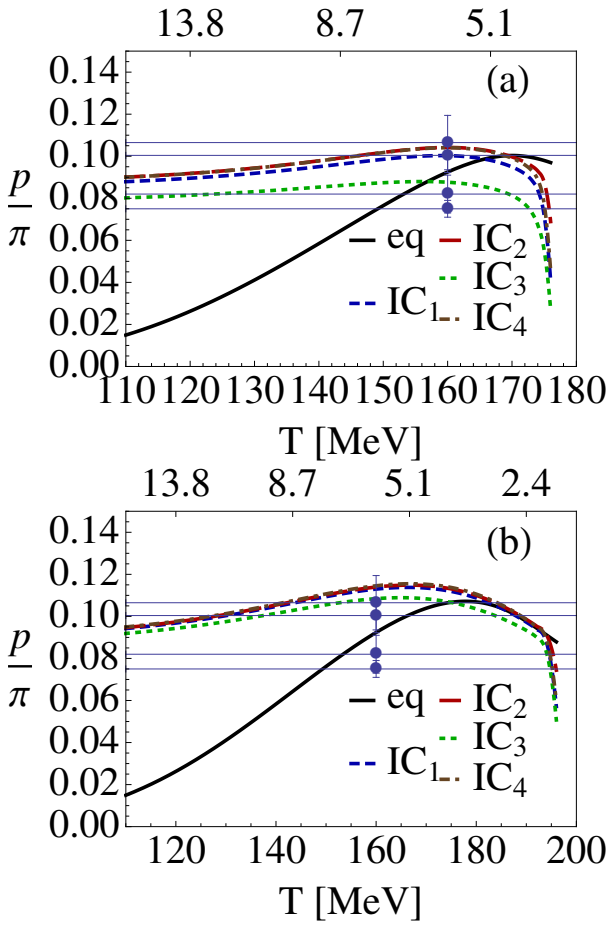

Figure 3.11: Results for the ratio of p/π^- with various initial conditions for (a) $T_H = 176$ MeV or (b) $T_H = 196$ MeV. Note that for STAR [5, 117] $p/\pi^-0.11$ and $\bar{p}/\pi^- = 0.082$ and for PHENIX [118] $p/\pi^-0.10$ (p/π^+ is actually measured but we convert it to p/π^- to match STAR) and $\bar{p}/\pi^- = 0.047$.

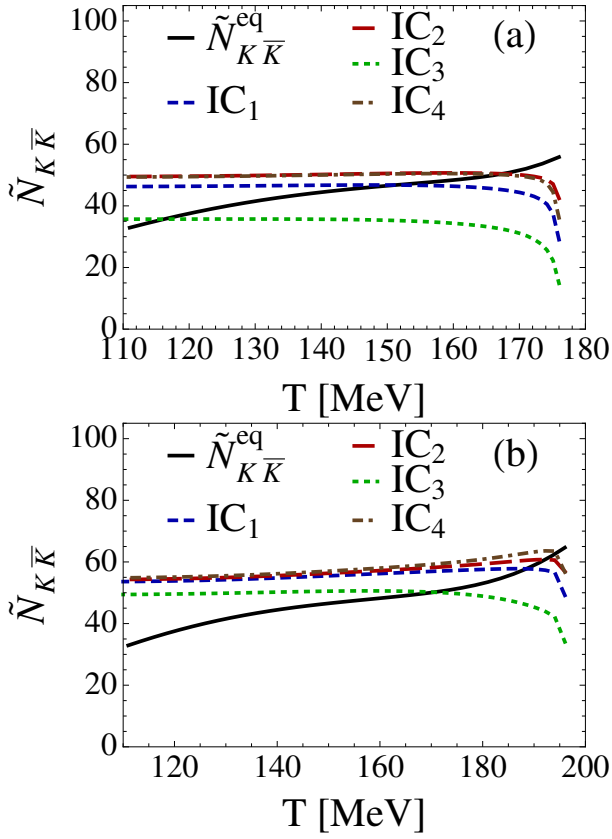

Figure 3.12: Results for the K's with various initial conditions for (a) $T_H = 176$ MeV and (b) $T_H = 196$ MeV.

match the experimental data early on at around $T = 190$ MeV. However, they become briefly overpopulated around $T = 160 - 170$ MeV but then quickly return to the experimental values, except for the case when we have the initial conditions such that the pions are overpopulated. This could imply that there are a few too many Hagedorn states and a fit for the Hagedorn states with a lower A (degeneracy of the Hagedorn states) may produce better results.

As with the protons, the total number of kaons are also slightly dependent on our chosen initial conditions, more specifically, our choice in β_i. In Fig. 3.12 and Fig. 3.13 the temperature of the evolving system after the phase transition at which chemical equilibrium among standard hadrons is basically reached and maintained is between $T = 160 - 170$ for $T_H = 176$ MeV and they have also already reached chemical equilibrium by $T = 170$ for $T_H = 196$ MeV, below which the Hagedorn states basically die out. The one exception is when the Hagedorn states begin underpopulated i.e. that $\beta_i < 1$. In this case, the kaon pairs take longer to reach chemical equilibrium. However, when we look at K/π in Fig. 3.14, lower β_i actually fits the data better.

Moreover, the pions again remain roughly at chemical equilibrium throughout the expansion as seen in Fig. 3.12 and Fig. 3.13 . While the pion graphs look roughly similar in Figs. 3.9-3.13, they are not. The difference is how the pions are affected in the presence of a $p\bar{p}$ pair compared

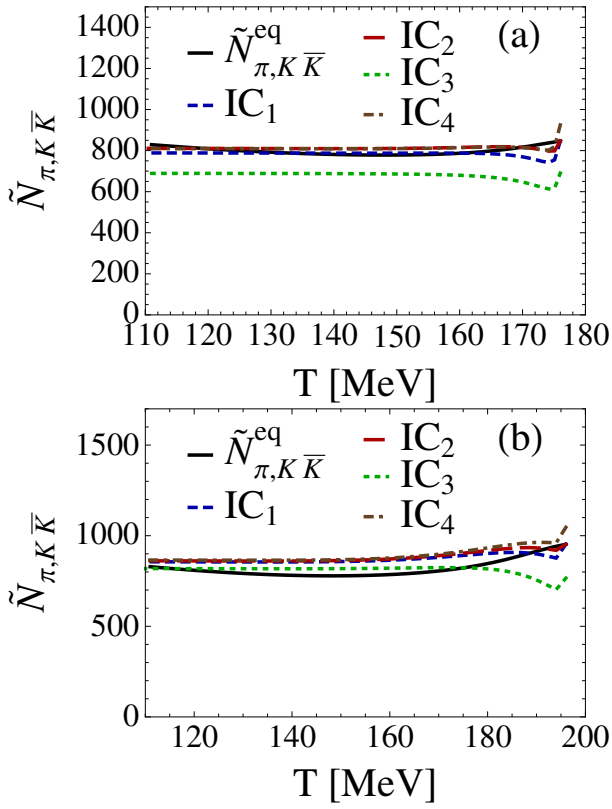

Figure 3.13: Results for the π's with various initial conditions for (a) $T_H = 176$ MeV and (b) $T_H = 196$ MeV.

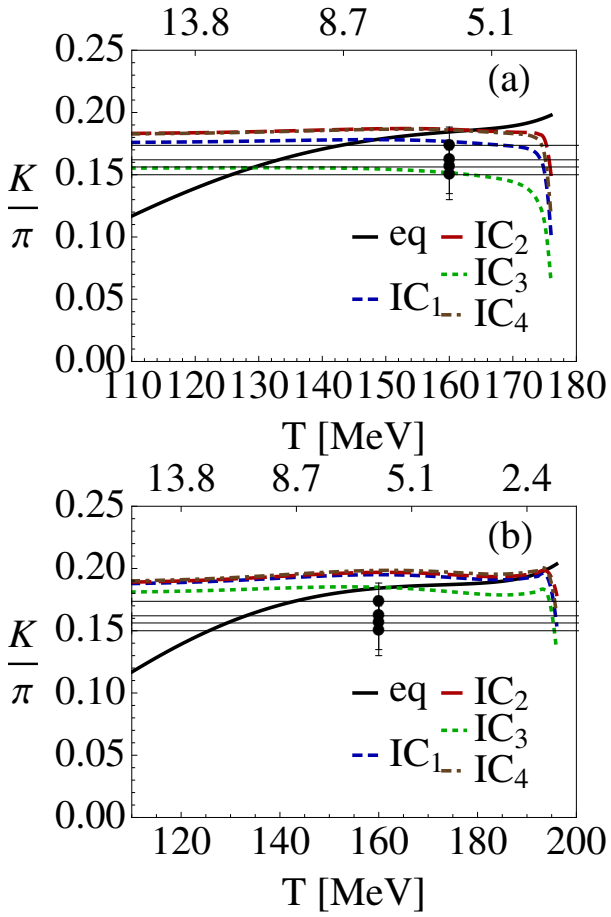

Figure 3.14: Results for the ratio of K^+/π^- with various initial conditions for (a) $T_H = 176$ MeV or (b) $T_H = 196$ MeV. Note that for STAR [5, 117] $K^+/\pi^- = 0.16$ and $K^-/\pi^- = 0.15$ and for PHENIX [118] $K/\pi^-0.174$ (K/π^+ is actually measured but we convert it to K/π^- to match STAR) and $\bar{K}/\pi^- = 0.162$.

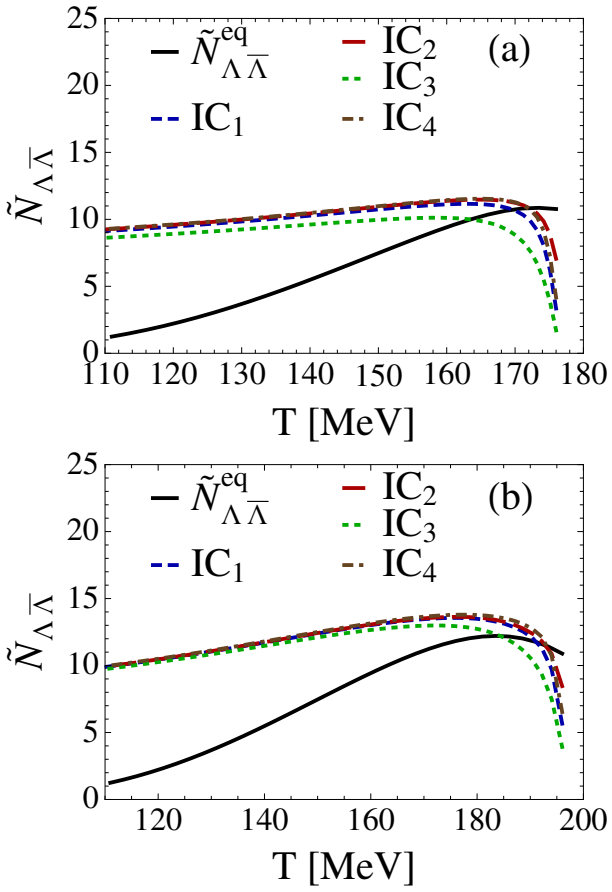

Figure 3.15: Results for the Λ's with various initial conditions for (a) $T_H = 176$ MeV and (b) $T_H = 196$ MeV.

to a decay that includes a kaon anti-kaon pair.

In Fig. 3.14 the ratio of kaons to pions is shown for $T_H = 176$ MeV and for $T_H = 196$ MeV. For $T_H = 176$ MeV our results are roughly at the upper edge of the experimental values. However, for $T_H = 196$ MeV our results are slightly higher than the experimental values. Although, the results at $T = 110$ MeV are almost exactly those of the uppermost experimental data point.

We can also observe the effects of the expansion on the $\Lambda\bar{\Lambda}$ pairs as seen in Fig. 3.15 and Fig. 3.16. We see that both reach the experimental values almost immediately ($T > 170$ for $T_H = 176$ MeV and around $T = 190$ for $T_H = 196$ MeV). The one exception is again for an underpopulation of Hagedorn states, which reaches chemical equilibrium at $T \approx 165$ for $T_H = 176$ MeV and already by $T = 170$ for $T_H = 196$ MeV).

The ratio of Λ/π's is shown in Fig. 3.17. In both cases the Λ/π's match the experimental values extremely well. For $T_H = 176$ MeV our results reach the equilibrium values at $T \approx 170$ MeV and for $T_H = 196$ MeV the experimental values are reached already by $T \approx 170$ MeV.

A summary graph of all our results is shown in Fig. 3.18. The gray error bars cover the range of error for the experimental data points from both STAR [5, 117] and PHENIX [118].

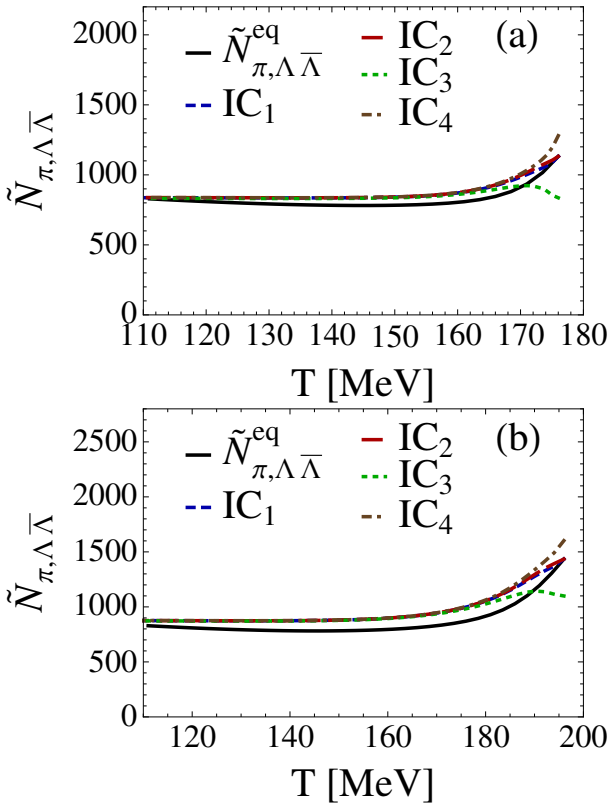

Figure 3.16: Results for the π's with various initial conditions for (a) $T_H = 176$ MeV and (b) $T_H = 196$ MeV.

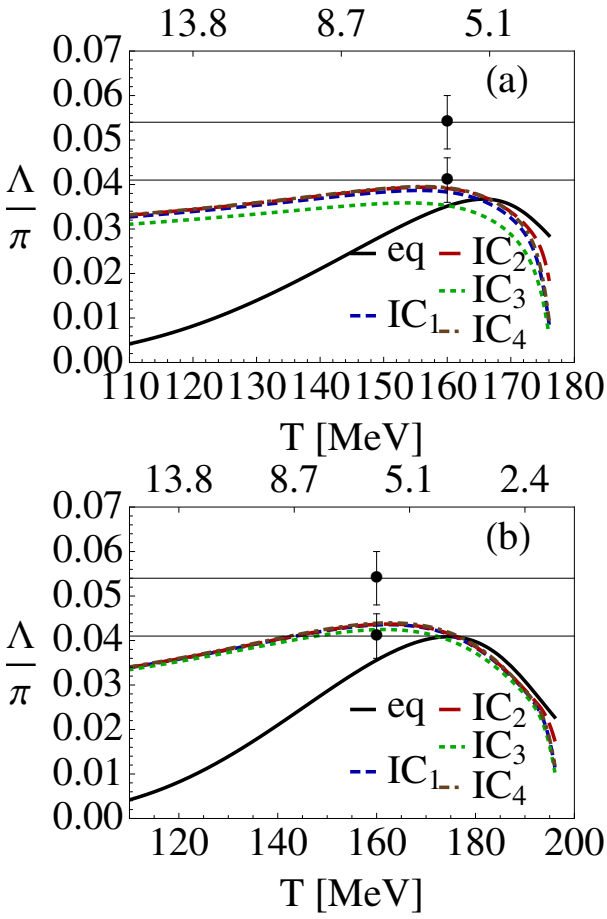

Figure 3.17: Results for the ratio of Λ/π^-'s with various initial conditions for (a) $T_H = 176$ MeV or (b) $T_H = 196$ MeV. Note that for STAR [5, 117] $\Lambda/\pi^- = 0.54$ and $\bar{\Lambda}/\pi^- = 0.41$ and Λ/π is not measured for PHENIX.

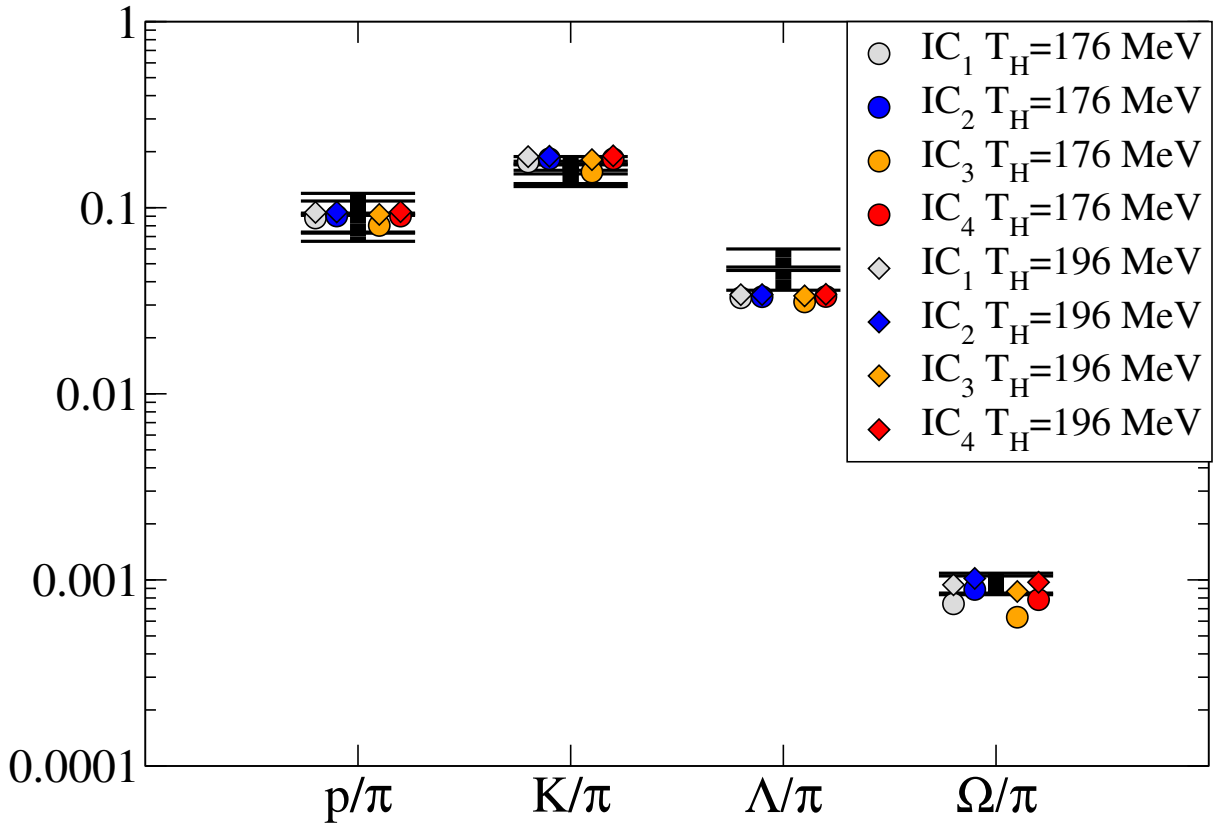

Figure 3.18: Plot of the various ratios including all initial conditions defined in Tab. 3.2. The points show the ratios at $T = 110$ MeV for the various initial conditions (circles are for $T_H = 176$ MeV and diamonds are for $T_H = 196$ MeV). The experimental results for STAR [5, 117] and PHENIX [118] are shown by the gray error bars.

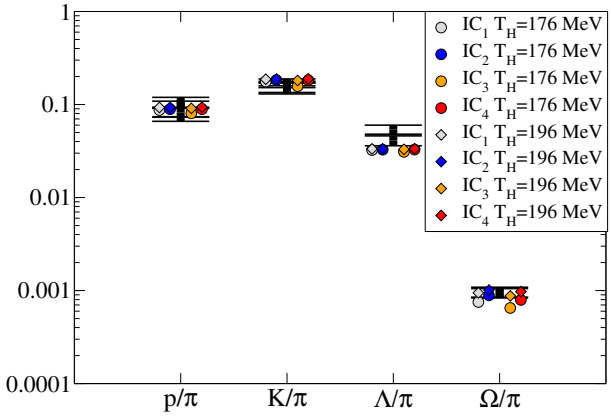

Figure 3.19: Plot is identical to Fig. 3.18, however, Γ_i^{hi} from Eq. (2.14) is used.

The points show the range in values for the various initial conditions at $T = 110$ MeV. We see in our graph that our freezeout results match the experimental data well.

What the graphs in Figs. 3.9-3.17 show us is that a dynamical scenario is able to explain chemical equilibration values that appear in thermal fits by $T = 160$ MeV. In general, $T_H = 176$ MeV and $T_H = 196$ give chemical freeze-out values in the range between $T = 160 - 170$ MeV. These results agree well with the chemical freeze-out temperature found in [63].

Moreover, the initial conditions have little effect on the ratios and give a range in the chemical equilibrium temperature of about ~ 5 MeV, which implies that information from the QGP regarding multiplicities is washed out due to the rapid dynamics of Hagedorn states. Lower β_i does slow the chemical equilibrium time slightly. However, as seen in Fig. 3.18 they still fit well within the experimental values. Furthermore, in [58] we showed the the initial condition play pretty much no role whatsoever in the ratios of K/π^+ and $(B + \bar{B})/\pi^+$, thus, strengthening our argument that the dynamics are washed out following the QGP.

While the variance in the chemical equilibration time arising from the initial conditions may seem contradictory to the K/π^+ and $(B + \bar{B})/\pi^+$ ratios in [58], it can be explained with the pion populations. In Figs. 3.9-3.13 quicker chemical equilibration times and, thus, larger total baryon/kaon numbers translated into a larger number of pions in the system. Thus, the K/π^+ and $(B + \bar{B})/\pi^+$ ratios do not depend on the initial conditions.

3.2.1 Dependence on Decay Width

Up until this point we have used a decay width dependence on the mass, which was calculated using the light hadrons from the particle data book [65] as shown in Fig. 2.8. It is clear to see in Fig. 2.8 that the decay widths do not follow a very consistent behvior. Thus, it is important to also look at the effects of changing the decay on the final particle ratios. At first we see if the upper and lower bounds that we found on the decay widths have any affect. In Fig. 3.19 and Fig. 3.20 we see that the bounds of the decay with, which were dependent on the upper/lower bounds of the the measured particle decay widths do not have a significant effect on the final state of the particle ratios.

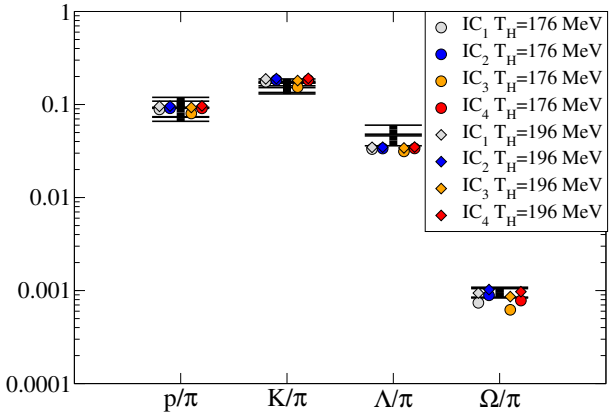

Figure 3.20: Plot is identical to Fig. 3.18, however, the lower bound of the Γ_i^{lo} from Eq. (2.13) is used.

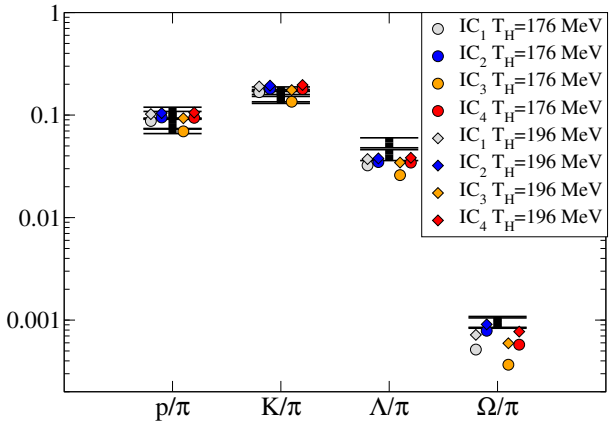

Figure 3.21: Plot is identical to Fig. 3.18, however, the decay widths are divided in half.

To further investiage the dependence on the decay width when return to Γ_i in Eq. (2.12) be we see what happens, if one were to divide the decay width in half $\Gamma_i' \equiv \Gamma_i/2$. We find that the particle ratios still match surprisingly well as seen in Fig. 3.21. The same can be said if we take $\Gamma_i' \equiv \Gamma_i/4$ as seen in Fig. 3.22.

In Fig. 3.21 the p/π's, K/π's, and Λ/π's all still fit within the experimental data points wheras the Ω/π's are below the experimental data. This indiciates that (with the exception of the Ω/π's) there is still a significant amount of leeway for the decay widths. Furthermore, if the decays widths are in turn divided by a fourth than the p/π's and K/π's match the experimental data points well still. However, the Λ/π's are somewhat below the experimental data points (especially for $T_H = 176$ MeV) and the Ω/π's are substantially underpopulated. If it turns out that we overperdict the decay widths in this paper and they are significantly smaller this could imply that strange baryons (and multi-strange baryons) require decays from strange and/or baryonic Hagedorn states and that non-strange, mesonic Hagedorn states alone are not enough to populate them.

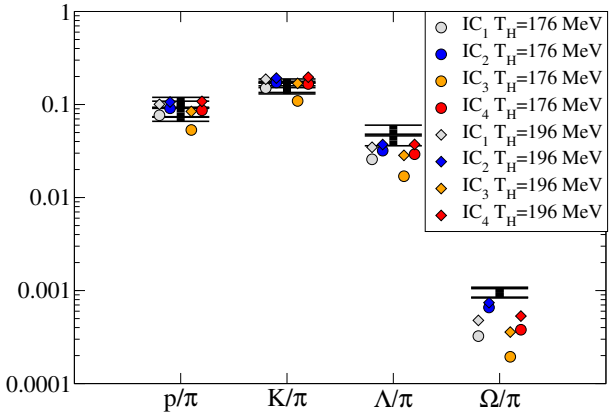

Figure 3.22: Plot is identical to Fig. 3.18, however, the decay widths are divided in fourth.

3.3 Production of $\Omega\bar{\Omega}$

We can also use our model to investigate the possibility of Ω's. In [44], they discussed the possibility of Ω's being produced from the following decay channels:

$$\begin{aligned} HS &\leftrightarrow \Omega\bar{\Omega} + X \\ HS\,(sss\bar{q}\bar{q}\bar{q}) &\leftrightarrow \Omega + \bar{B} + X \\ HS_B(sss) &\leftrightarrow \Omega + X. \end{aligned} \tag{3.24}$$

The first decay channel of a mesonic non-strange Hagedorn state we can implement straightforwardly with our model by employing the canonical branching ratio via Fig. 2.9. The results are shown in Fig. 3.23 for $T_H = 176$ MeV, in Fig. 3.24 for $T_H = 196$ MeV, and the Ω/π ratio is shown in Fig. 3.25. We are able to find the average number of Ω's using a canonical model as seen in Fig. 2.9. We see that, using only the first reaction, we are still impressively able to adequately populate the $\Omega\bar{\Omega}$ pairs so that they roughly match the experimental data. On the other hand, from Fig. 3.2 we see that for the Ω particle the equilibration time is short only very close to T_c. The scenario is thus more delicate. If one would take, for example, one half the decay width of that of Eq. 2.12 as seen in Fig. 3.21, or one fourth of the decay width as in Fig. 3.22, the total production of Ω is not sufficient up to 25 %, or up to 50%, respectively, to meet the experimental yield (the other ratios are not significantly affected by such a change of the decay width).

In a future work, it would be interesting to observe the other decay channels as given in Eq. 3.24 and advertised in [44]. The second reaction includes a mesonic, three times strange Hagedorn state whereas the third decay channel includes a baryonic, strange Hagedorn state. Both states are much more likely to directly decay into a Ω. These are, admittedly, exotic states, but should also occur in the spirit of Hagedorn states. In order to observe these decay channels a method, e.g. a microscopic quark model, must be found to find the appropriate Hagedorn spectrum for strange mesonic/baryonic Hagedorn states.

In [81] a canonical model was used in order to calculate branching ratios, more specifically, the average number of baryons and mesons that a single Hagedorn state could decay into. One

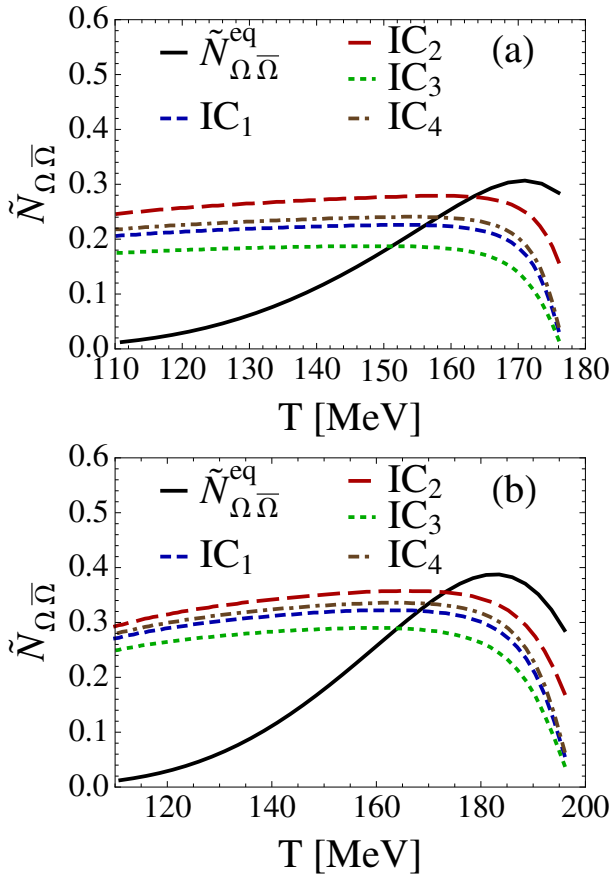

Figure 3.23: Results for the Ω's with various initial conditions for (a) $T_H = 176$ MeV and (b) $T_H = 196$ MeV.

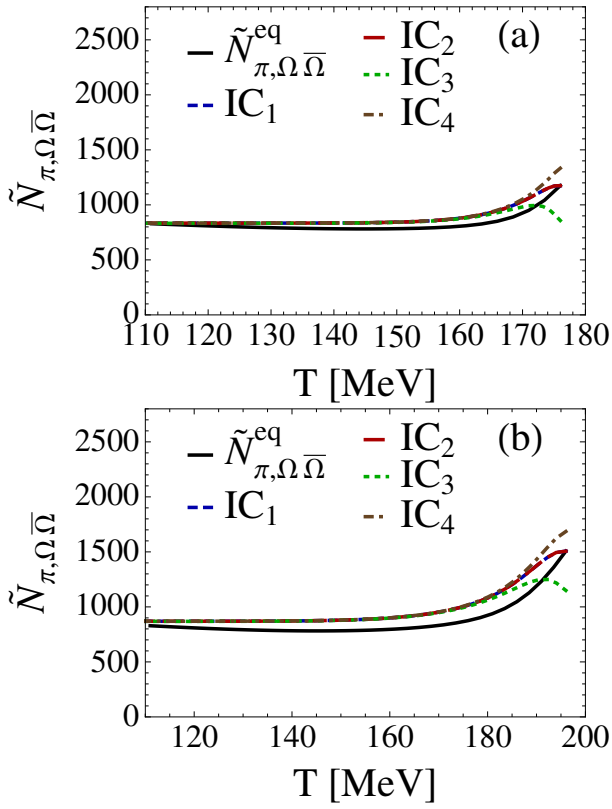

Figure 3.24: Results for the π's with various initial conditions for (a) $T_H = 176$ MeV and (b) $T_H = 196$ MeV.

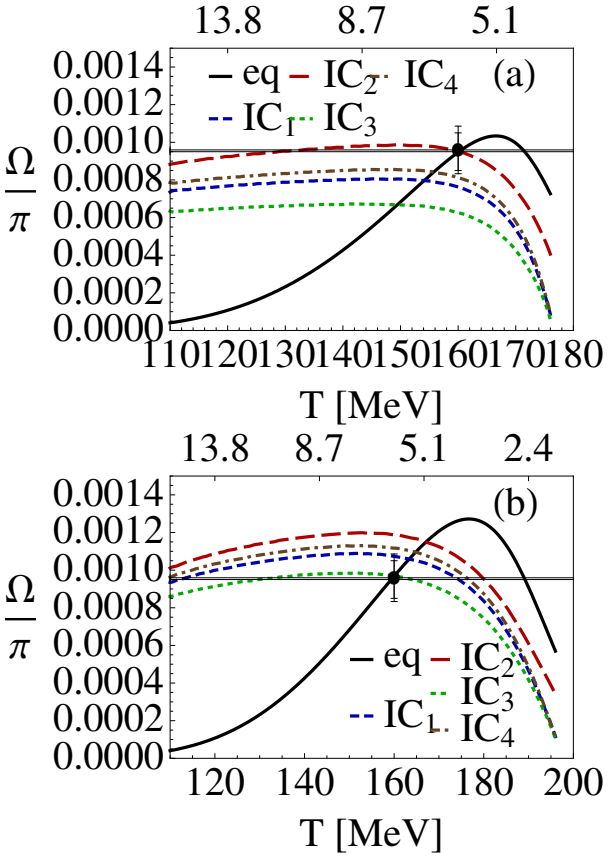

Figure 3.25: Results for the ratio of Ω/π^-'s with various initial conditions for (a) $T_H = 176$ MeV or (b) $T_H = 196$ MeV. Note that for STAR $\Omega/\pi^- = 9.5 \times 10^{-4}$ and $\bar{\Omega}/\pi^- = 9.6 \times 10^{-4}$ STAR [5, 117] and Ω/π is not measured for PHENIX.

example of this was shown already in Fig. 2.9. The canonical model observes the conservation of charge, Q, baryon number, B, and strangeness, S. In this thesis we use the results only when $B = S = Q = 0$, which would be for non-strange, electrical neutral mesons. The canonical model considers only clusters with the conserved quantities that have a certain mass, which we assume describe Hagedorn states. However, in [81] other configurations of B, S, and Q were considered, which means that we could use these results for the branching ratios of strange and/or baryonic Hagedorn states.

Chapter 4

Effects of Hagedorn States on Transport Coefficients

4.1 Introduction

Collective flow measurements [5] performed at RHIC indicate that the new state of matter produced in heavy ion collisions behaves almost as a perfect liquid [82]. In fact, the large elliptic flow coefficient measured at RHIC [5] supports the idea that this new state of matter is a strongly interacting quark-gluon plasma [17] characterized by a very small shear viscosity to entropy density ratio that is compatible with the lower bound $\eta/s \geq 1/(4\pi)$ [83] derived within the anti-de Sitter/conformal field theory (AdS/CFT) correspondence [84]. It was further conjectured by Kovtun, Son, and Starinets (KSS) [61] that this bound holds for all substances in nature. Possible counterexamples that would violate the bound involving nonrelativistic systems with very large number of particle species were discussed in [85, 86].

Recent lattice calculations [87] in pure glue $SU(3)$ gauge theory have shown that η/s remains close to the KSS bound at temperatures not much larger than T_c. Additionally, calculations within the BAMPS parton cascade [88], which includes inelastic gluonic $gg \leftrightarrow ggg$ reactions, showed that $\eta/s \sim 0.13$ in a pure gluon gas [89]. Moreover, it was argued in [90] that this ratio should have a minimum at (or near) the phase transition in quantum chromodynamics (QCD). This is expected because η/s increases with decreasing T in the hadronic phase [91] while it increases with T in the deconfined phase according to the perturbative calculations done in [92]. Note, however, that in general perturbative calculations are not reliable close to T_c (see, however, Ref. [93]).

Before our work [30], there have been several attempts to compute η/s in the confined phase using the known hadrons and resonances [94, 95, 96, 97]. However, these studies have not explicitly considered that the hadronic density of states in QCD is expected to be $\sim \exp(m/T_H)$ for sufficiently large m [48, 98], where $T_H \sim 150 - 200$ MeV is the Hagedorn temperature [48]. This hypothesis was originally devised to explain the fact that an increase in energy in pp and $p\bar{p}$ collisions does not lead to an increase in the average momentum per particle but rather to production of more particles of different species [48]. Moreover, hadron resonance models that include such rapidly increasing density of states are known to have a "limiting" temperature,

T_{max}, beyond which ordinary hadronic matter cannot exist [48].

In this chapter, a hadron resonance gas model which includes all the known particles and resonances with masses $m < 2$ GeV [65] and also an exponentially increasing number of Hagedorn states (HS) [30, 55, 56] is used to provide an upper limit on η/s for hadronic matter close to the critical temperature that is comparable to $1/4\pi$. Additionally, we show that our model provides a good description of the recent lattice results [8] for the trace anomaly and also the speed of sound, c_s, close to $T_c = 196$ MeV. We also study how the inclusion of HS affects the bulk viscosity to entropy density ratio, ζ/s, of hadronic matter near T_c.

4.2 Trace Anomaly and the Speed of Sound

The main assumption behind hadron resonance models is that the thermodynamic properties of an interacting gas of hadrons can be described by a free gas with the same hadrons and their respective resonances. For instance, it is known [99] that the pressure of a gas of interacting pions calculated within the virial expansion nearly coincides with that of a free gas of pions and ρ mesons. In this case there is an exact cancelation between the attractive and repulsive S-wave channels but the same is not true for an interacting gas of pions, kaons, and nucleons [100]. Thus, in general one also has to include the repulsive interactions between the hadrons when computing thermodynamic functions [70, 100, 101].

Here we assume that attractive interactions can be described by the inclusion of resonances which for large masses follow a Hagedorn spectrum as discussed in Chapter 2. The system's mass spectrum is assumed [55, 56] to be a sum over discrete and continuous states $\rho(m) = \rho_{HG}(m) + \rho_{HS}(m)$, where $\rho_{HG}(m) = \sum_i^{M_0} g_i\, \delta(m - m_i)\, \theta(M_0 - m)$ involves a sum over all the known hadrons and resonances [65] with their respective degeneracy factors up to $M_0 < 2$ GeV [72] and for larger masses it is shown in Eq. (1.15) where we take $m_0 = 0.5$ GeV, $A = 0.5$ GeV$^{\frac{3}{2}}$ [55], and $T_H = T_c$. As mentioned in Chapter 2, effects from repulsive interactions are included using the excluded-volume approach derived in [70] where the volume excluded by a hadron equals its energy divided by $4B$, where B plays the role of an effective MIT bag constant. The thermodynamic quantities can be obtained using Eq. (2.3) and the standard thermodynamic identities at zero baryon chemical potential [70]. When $P_{pt}(T_c)/4B < 1$ there is still a limiting temperature that is larger than T_c because then the denominator is then less than 1 in Eq. (2.3), which means that at $T^* = T_H$ then $T > T_H$. We take $B^{1/4} = 0.34$ GeV in our calculations, which implies that $T_{max} > T_c$. We restrict our discussion to $T \leq T_c$ because at higher temperatures a description involving quarks and gluons should be more adequate.

Our results for the trace anomaly are shown in Fig. 2.2 where the mass of the heavier Hagedorn state was set to be $M_{max} = 20$ GeV. Note that the inclusion of HS correctly captures the trend displayed by the lattice data in the transition region whereas the hadron gas curve does not. This remains true if other values of B are used. We checked that our results did not change appreciably in this temperature range when M_{max} is increased to 80 GeV. This happens because the divergences normally associated with the limiting temperature only occur in this case at $T_{max} \sim 210$ MeV. Were $T_H < T_c$, the dependence of the thermodynamic quantities with M_{max} would be much more pronounced. In general, a very rapid increase in the number of particle species (specifically heavier species) around T_c is expected to strongly reduce the speed

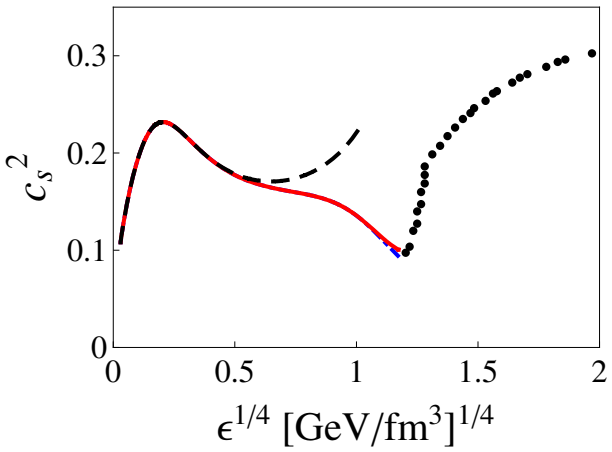

Figure 4.1: c_s^2 for the model including HS with $2 < M < 12$ GeV (solid red line) and for the hadron gas model of Ref. [72] which does not include HS (dashed black curve). The lattice results for the $p4$ action with $N_\tau = 6$ [8] are depicted in the dotted curve. The dotted-dashed blue curve was computed using HS with $2 < M < 80$ GeV.

of sound $c_s^2 = dP/d\epsilon$ at the phase transition. While $c_s^2 \to 0$ at the transition would certainly lead to very interesting consequences for the evolution of the RHIC plasma [102], recent lattice simulations have found that $c_s^2 \simeq 0.09$ near T_c [8]. It is shown in Fig. 7.3 that $c_s^2(T \sim T_c) \sim 0.09$ in the model with HS while for the model without them $c_s^2 \sim 0.25$ near the transition. Note that when $M_{max} = 80$ GeV (dashed blue curve) c_s^2 is only a bit smaller than 0.09 near the phase transition. Other quantities such as the total entropy density near T_c are found to agree with lattice results within the uncertainties present in those calculations [68].

4.3 Shear Viscosity

The total shear viscosity of our multi-component system computed within kinetic theory [103] is

$$\eta_{tot} \sim \alpha \sum_i n_i \langle p_i \rangle \lambda_i, \tag{4.1}$$

where n_i is the number density, $\langle p_i \rangle$ is the average momentum, and λ_i is the mean free path for discrete states and HS ($\alpha \sim \mathcal{O}(1)$). The derivation of Eq. 4.1 for the case of a fluid composed of a single type of particles is shown in section 4.3.1 and then generalized for a multi-particle fluid and used to determine the shear viscosity contribution from the Hagedorn states in section 4.3.2.

4.3.1 Derivation of Shear Viscosity for Non-relativistic Dilute Gas

The cartoon in Fig. 4.2 illustrates a fluid flowing in the positive x direction between two plates. The lower plate is fixed and has no velocity whereas the upper plate flows with the liquid at a speed of u_0. Thus, a gradient of the flow $\partial u_x/\partial z$ appears. The distance between the plates is L. Additionally at some point where $z = const.$ the fluid below exerts a stress P_z (a mean force per

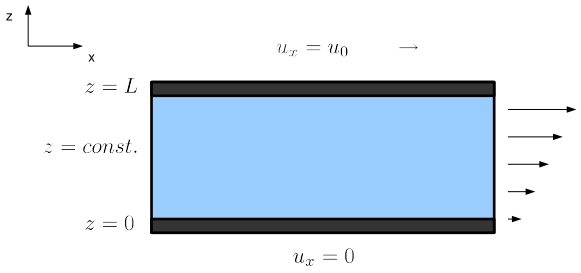

Figure 4.2: Two plates contain a fluid flowing in the positive x direction. The lower plate is at rest and the upper plate has the velocity u_0.

unit area) on the fluid above and according to Newton's third law the fluid above exerts P_z on the fluid below. Moreover, P_z is simply a measurement of the mean pressure in the fluid. Thus, when the fluid is in equilibrium $P_{zx} = 0$ (z for orientation of the plane and x the component of the forced exerted on the plane), otherwise known as the pressure tensor.

When the fluid is out of equilibrium such as in Fig. 4.2, the flow velocity in the z direction depends on z i.e. $u_z(z)$. Thus, $\partial u_x/\partial z \neq 0$ and $P_{zx} \propto \partial u_x/\partial z$. Assuming that $\partial u_x/\partial z$ is small, we can expand use a power series expansion where only the first term is needed. Thus, we have the equation

$$P_{zx} = -\eta \frac{\partial u_x}{\partial z} \tag{4.2}$$

where η is the viscosity. The minus sign is introduced in order to ensure that the viscosity is positive. For instance, if u_z increases with z ($\partial u_x/\partial z > 0$) then the fluid below slows down the fluid above and exerts a force in the $-x$ direction i.e. P_{zx}.

Assuming that we have a dilute gas (a good assumption for the hadron gas phase) and suppose that mean fluid velocity is dependent on z such that $u_x(z)$, then the stress P_{zx} arises because particles above a plane $z = constant$ have a somewhat larger component of x than those below. Basically, the gas below the plane gains momentum in the x direction from the molecules above the plane.

Given that there are n molecules per unit volume, roughly one-third of them have velocities in the z direction and half of these (so $n/6$) have the mean velocity $\bar{v}$ in the $+z$ direction. Then on average $n\bar{v}/6$ molecules in unit of time cross a unit area of the plane z=constant. Additionally, the particles that have crossed the plane from below experienced on average their last collisions within a distance of λ, where λ is the mean free path, below the plane. Therefore, each particle transfers across the plane a mean x component of moment $p_x = mu_x(z - \lambda)$. Thus, the mean x compnent of momentum transported upward per unit time per unit area is

$$\bar{p}_x + = \frac{1}{6} n\bar{v} m u_x(z - \lambda) \tag{4.3}$$

and downward is

$$\bar{p}_x- = \frac{1}{6}n\bar{v}mu_x(z+\lambda). \tag{4.4}$$

Then the stress P_{zx} is then the net molecular transport of the x component of momentum per unit time per unit area i.e.

$$\begin{aligned} P_{zx} &= \frac{1}{6}n\bar{v}mu_x(z-\lambda) - \frac{1}{6}n\bar{v}mu_x(z+\lambda) \\ &= \frac{1}{6}n\bar{v}m\left[u_x(z-\lambda) - u_x(z+\lambda)\right]. \end{aligned} \tag{4.5}$$

Then $u_x(z)$ can be expanded using a taylor series where higher order terms are neglected since the velocity gradient $\partial u_x/\partial z$ is assumed to be small so that the stress is

$$\begin{aligned} P_{zx} &= \frac{1}{6}n\bar{v}m\left[-2\frac{\partial u_x}{\partial z}l\right] \\ &= -\eta\frac{\partial u_x}{\partial z} \end{aligned} \tag{4.6}$$

where

$$\eta = \frac{1}{3}n\bar{v}m\lambda = \frac{1}{3}n\bar{p}\lambda. \tag{4.7}$$

4.3.2 Shear Viscosity to Entropy Density Ratio

In kinetic theory, the total shear viscosity of a gas composed of different types of particles is given in (4.1). Basically one has to sum over the individual contributions of each particle species but now the mean free path of a given species is $\lambda_i = \left(\sum_j n_j\,\sigma_{ij}\right)^{-1}$, with σ_{ij} being the scattering cross section.

Due to their very large mass, the particle density of a HS is much smaller than that of discrete states. Thus, one can neglect the small contribution to the mean free path from terms involving the interaction between the standard hadrons and the HS. In this case, $\eta_{tot} = \eta_{HG} + \eta_{HS}$ where η_{HG} is the shear viscosity computed using only the interactions between the standard hadrons while

$$\eta_{HS} = \frac{1}{3}\sum_i n_i\langle p\rangle_i\,\lambda_i \tag{4.8}$$

includes only the contribution from HS, which move non-relativistically since $m_{HS}/T \gg 1$ and is clearly taken from Eq. (4.7). Note that the approximation for η_{tot} used here provides an upper bound for this quantity since the inclusion of the interactions between HS and the standard hadrons would only decrease η_{tot}. Using the results above, one sees that

$$\left(\frac{\eta}{s}\right)_{tot} \leq \frac{s_{HG}}{s_{HG}+s_{HS}}\left[\left(\frac{\eta}{s}\right)_{HG} + \frac{\eta_{HS}}{s_{HG}}\right]. \tag{4.9}$$

While the entropy dependent prefactor in Eq. (4.9) can be easily determined using our model, the detailed calculation of η_{HG} and η_{HS} requires the knowledge about the mean free paths of the different particles and resonances in the thermal medium.

In the non-relativistic approximation, we can set

$$\langle p_i \rangle = m_i \langle v_i \rangle = \sqrt{8 m_i \, T/\pi} \tag{4.10}$$

in Eq. (4.9). Note that HS with very large m_i's are more likely to quickly decay. We assume that $\lambda_i = \tau_i \, \langle v_i \rangle$ where $\tau_i \equiv 1/\Gamma_i = 1/(0.151 \, m_i - 0.0583)$ GeV^{-1} is the inverse of the decay width of the i^{th} HS obtained from a linear fit to the decay widths of the known resonances in the particle data book [55, 56, 77] discussed in Chapter 2. Our choice for λ_i gives the largest mean free path associated with a given state because it neglects any possible collisions that could occur before it decays on its own. The inclusion of collisions here would only shorten λ_i, which would further decrease η_{tot}. Further studies of the relationship between HS and η could be done, for instance, using the cross sections discussed in [74]. Substituting the results above in we find that

$$\eta_{HS} = 8T \sum_i n_i \tau_i / 3\pi. \tag{4.11}$$

The remaining ratio $(\eta/s)_{HG}$ has been computed in Refs. [95, 96, 97] using different models and approximations. Since our main goal is to understand the effects of HS on $(\eta/s)_{tot}$, here we will simply use the values for $(\eta/s)_{HG}$ obtained in some of these calculations to illustrate the importance of HS. We chose to obtain $(\eta/s)_{HG}$ for a gas of pions and nucleons from Fig. 5 in [95] and for a hadron resonance gas with (constant) excluded volume corrections from [96]. Note that the results for η/s obtained from the calculation that included many particles and resonances [96] are already much smaller than those found in [95] where only pions and nucleons are considered. A linear extrapolation of the results in [95, 96] was used to obtain their η/s values at high temperatures. One can see in Fig. 4.3 that $(\eta/s)_{tot}$ drops significantly around T_c because of HS. This result is especially interesting because η/s in the hadronic phase is thought to be too large (according to viscous hydrodynamics calculations) to be compatible with elliptic flow data. One can see that the contributions from HS should lower η/s to near the KSS bound. Thus, the drop in η/s due to HS could explain the low shear viscosity near T_c already in the hadronic phase. We used $M_{max} = 20$ GeV in the calculations shown in Fig. 4.3 but the results do not change significantly if M_{max} is increased by a factor of 4.

4.4 Bulk Viscosity

The large value of the trace anomaly near T_c observed on the lattice has been used as an indication that ζ/s of QCD may be large at the phase transition [104, 105]. This is very different than at high temperatures where ζ/s is predicted to be small [106]. This may have some interesting phenomenological consequences such as the formation of clusters at freeze-out [107]. Using the QCD sum rules derived in [108], one can extract the (zero-momentum) Euclidean correlator of the trace of the energy-momentum tensor, θ^μ_μ, as follows

$$\begin{aligned} G^E(0,\mathbf{0}) &= \int d^4x \, \langle \theta^\mu_\mu(\tau,\mathbf{x}) \theta^\nu_\mu(0,\mathbf{0}) \rangle \\ &= (T\partial_T - 4)\,(\epsilon - 3p)\,, \end{aligned} \tag{4.12}$$

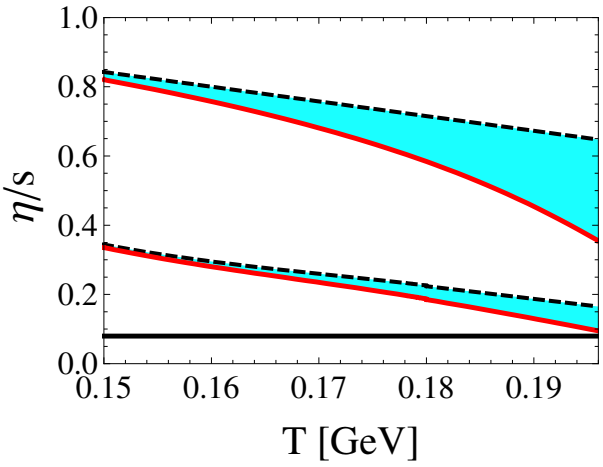

Figure 4.3: η/s is shown for a gas of pions and nucleons [95] (upper dashed black line) and for a hadron resonance gas with (constant) excluded volume corrections [96] (lower dashed black line). An upper bound on the effects of HS on η/s is shown in solid red lines. The blue band between the curves is used to emphasize the effects of HS. The solid black line at the bottom is the AdS/CFT lower bound $\eta/s = 1/4\pi$ [61].

the derivation of which is shown in Appendix E. The authors of Ref. [105] have argued that ζ can be obtained via G^E using $\pi\rho(\omega, \mathbf{0})/9\omega = \zeta\omega_0^2/(\omega^2 + \omega_0^2)$ as an ansatz for the small frequency limit of the $\langle\theta\theta\rangle$ spectral density at zero spatial momentum, $\rho(\omega, \mathbf{0})$. The parameter $\omega_0(T)$ defines the energy scale at which perturbation theory is applicable. The validity of this ansatz has been recently studied in Refs. [109]. Here we assume that this ansatz can at least capture the qualitative behavior of ζ around T_c and we use it to estimate how HS change the ζ/s close to T_c. The results for $\zeta/s \equiv G^E(0)/(9\omega_0\, s)$ are shown in Fig. 4.4 where $\omega_0 = 1$ GeV. Note that while ζ/s decreases near T_c for the hadron gas model with $m < 2$ GeV, when HS are included ζ/s increases close to T_c and this enhancement does not vary much with M_{max}.

Summarizing, in this chapter we used a hadron resonance gas model including all the known particles and resonances with masses $m < 2$ GeV and also an exponentially rising level density of Hagedorn states for $m > 2$ GeV to obtain an upper bound on η/s for hadronic matter near T_c that is comparable to the KSS bound $1/(4\pi)$. This indicates that the small η/s necessary to explain the large elliptic flow observed at RHIC could be already reached in the hadronic phase. It is clear that Hagedorn states with masses above $m > 2$ GeV are needed for a small η/s in the hadronic phase because URQMD using only the know hadrons has been used to calculate η/s and found that $\eta/s \approx 1$ [110]. Additionally, the results in this section were recently independently confirmed in [111].

Also, the large trace anomaly and the small speed of sound near T_c MeV computed within this model agree well with recent lattice calculations [8]. An estimate for the bulk viscosity of QCD using the proposal written by [105] generally indicates that HS increase ζ/s close to T_c.

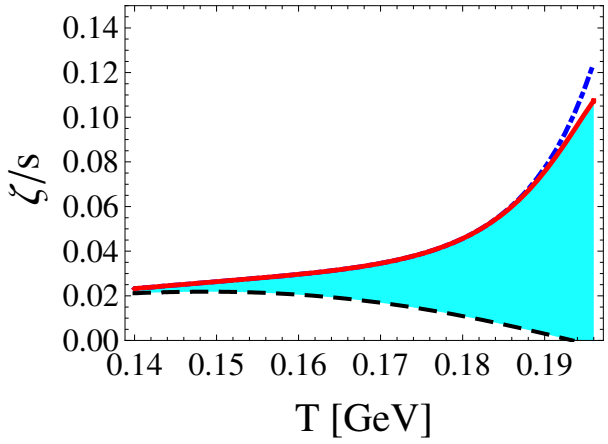

Figure 4.4: Estimates for $\zeta/s \equiv G^E(0)/(9\omega_0\, s)$ ($\omega_0 = 1$ GeV) for a model that includes HS with $2 < m < 20$ GeV (solid red line) and $2 < m < 80$ GeV (dotted-dashed blue line) and a hadron gas model with $m < 2$ GeV (black dashed line).

Chapter 5

Thermal Fits + Hagedorn States

5.1 Introduction

Lattice QCD is the main non-perturbative theoretical tool used to probe bulk thermodynamics quantities of QCD such as its pressure, entropy density, and the speed of sound. The QCD phase transition at vanishing baryonic chemical potential is a (rapid) crossover where the thermodynamic quantities vary significantly near a critical temperature, whose value lies between $170-200$ MeV. In fact, according to the Bielefeld-BNL/RIKEN-Columbia collaboration (RBC-Bielefeld) the critical temperature is around $T_c = 196$ MeV [8] (although recently it has been concluded that the range could be $T_c = 180 - 200$ MeV [68]) whereas the Budapest/Marseille/Wuppertal (BMW) collaboration has found a lower value $T_c = 176$ MeV [9]. Because the value of the critical temperature is vital to many phenomenological models of QCD, it is clearly important to find experimentally driven signals able to distinguish between these two critical temperature regions. We shall show that thermal fits for the measured particle ratios in Au+Au collisions at $\sqrt{s_{NN}} = 200$ GeV at RHIC can provide some nontrivial information about the critical temperature of the QCD phase transition at nonzero baryonic chemical potential as long as effects from highly massive Hagedorn resonances are included.

Thermal fits computed within a grand canonical statistical models are normally used to reproduce hadron yield ratios in heavy ion collisions [72, 112, 45, 46, 113, 114]. Thermal models computed at AGS, SIS, SPS, and RHIC energies can be used to construct a chemical freeze-out line in the QCD phase diagram [115, 116], which is shown in Fig. 5.1. For Au+Au collisions at RHIC at $\sqrt{s_{NN}} = 200$ GeV, specifically, estimates for the chemical freeze-out temperature and baryon chemical potential range from $T_{ch} = 155-169$ MeV and $\mu_b = 20-30$ MeV [46, 113, 114]. These thermal models give reasonable fits to the experimental data, which leads to the conclusion that chemical freeze-out is reached in these experiments.

As discussed in previous chapters, it was thought that the chemical freeze-out temperature and the critical temperature coincided because early calculations for T_c were around $T_c = 160-170$ MeV, which is where the chemical freezeout temperature lies. However, recent lattice results indicate a higher critical temperature, which leads to a difference of $\Delta T = 7 - 45$ MeV between T_c and T_{ch}. At SPS this difference was explained by allowing hadrons, especially exotic anti-baryonic states, to be "born" out of chemical equilibrium at T_c and reach chemical

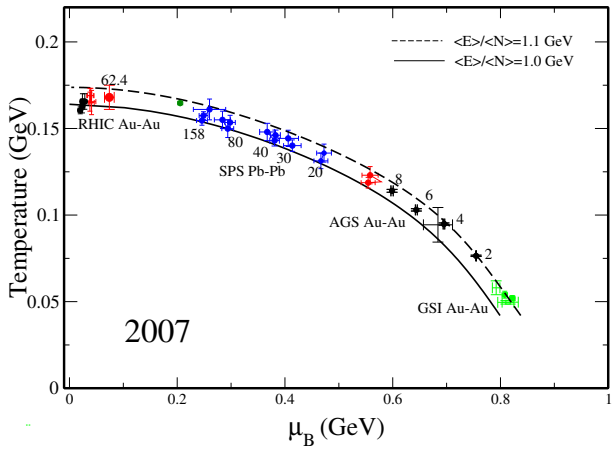

Figure 5.1: Temperatures and baryonic chemical potentials which are determined using thermal fits for various experiments. Taken from [115].

equilibrium through multi-mesonic collisions [36, 37] because chemical equilibration times of binary collisions are too long [35]. At RHIC, multi-mesonic collisions are no longer adequate to explain chemical equilibration times [39, 40] and this has led some to believe that hadrons are "born" in chemical equilibrium [42, 43]. A way out of this scenario involving an overpopulation of pions and kaons has been suggested in [41]. Another solution that has provided very promising results is the inclusion of Hagedorn states, which are heavy resonances with an exponentially growing mass spectrum [48] that open up the phase space and help drive hadrons quickly into chemical equilibrium [44, 55, 56, 58]. When a reaction of the form

$$n\pi \leftrightarrow HS \leftrightarrow n\pi + X\bar{X} \tag{5.1}$$

is used where $X\bar{X} = p\bar{p},\ K\bar{K},$, $\Lambda\bar{\Lambda}$ or $\Omega\bar{\Omega}$, hadrons are able to reach chemical equilibrium at about $T_{ch} \approx 160$ MeV [55, 56] using various lattice critical temperatures [56], see also Chapter 3. Moreover, it was shown that p/π, K/π, Λ/π and Ω/π ratios match RHIC data well [55, 56].

As we have seen in previous chapters, not only have Hagedorn states provided a mechanism for explaining the temperature difference between T_c and T_{ch}, but they have also been used to find a low η/s in the hadron gas phase [30] and see Chapter 4, which nears the string theory bound $\eta/s = 1/(4\pi)$ [61]. Calculations of the trace anomaly including Hagedorn states also fits recent lattice results well and correctly describe the minimum of c_s^2 near the phase transition found on the lattice [30]. Furthermore, estimates for the bulk viscosity including Hagedorn states in the hadron gas phase indicate that ζ/s has a peak near T_c.

Since Hagedorn states have been shown to affect the chemical equilibration times, thermodynamic properties, and transport coefficients of hadron resonance gases close to T_c it is natural to expect that they may also be relevant in the thermal description of particle ratios. Moreover, because Hagedorn states are dependent on the limiting Hagedorn temperature $T_H = T_c$, a relationship between the chemical freeze-out temperature and the critical temperature can be found by including Hagedorn states in thermal fits. This uniquely gives us the ability to distinguish between different critical temperature regions depending on the quality of the fit obtained using

the statistical model.

5.2 Model

In this chapter we use a grand-canonical model to describe the particle densities from which we can calculate the corresponding ratios as described in detail in [72]. We do not include any strangeness suppression factor or, in other words, we assume $\gamma_s = 1$. Unlike in previous chapters we do not assume that $\mu_b = 0$ but rather we allow change the baryonic chemical potential (and also temperature) to best fit the data.

In order to calculate the baryonic chemical potential μ_b and the strange chemical potential μ_s we use the following conservation relation

$$0 = \frac{\sum_i n_i S_i}{\sum_i n_i B_i}, \tag{5.2}$$

which means that the total strangeness per baryon number is held at zero. There n_i is the density of the i^{th} particle that has a corresponding baryon number B_i and strangeness S_i. The Hagedorn states are implemented in our model as previously discussed in Chapter 2. Furthermore, as in Chapter 3, we use two different scenarios regarding T_H. First we assume that $T_H = T_c$, and then we consider the two different different lattice results for T_c: $T_c = 196$ MeV for the RBC-Bielefeld collaboration [8] and $T_c = 176$ MeV from the BMW collaboration [9]. Furthermore, we take into account effects from repulsive interactions between the hadrons [70, 71] via excluded-volume corrections [70]. Only mesonic, non-strange Hagedorn states are considered in our calculations.

In our model we do not just consider the direct number of hadrons but also the indirect number that comes from other resonances. For example, for pions we consider also the contribution from resonances such as ρ's, ω's etc. The number of indirect hadrons can be calculated from the branching ratios for each individual species in the particle data book [65]. Moreover, there is also a contribution from the Hagedorn states to the total number of pions, kaons, and so on as described in [55, 56]. Thus the total number of "effective" pions can be described by

$$\tilde{N}_\pi = N_\pi + \sum_i N_i \langle n_i \rangle \tag{5.3}$$

whereas the total number of "effective" protons, kaons, or lambdas (generalized as X) can be described by

$$\tilde{N}_X = N_X + \sum_i N_i \langle X_i \rangle \tag{5.4}$$

where $\langle X \rangle$ is the average number of X = p's, K's, or Λ's. We take all $\langle X_i \rangle$'s from the micro-canonical model [75] discussed in Chapter 2. Here N is the total number of each species and $\langle n_i \rangle$ is the average number of pions that each Hagedorn state decays into. We have discussed this also in other chapters but we reiterate the equations to ease understanding. We assume here that the branching ratios can be obtained from a microcanonical calculation. Such a description is, for instance, also appropriate for describing the annihilation of p and anti-p.

It is important to note here that because the Hagedorn states always produce pairs of $X\bar{X}$'s that the entire contribution to ratios like K^+/K^- must come from the known particles. Therefore, in our calculations the baryonic chemical potential, which is directly related to the strange chemical potential, is somewhat inflated. If we were to include baryonic and/or strange Hagedorn states then μ_b would be lower.

In order to get an idea of the quality of the thermal fits, we define χ^2 as

$$\chi^2 = \sum_i \frac{\left(R_i^{exp} - R_i^{therm}\right)^2}{\sigma_i^2} \tag{5.5}$$

where R_i^{therm} is our ratio of hadron yields calculated within our thermal model whereas R_i^{exp} is the experimentally measured value of the hadron yield with its corresponding error σ_i^2.

In this work we look at only the experimental values at mid-rapidity and we used only the systematic error given by each respective experiment. We vary the temperature and μ_b according to the conservation laws in Eq. (5.2), in order to get the smallest χ^2. We use the experimental data from both STAR [117] and PHENIX [118] for Au+Au collisions at RHIC at $\sqrt{s_{NN}}$=200 GeV. Specifically, we observe the ratios: π^-/π^+, $\bar{p}/p$, K^-/K^+, K^+/π^+, p/π^+, and $(\Lambda + \bar{\Lambda})/\pi^+$. All of which are calculated by STAR [117]. However, only π^-/π^+, $\bar{p}/p$, K^-/K^+, K^+/π^+, p/π^+ are given by PHENIX. Because there is such a difference between p/π^+ from PHENIX and STAR we choose only the value from STAR so that we can compare are results to [113] where they also exclude p/π^+ from PHENIX. It should be noted that Ref. [113] includes more ratios than we do such as multi-strange particles and resonances, which are not include in this paper. This is because the purpose of the present study is not to confirm their results, which have already been confirmed in [114], but rather to compare thermal fits that include the contribution of Hagedorn states and those that exclude them.

5.3 Results

The following results are given for the minimal χ^2 for a given μ_b and T_{ch}. Initially, we found the thermal fit for a hadron gas excluding Hagedorn states, which is shown in Fig. 5.2. There $T_{ch} = 160.4$ MeV, and $\mu_b = 22.9$ MeV, which gave $\chi^2 = 21.2$. Our resulting temperature and baryonic chemical potential are almost identical to that in [113] where $T_{ch} = 160.5$ and $\mu_b = 20$ MeV.

The inclusion of Hagedorn states is our primary interest. Starting with the fit for the RBC-Bielefeld collaboration, we obtain $T_{ch} = 165.9$ MeV, $\mu_b = 25.3$ MeV, and $\chi^2 = 20.9$, which is shown in Fig. 5.3. The χ^2 is actually slightly smaller than in Fig. 5.2. The contributions of the Hagedorn states to the total number of the various species at this temperature and chemical potential are shown in Tab. 5.1.

When we consider the lattice results from BMW, which are at the lower end of the critical temperature spectrum where $T_c = 176$ MeV, we find $T_{ch} = 172.6$ MeV, $\mu_b = 39.7$ MeV, and $\chi^2 = 17.8$. The lower critical temperature seems to have a significant impact on the thermal fit. The lower χ^2 is due to the larger contribution of Hagedorn states at at $T_{ch} = 172.6$ MeV, which is much closer to T_c. The contributions of the Hagedorn states to the total number of the

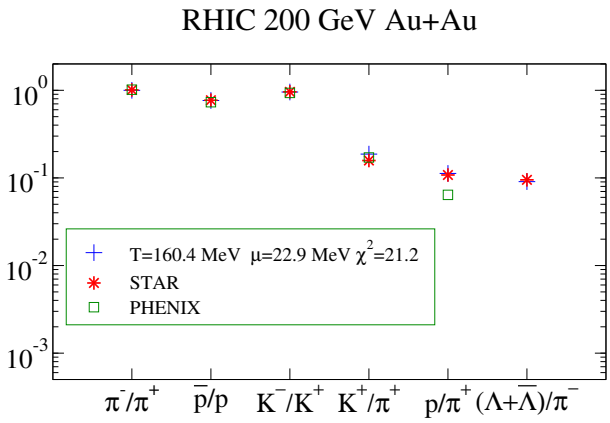

Figure 5.2: Thermal fits for Au+Au collisions at RHIC at $\sqrt{s_{NN}} = 200$ GeV when no Hagedorn states are present.

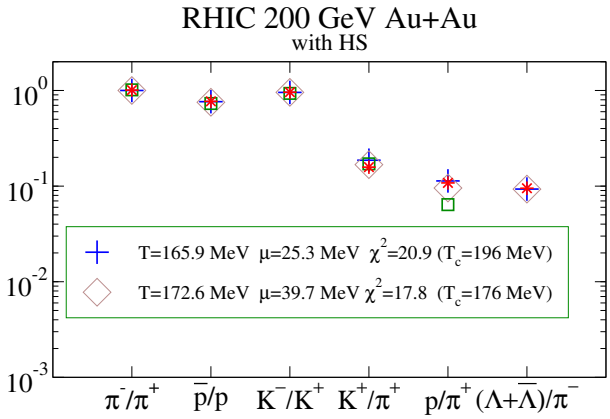

Figure 5.3: Thermal fits including Hagedorn states for Au+Au collisions at RHIC at $\sqrt{s_{NN}} = 200$ GeV.

various species at this temperature and chemical potential are about $30-50\%$ as shown in Tab. 5.1.

The difference in the χ^2's for BMW and RBC-Bielefeld collaboration is directly related to the contribution of Hagedorn states in the model. Because the RBC-Bielefeld critical temperature region is significantly higher than its corresponding chemical freeze-out temperature the contribution of the Hagedorn states is minimal at only 4-11% (see Tab. 5.1.). To further prove this point we can vary the parameters that define the influence of Hagedorn states in the model. If, for instance, we double the maximum mass we see in Fig. 5.4 that our thermal fits are not affected. This effect arises the true limiting temperature after volume corrections is larger than the critical temperature [30]. The effects of changing the maximum mass are only seen at temperatures larger than the critical temperature, which are not considered in this study.

While the maximum mass does not affect the quality of the fit, the parameter A, which is essentially the degeneracy of the Hagedorn states, does. The results of this are shown in Fig. 5.5. If we double A then we find that the minimum χ^2 for $T_c = 196$ MeV has dropped down

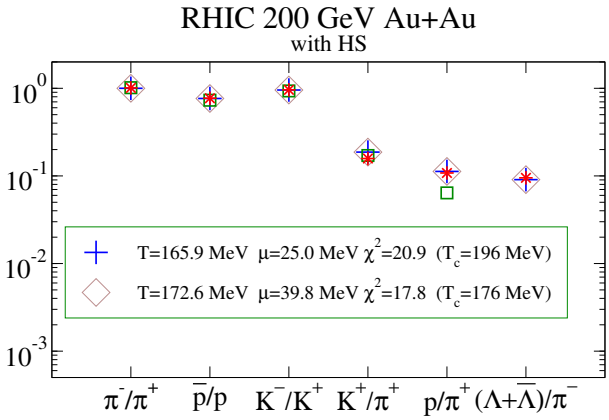

Figure 5.4: Thermal fits including Hagedorn states for Au+Au collisions at RHIC at $\sqrt{s_{NN}} = 200$ GeV when the maximum mass of the Hagedorn states is doubled.

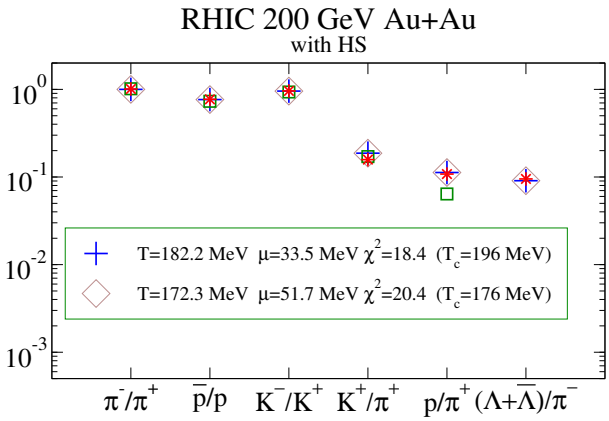

Figure 5.5: Thermal fits including Hagedorn states for Au+Au collisions at RHIC at $\sqrt{s_{NN}} = 200$ GeV when the degeneracy of the Hagedorn states is doubled.

to $\chi^2 = 18.4$, which is only slightly higher than the best fit for $T_c = 176$ MeV in Fig. 5.3. This indicates that at $T_c = 196$ MeV more Hagedorn states would be needed in order to get a better fit. However, we also see that for $T_c = 176$ MeV and A=1.0 GeV$^{3/2}$ that $\chi^2 = 20.4$. The reason for this is that there is an overpopulation of Hagedorn states. If we look at the contribution of Hagedorn states to the individual particle species we see that the optimal contribution of Hagedorn states is around $\approx 40 \pm 10\%$, which is what we get for the fits $T_c = 176$ MeV, A=0.5 GeV$^{3/2}$, M=15 GeV and $T_c = 196$ MeV, A=1.0 GeV$^{3/2}$, M=20 GeV as seen in Tab. 5.1.

A summary of our results is seen in Tab. 5.2. We find that the inclusion of Hagedorn states should not only provide a better fit but they also affect the chemical freeze-out temperature and the baryonic chemical potential. The more mesonic Hagedorn states are present the larger μ_b becomes. Furthermore, our fits also have higher T_{ch}'s than seen in the fit without the effects of Hagedorn states.

In this chapter we assumed that the particle ratios measured in Au+Au collisions at RHIC

T_c (MeV)	A (GeV$^{3/2}$)	M (GeV)	π's	K's	p's	Λ's
176	0.5	15	48.5%	41.6%	29.1%	41.0%
196	0.5	20	11.2%	10.5%	4.7%	6.2%
176	0.5	30	48.7%	41.6%	29.1%	41.2%
196	0.5	40	11.2%	10.5%	4.7%	6.2%
176	1.0	15	62.5%	56.0%	40.6%	53.4%
196	1.0	20	44.0%	38.9%	21.9%	30.3%

Table 5.1: Contribution of the Hagedorn states to the total number of hadron species.

T_c (MeV)	A (GeV$^{3/2}$)	M (GeV)	T_c (MeV)	μ_b (MeV)	χ^2
176	0.5	15	172.6	39.7	17.8
196	0.5	20	165.9	25.3	20.9
176	0.5	30	172.6	39.8	17.8
196	0.5	40	165.9	25.0	20.9
176	1.0	15	172.3	51.7	20.4
196	1.0	20	182.2	33.5	18.4

Table 5.2: Comparison of the chemical freeze-out temperature, baryonic chemical potential, and χ^2 for various fits including Hagedorn states.

at $\sqrt{s_{NN}} = 200$ GeV admit a purely statistical description at chemical freeze-out. Our results for thermal fits without Hagedorn states concur well with other thermal fit models [113] where the chemical freeze-out temperature ($T_{ch} = 160.4$ MeV) is almost identical and the baryonic chemical potential ($\mu_b = 22.9$ MeV) is only slightly larger. The thermal fit with the known particles in the particle data group provides a decent fit with $\chi^2 = 21.2$. However, the inclusion of Hagedorn states provides an even better fit to the experimental data where $\chi^2 = 17.8$ for the BMW collaboration and $\chi^2 = 20.9$ for the RBC-Bielefeld collaboration. This provides further evidence [30, 55, 56, 58] that Hagedorn states should be included in a description of hadronic matter near T_c.

Furthermore, because Hagedorn states provide a bridge between the chemical freeze-out temperature and the critical temperature, we were able to make a qualified statement about which critical temperature region is more appropriate according to the quality of the thermal fits. We find that lower critical temperature regions are somewhat favored in this study because more Hagedorn states are present close to the chemical freeze-out temperature and that a substantial number of Hagedorn states (i.e. a contribution of about 40% to the total particle numbers) are needed in order to provide the best fit to the hadron yield ratios.

A lower χ^2 can be obtained for the higher critical temperature region when we double the degeneracy of the Hagedorn states, which would lead to a mismatch between our thermodynamic quantities and those computed on the lattice (recall that the parameters that define the exponential spectrum in this case are obtained by fitting the results of the RBC-Bielefeld collaboration at $\mu_b = 0$). As we can see from Tab. 5.2 a change in the parameters even when they are doubled

still gives a better fit than the thermal fits without Hagedorn states because a contribution of Hagedorn states as small as 4-11% still contribute enough to lower χ^2. Therefore, this reconfirms the importance of including Hagedorn states in the hadron gas phase and, consequently, in the computation of thermal fits. Moreover, our results indicate that hadronization and chemical equilibration do not need to occur at the same temperature in order to explain RHIC data.

Chapter 6

Summary and Outlook

In this work we have used an old idea, Hagedorn states, to understand the new physics involved in hadronic matter close to T_c formed in relativistic heavy ion collisions. The idea that hadronic resonances follow an exponential mass spectrum came from Hagedorn in the 1960's. However, today the ramifications of this idea are still being explored as these states appear to play an important role in the physics close to T_c at RHIC. Since Hagedorn's initial work, many new resonances have been discovered and they still fit an exponential mass spectrum up to $M = 2$ GeV. Beyond that point the mass spectrum flattens, deviating from an exponential behavior, which indicates that there are possible "missing" resonances. In this thesis, I assumed that these "missing" resonances indeed exist, which affects various signals of QGP because the previous assumptions about the hadron gas phase are significantly altered.

Dynamical reactions with the known hadronic particles cannot account for the particle abundances seen at RHIC. The chemical equilibration times are too long and do not fit within the calculated time scale of the hadronic fireball. This has led to the assumption that the chemical freeze-out temperature and the critical temperature coincide. However, we have shown in Chapter 3 under the assumption that these heavy, quickly decaying Hagedorn states exist that chemical equilibrium can be achieved on short enough time scales that fit within a hadronic, cooling fireball i.e. on the order of $\approx 1 - 2\ fm/c$. Moreover, Hagedorn states states provide a very efficient way for incorporating multi-hadronic interactions (with parton rearrangements). This work indicates that the population and repopulation of potential Hagedorn states close to phase boundary can be the key source for a dynamical understanding of generating and chemically equilibrating the standard and measured hadrons.

In this thesis only the following hadrons were considered: pions, protons, kaons, lambdas, and omegas, as described in Chapter 2. However, a possible future outlook would be to consider a wider range of hadrons using branching ratio data from a microcanonical or canonical model. Due to the large decay width of Hagedorn states and their prominence close to T_c it is reasonable to believe that all light and strange hadrons will be able to quickly reach chemical equilibrium. In fact, according to our chemical equilibration time estimates Eq. (3.8), the only component of the time scale that would be affected is $N^{eq}_{X\bar{X}}/\langle X\rangle$ (recall that $\Gamma_{i,X\bar{X}} = \langle X\rangle\Gamma_i$ where Γ_i is unaffected by our choice in X). Both $N^{eq}_{X\bar{X}}$ and $\langle X\rangle$ should increase/decrease roughly by the same order of magnitude in the system because both are calculated in statistical models, which

are dependent on the same quantities: temperature, volume, chemical potential, mass of the particle, degeneracy, and its quantum numbers. Thus, it is possible that Hagedorn states can account for all particles reaching chemical equilibrium close to T_c.

Furthermore, our analytically derived chemical equilibration time depends only on the temperature, decay widths, and branching ratios, but not the initial conditions. While this changes slightly when an expanding fireball is considered, the initial conditions still only play a small role and only minimally affect the 'freeze-out' temperature at which chemical equilibrium is reached (the summary graph in Fig. 3.18 illustrates this nicely). This demonstrates that regardless of the population of hadrons cooling out of the QGP phase, the initial conditions are washed out and the hadrons can reach chemical equilibrium by the freezeout temperatures found in [63]. Moreover, the particle ratios p/π, K/π , Λ/π, and also Ω/π match the experimental values regardless of the initial conditions. Especially, in Fig. 3.18 one can see: Regardless of the initial conditions, our dynamical scenario can match experimental data. We do find, however, that $T_H = 196$ MeV fits within the experimental data box for K/π whereas $T_H = 176$ MeV is slightly above. This appears to reconfirm the findings in [63]. Our results imply that both lattice temperatures can ensure that the hadrons reach their chemical equilibrium values by $T = 160 - 170$ MeV. Although the ratios for $T_H = 176$ MeV do fit the data somewhat better, both match the experimental values reasonably well. This implies that independent of the critical temperature the hadrons are able to reach chemical freeze-out.

These results raise the idea that the strangeness enhancement observed in heavy ion collisions may not be a true signature for the formation of the QGP since it could be explained using only the physics within the hadronic phase. Thus, it would interesting in the future to include strange and/or baryonic Hagedorn states (currently, only non-strange, mesonic Hagedorn states have been used). With these new Hagedorn states new decay channels could be considered, which might contribute to multi-strange particles such as Ω.

One clear extension of my work is to include a finite baryon chemical potential μ_b, which is currently held at $\mu_b = 0$ in all dynamical calculations (the thermal fits do include finite μ_b but all those calculations are done in equilibrium). In order to implement this, the decay channels must also include effects from finite μ_b whereas in the current work the total baryon number is set to zero i.e. a baryon anti-baryon pair is always produced instead of a single baryon. Another interesting possibility is to include Hagedorn states in numerical transport theory descriptions of the hadronic phase. Current transport models only include binary reactions when detailed balance is preserved (in general $2 \rightarrow 3$ reactions are possible but only if the backreactions are not included). Even though my work, thus far, has always included multi-mesonic reactions, it should be possible to include Hagedorn states via binary reactions in a ladder approach. There, a heavy Hagedorn state could decay into a lighter Hagedorn state plus a hadron.

Because of the success of decays from Hagedorn states in reproducing experimental particle ratios, it was only logical to extend their use to other areas. Hadronic models with the known particles are not able to reproduce the low shear viscosity to entropy density ratio that seems to be required to explain the large elliptic flow observed at RHIC. One might expect that by increasing the number of particles in a gas the mean free path would subsequently decrease, which would in effect decrease the total η/s. In fact, including the "missing" Hagedorn states also decreases η/s for hadronic matter near T_c near to the string theory value $1/(4\pi)$ as seen in Chapter 4. Moreover, according to the general result that small η/s implies strong jet quenching

[120], our significant reduction of η/s indicates that hadronic matter near the phase transition is more opaque to jets than previously thought. Since the system should spend most of its time near T_c (because of the minimum in the speed of sound), the fact that η/s can be very small in that region in the hadronic phase may imply that the key observables for the QGP, i.e., the strong quenching of jets and the large elliptic flow, can receive significant contributions from the hot Hagedorn resonance gas.

As discussed in the Chapter 1, the equation of state, i.e., the relationship between the pressure and energy density, is one of the necessary input parameters for hydrodynamics. Using only the known particles the equation state for the hadron gas phase one is not able to match that for the lattice near T_c if repulsive interactions are taken into account. In fact, we believe that repulsive interactions between hadrons in a Hagedorn gas should be included since there are no fundamental physical reasons to neglect them at such high temperatures (this was also Hagedorn's idea). However, note that at lower temperatures the repulsive interactions do not contribute significantly and a sudden freeze-out scenario is still valid.

Hydrodynamic simulations of heavy ion collisions typically use either the simplified $\epsilon = 3p$ that describes a non-interacting ideal gas (or conversely an infinitely strong interacting conformal plasma such $\mathcal{N} = 4$ super-symmetric Yang Mills [**?**]) or an interpolation between an equation of state based on lattice results above T_c and an ansatz for the equation state of hadronic matter using the known hadrons. The latter is currently used more often. However, an interpolation at T_c is required because the equations of state do not match at the transition and at best a guess must be made to connect the two because hydrodynamics requires a continuous equation of state. This can be avoided with the inclusion of Hagedorn states in determining the hadronic equation of state (here the pressure and energy are related via the speed of sound, c_s^2 and the trace anomaly also matches the lattice well) because it uniquely matches the lattice results at T_c and, thus, no interpolation is required. Note that once the mass of the hadrons computed on the lattice match the physical masses the value of the model parameters determined by the fit to the lattice data near T_c will be slightly different but this change can be straightforwardly incorporated in our calculations. It would be interesting to use the calculated equation of state here in hydrodynamic simulations. In fact, one could study how the temperature dependence of viscous coefficients, which so far has been mostly neglected in the viscous hydrodynamic simulations, affects key signatures of QGP formation such as the elliptic flow of hadrons.

Finally, in Chapter 5 I continued my research into the effects of the missing Hagedorn states in thermal fits. I assumed that the particle ratios measured in Au+Au collisions at RHIC at $\sqrt{s_{NN}} = 200$ GeV admit a purely statistical description at chemical freeze-out. The results for thermal fits without Hagedorn states concur well with other thermal fit models [113] where the chemical freeze-out temperature ($T_{ch} = 160.4$ MeV) is almost identical and the baryonic chemical potential ($\mu_b = 22.9$ MeV) is only slightly larger. The thermal fit with the known particles in the particle data group provides a decent fit with $\chi^2 = 21.2$. However, the inclusion of Hagedorn states provides an even better fit to the experimental data. In fact, we find $\chi^2 = 17.8$, $T_{ch} = 172.6$ MeV, and $\mu_b = 39.7$ MeV for the BMW collaboration while for the RBC-Bielefeld collaboration we obtained $\chi^2 = 20.9$, $T_{ch} = 165.9$ MeV, and $\mu_b = 20.9$ MeV. This implies [30, 55, 56, 58] that Hagedorn states are important in a description of hadronic matter near T_c. Since the chemical freeze-out temperature was found to increase from 160 MeV to roughly 165 MeV (RBC-Bielefeld) or 172 MeV (BMW) when including Hagedorn states, this exemplifies the

degree of uncertainty in extracting chemical freeze-out thermodynamical parameters by means of such thermal analyzes.

Furthermore, it would be interesting to calculate the hadronic susceptibilities, which can be done by taking the second derivative of the free energy with respect to the chemical potential. The susceptibilities are interesting because lattice calculations show that quadratic fluctuations increase rapidly in the phase transition region and continue to increase about T_c until they near the ideal-gas value at $T \approx 2T_c$. Because my statistical model including Hagedorn states matches lattice data well, it would be interesting to see if it has the same results for the susceptibilities in the hadronic phase. It would be also interesting to study the new properties of hadronic matter that appear near the conjectured QCD critical point.

Hopefully, in the next few years results from LHC will begin to flood scientific conferences and papers. Thus, it is normal to wonder what role the Hagedorn states will play at LHC. The work I have done on dynamical chemical equilibrium using Hagedorn states should be almost entirely unaffected by a longer QGP phase during the collision. The reason is that all calculations are made following the cooling into the hadronic phase, so as long as the temperature is close to T_c it is irrelevant how long QGP has existed beforehand. Furthermore, because the initial number of hadrons following freeze-out is washed out because of the quick decays of Hagedorn states, even if the initial conditions for the protons, pions, etc. at LHC are different then at RHIC, this difference will not affect my results. Here I have assumed that $\mu_b = 0$, which means that if anything my calculations are even more applicable at those higher collision energies because LHC has a smaller chemical potential than RHIC.

The only step in our calculations that could be affected by different results from LHC is the way the fireball expansion is setup. In Eq. (2.22) the term $\frac{dN_\pi}{dy}$ is taken from experimental results in [78]. Therefore, if the number of pions is drastically increased it could possible affect our results. Because the entropy density at a given temperature would be unchanged an increase in the number of pions would increase the volume, which would in turn increase the total number of particles. However, our time scale estimate in Eq. (3.8) would be unaffected by a change in the volume because this factor would be cancelled out. Obviously, the caluclated particle ratios would remain the same because the volume would cancel. Thus, if the mechanism proposed in this thesis indeed correctly captures the corresponding physics at RHIC, one should still expect to see quick chemical equilibration times at LHC.

A change in the total number of pions would also have no effect on η/s because the volume cancels out. As for the trace anomaly, c_s^2, and the bulk viscosity they would be unaffected. The same goes for thermal fits because the volume would be cancelled out due to only considering particle ratios. Therefore, we conclude that the "missing" Hagedorn states discussed in this thesis should be just as vital to understand the physics at the new energy frontier at the LHC as it has been at RHIC and SPS.

Chapter 7

Zusammenfassung

Die vorliegende Arbeit greift das bekannte Konzept von Hagedornzuständen auf, um damit neue physikalische Effekte in hadronischer Materie nahe der kritischen Temperatur T_c[1] in einem Beschleunigerring für relativistische Schwerionen zu untersuchen. Dieses Konzept wurde in den 1960er Jahren von Rolf Hagedorn eingeführt und beruht darauf, dass hadronische Resonanzen einem exponentiellen Spektrum folgen. Seit den Arbeiten von Hagedorn wurden viele neue Resonanzen gefunden, jedoch weisen sie bis zu einer Masse von $M = 2$ GeV weiterhin ein exponentielles Spektrum auf. Für größere Massen flacht das Spektrum allerdings ab, was darauf hinweist, dass bislang noch nicht alle Resonanzen bekannt sind. In dieser Arbeit wird die Existenz solcher Resonanzen angenommen und ihre Auswirkungen auf verschiedene Signaturen des Quark-Gluon Plasmas untersucht.

Dynamische Zerfälle der bekannten hadronischen Teilchen können die Anzahl der verschiedenen am RHIC (dem Relativistic Heavy-Ion Collider am Brookhaven National Laboratory on Long Island, USA) auftretenden Teilchen nicht erklären. Die Zeitskala des chemischen Gleichgewichtes ist zu groß und sie stimmt nicht zu der berechneten Zeitskala des expandierenden hadronischen Feuerballs überein. Dies führte zu der Annahme, dass die Temperatur des chemischen Ausfrierprunktes (d.h. die Temperatur, an dem Teilchen nicht mehr durch Stöße miteinander wechselwirken) und die kritische Temperatur übereinstimmen. In dieser Arbeit konnte gezeigt werden, dass unter Hinzunahme der bereits erwähnten schweren, schnell zerfallenden Hagedornzustände das chemische Gleichgewicht innerhalb von $\approx 1 - 2\frac{fm}{c}$ erreicht werden kann. Diese Zeitskala stimmt mit einem expandierenden, sich abkühlenden Feuerball überein. Darüber hinaus bieten Hagedornzustände einen wirksamen Mechanismus, die Wechselwirkung von Hadronen untereinander zu beschreiben. Die Ergebnisse dieser Arbeit weisen darauf hin, dass die Besetzung potentieller Hagedornzustände nahe der Phasengrenze eine essentielle Rolle im Verständnis der dynamischen Prozesse spielt, die zur Produktion und zur Ausbildung des chemischen Gleichgewichtes der gemessenen Hadronen führen.

Diese Arbeit betrachtet nur die folgenden Hadronen: Pionen, Protonen, Kaonen, Lambdas und Omegas. Zukünftig wäre eine Erweiterung des in der Arbeit vorgestellten Modells denkbar, das eine größere Auswahl von Hadronen berücksichtigt und dabei Verzweigungsverhältnisse (sog.

[1] Die kritische Temperatur bestimmt den Phasenübergang von der hadronischen Materie zum Quark-Gluon Plasma.

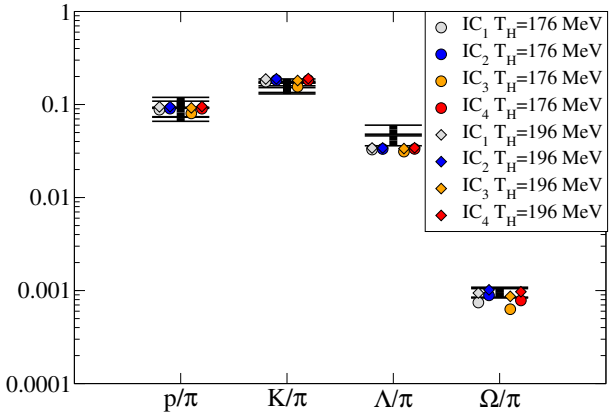

Figure 7.1: Diagramm der verschiedenen Teilchenverhältnisse bei verschiedenen Anfangsbedingungen. Die Punkte stellen die Teilchenverhältnisse bei $T = 110$ MeV dar, wobei unterschiedliche Hagedorntemperaturen von $T_H = 176$ MeV (Kreise) und ein $T_H = 196$ MeV (Rauten) betrachten werden. Die experimentellen Ergebnisse für STAR [5, 117] und PHENIX [118] sind durch graue Balken angezeigt.

branching ratios) zwischen den verschiedenen Hadronen in Betracht zieht, die anhand von kanonischen oder mikrokanonischen Modellen gewonnen werden können. Aufgrund der großen Zerfallsbreite der Hagedornzustände und ihres Einflusses nahe T_c kann man davon ausgehen, dass alle leichten und seltsamen Teilchen schnell das chemische Gleichgewicht erreichen. Es lässt sich zeigen, dass die chemische Zeitskala die Form

$$\tau_{X\bar{X}} = \frac{N^{eq}_{X\bar{X}}}{\sum_i \Gamma_{i,X\bar{X}} N^{eq}_i} \tag{7.1}$$

annimmt. Daher ist $N^{eq}_{X\bar{X}}/\langle X\rangle$ die einzige Komponente der Zeitskala, auf die eine Änderung eines Verzweigungsverhältnisses einwirken würde, da die Relation $\Gamma_{i,X\bar{X}} = \langle X\rangle\Gamma_i$ gilt, wobei Γ_i unabhängig von der Wahl von X ist. Die Terme $N^{eq}_{X\bar{X}}$ und $\langle X\rangle$ nehmen ungefähr mit der gleichen Größenordnung im System zu/ab, weil sie die gleiche Abhängigkeiten von der Temperatur, dem Volumen, dem chemisches Potential, der Masse, dem Entartungswert und den verschiedenen Quantenzahlen aufweisen. Daher ist es möeglich, dass aufgrund der Hagedornzustände alle Teilchen chemiches Gleichgewicht erreichen können.

Unsere analytisch abgeleitete Zeitskala des chemischen Gleichgewichtes hängt ausschließlich von der Temperatur, der Zerfallsbreite und Verzweigungsverhältnissen zwischen verschiedenen Hadronen, aber nicht von den gewählten Anfangsbedingungen ab. Dies ändert sich jedoch, wenn ein expandierender Feuerball betrachtet wird. Allerdings spielen auch dann die Anfangsbedingungen nur eine untergeordnete Rolle und haben nur eine minimale Wirkung auf die Temperatur, an der das chemische Gleichgewicht erreicht wird (siehe Fig. 7.1). Dies verdeutlicht, dass trotz der Bevölkerung verschiedener hadronischer Zustände während der Abkühlphase aus dem QGP die Anfangsbedingungen nahezu vollständig verwaschen und die Hadronen bei einer Temperatur von $T_{ch} = 160$ MeV ein chemisches Gleichgewicht erreichen, die als typische chemische Ausfriertemperatur angesehen werden kann (siehe [63]). Darüber hinaus stimmen die mit unserem dynamischen Modell berechneten Teilchenverhältnisse p/π, K/π , Λ/π und Ω/π unabhängig von

den gewählten Anfangsbedingungen gut mit den experimentell gemessenen Werten überein wie Fig. 7.1 zeigt. Die einzige Ausnahme hierbei bildet das Verhältnis K/π, das für eine Hagedorntemperatur von $T_H = 176$ MeV, jedoch nicht für ein $T_H = 196$ MeV innerhalb der Fehlerbalken liegt. Diese Ergebnisse implizieren, dass beide Hagedorntemperaturen von $T_H = 176$ MeV und $T_H = 196$ MeV, die anhand von verschiedenen Lattice-QCD Rechnungen bestimmt wurden, ein chemisches Gleichgewicht zwischen $T = 160 - 170$ MeV erzeugen. Obwohl die Verhältnisse für eine Hagedorntemperatur von $T_H = 176$ MeV die experimentellen Daten etwas besser zu beschreiben scheinen, führen beide Temperaturen zu einer guten Übereinstimmung mit den experimentellen Werten. Dies weist darauf hin, dass die Hadronen das chemische Gleichgewicht unabhängig von der kritischen Temperatur erreichen.

Diese Ergebnisse werfen die Frage auf, ob der in Schwerionenkollisionen beobachtete Anstieg seltsamer Teilchen ein eindeutiges Indiz für die Ausbildung des QGP ist, da dieser Effekt auch allein anhand der Physik in der Hadrongas-Phase erklärt werden kann. Daher wäre es interessant, unser Modell um seltsame und/oder baryonische Hagedornzustände zu erweitern (bisher haben wir nur nicht-seltsame, mesonische Hagedornzustände berücksichtigt). Mit diesen neuen Hagedornzuständen könnten außerdem zusätzliche Zerfallskanäle berücksichtigt werden, die zur Produktion von Teilchen beitragen könnten, die wie das Ω aus mehreren seltsamen Teilchen aufgebaut ist.

Da die experimentell gemessenen Teilchenverhältnisse sehr gut durch den Zerfall von Hagedornzuständen reproduziert werden konnten, wurde ihre Anwendung auch auf andere Gebiete ausgedehnt. Aus hadronische Modellen, die alle bekannten Teilchen berücksichtigen, lässt sich kein Verhältnis von Scherviskosität zu Entropiedichte (η/s) ableiten, das klein genug wäre, um den großen elliptischen Fluss zu beschreiben, der am RHIC beobachtet wurde. Man könnte erwarten, dass durch die Erhöhung der Teilchenzahl in einem Gas die mittlere freie Weglänge deutlich nachlässt, was zu einem kleineren η/s führen würde. In der Tat führt auch die Hinzunahme der fehlenden Hagedornzustände zu einem kleineren Wert von η/s für hadronische Materie nahe T_c, der ungefähr den aus der Stringtheorie abgeleiteten Wert von $\eta/s = 1/(4\pi)$ hat, wie man Fig. 7.2 entnehmen kann. Da ein kleines η/s eine starkt Abschwächung von Jets bedeutet (das sog. Jet Quenching) [120], weist der aus unseren Rechnungen gewonnene, kleinere Wert von η/s darauf hin, dass hadronische Matterie nahe der Phasenübergang Jets stärker abschwächen dürfte als gedacht. Da sich das System (aufgrund des Minimums der auftretenden Schallgeschwindigkeit) längere Zeit in dem Bereich nahe der kritischen Temperatur T_c aufhalten sollte, könnte ein kleines η/s in diesem Bereich der Hadrongas-Phase bedeuten, dass die wichtige Signaturen des QGPs wie Jet Queching oder elliptischer Fluss stark vom heißen Hagedorn-Resonazgas beeinflusst werden.

Darüber hinaus bietet die Einbeziehung der Hagedornzustände die Möglichkeit, eine Zustandsgleichung abzuleiten, die ein Hadrongas kontinuierlich mit der aus Lattice-QCD Rechnungen bestimmten Zustandsgleichung für ein QGP verbindet (siehe Fig. 7.3). Bislang wurde häufig eine Interpolation zwischen den Lattice-QCD Resultaten und einem Hadrongas (ohne Hagedornzustände) verwendet. Es wäre äusserst interessant, eine derartige Zustandsgleichung in einem hydrodynamischen Modell zu verwenden. So ließe sich beispielsweise die Abhängigkeit der Transportkoeffizienten von der Temperatur untersuchen, die bislang größtenteils vernachlässigt wurde, jedoch einen Einfluss auf bestimmte Signaturen des QGPs wie den elliptischen Fluss von Hadronen haben könnte.

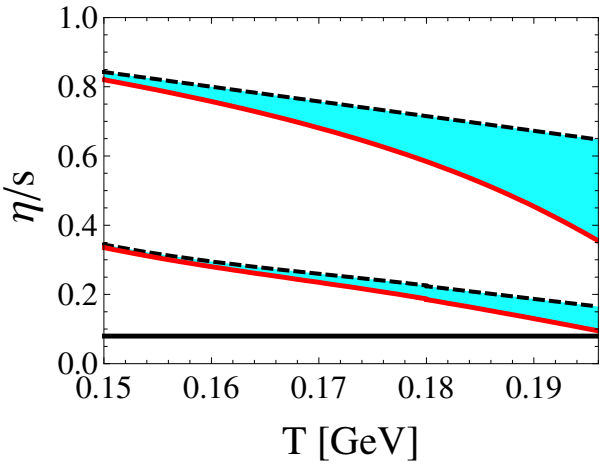

Figure 7.2: Das Verhältnis von η/s als Funktion der Temperatur T für ein Gas von Pionen und Nukleonen [95] (obere gestrichelte schwarze Linie) und für ein Hadron-Resonazgas [96] (untere gestrichelte schwarze Linie). Die rote durchgezogene Linie stellt die minimale Einwirkung von Hagedornzuständen auf das Verhältnis von η/s dar und das blaue Band verdeutlicht den möglichen Effekt von Hagedornzuständen. Die durchgezogene schwarze Linie repräsentiert den aus der Stringtheorie abgeleiteten Wert von $\eta/s = 1/4\pi$ [61].

Darüber hinaus beschäftigt sich die Arbeit auch mit der Auswirkung von Hagedornzuständen auf thermische Fits. Hierbei wurde angenommen, dass die in Au+Au Kollisionen am RHIC (bei Schwerpunktsenergien von $\sqrt{s_{NN}} = 200$ GeV) gemessenen Teilchenverhältnisse einer rein statistichen Beschreibung am chemischen Ausfrierspunkt folgen. Die aus unserem Modell gewonnenen thermischen Fits ohne Einbeziehung von Hagedornzuständen stimmen gut mit anderen thermischen Fits [113] überein, wobei wir fast dieselbe Ausfrierstemperatur ($T_{ch} = 160.4$ MeV) und ein nur leicht größeres baryonischchemisches Potenzial ($\mu_b = 22.9$ MeV) erhalten. Unter Berücksichtigung der von der Particle Data Group gemessenen Teilchen liefern die thermischen Fits mit einem $\chi^2 = 21.2$ ein zufriedenstellendes Ergebnis (siehe Fig. 7.4). Das Einbeziehen der Hagedornzustände jedoch liefert eine noch bessere Beschreibung der experimentellen Daten. Mit einem $\chi^2 = 17.8$ erhalten wir eine Ausfriertemperatur von $T_{ch} = 172.6$ MeV und ein baryochemisches Potential von $\mu_b = 39.7$ MeV für eine Hagedorntemperatur von $T_H = 176$ MeV, während wir für eine Hagedorntemperatur von $T_H = 196$ MeV bei einem $\chi^2 = 20.9$ eine Ausfriertemperatur von $T_{ch} = 165.9$ MeV und ein baryochemisches Potential von $\mu_b = 20.9$ MeV bestimmen konnten (siehe Fig. 7.5). Dies zeigt, wie wichtig Hagedornzustände für die Beschreibung hadronischer Materie nahe der kritischen Temperatur T_c ist [30, 55, 56, 58]. Hierbei verdeutlicht das Ansteigen der chemischen Ausfriertemperatur von $T_{ch} = 160$ MeV auf $T_{ch} = 165$ MeV bzw. $T_{ch} = 172$ MeV unter Berücksichtigung von Hagedornzuständen die Unsicherheiten beim Extrahieren der thermodynamischen Parameter am chemischen Ausfrierspunkt.

In den nächsten Jahren wird der Large Hadron Collider (LHC, zu Deutsch "Großer Hadronen-Speicherring") viele neue wissenschaftliche Ergebnisse hervorbringen. Somit stellt sich die Frage, welche Rolle Hagedornzustände am LHC spielen werden. Die in dieser Arbeit vorgestellten Ergebnisse für ein dynamisches chemisches Gleichgewicht sollten von einer längeren QGP-Phase

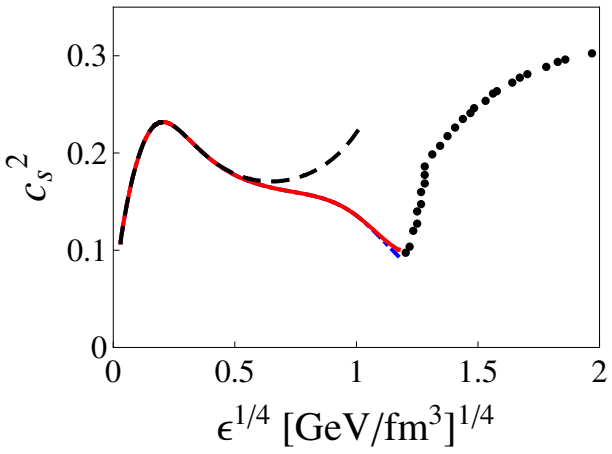

Figure 7.3: Das Quadrat der Schallgeschwindigkeit (c_s^2) als Funktion von $\varepsilon^2 1/4$ für ein dynamisches Modell mit Hagedornzuständen zwischen $2 < M < 12$ GeV (durchgezogene rote Linie) und für ein Hadrongas ohne Hagedornzustände (gestrichelte schwarze Linie) [72]. Die Punkte stellen die Ergebnisse aus Lattice-QCD Rechnungen dar [8]. Die blaue Linie wurde anahnd von Hagedornzuständen mit $2 < M < 80$ GeV berechnet.

nahezu unbeeinflußt bleiben. Der Grund hierfür ist, dass alle Berechunungen erst nach Erreichen der hadronische Phase gemacht wurden. Solange die Temperatur nahe der kritischen Temperatur T_c ist, ist es irrelevant, wie lange das QGP vorher existierte. Da die ursprüngliche Anzahl von Hadronen, die während des Ausfrierens erzeugt werden, aufgrund der schnellen Zerfälle aller Hagedornzuständen verwaschen ist, werden die Ergebnisse selbst dann nicht beeinflußt, wenn sich die Anfangsbedingungen für die unterschiedlichen Teilchen wie Pionen, Kaonen usw. von RHIC zu LHC unterscheiden. Da in dieser Arbeit das baryochemische Potential zu Null gesetzt wurde ($\mu_b = 0$) und am LHC vermutlich sehr kleine baryochemische Potentiale auftreten, kann das vorgestellt Modell sogar noch besser bei höheren Kollisionsenergien angewendet werden.

Jedoch könnte die Expansion des Feurballs am LHC die Ergebnisse durchaus beeinflussen, vornehmlich durch die Anzahl von Pionen. Da sich die Entropiedichte bei einer gegebenen Temperatur nicht verändert, würde ein solcher Anstieg der Pionenanzahl das Volumen vergrößern und damit zu einem Gesamtanstieg der Teilchenzahl führen. Die berechneten Teilchenverhältnisse blieben jedoch unbeeinflusst. Somit kann man erwarten, dass auch am LHC das chemische Gleichgewicht innerhalb sehr kurzer Zeit erreicht wird.

Eine Änderung in der Gesamtanzahl der Pionen hätte keine Wirkung auf das Verhältnis von η/s, da sich auch hier die Volumina gegenseitig wegheben. Ebenso bliebe die Zustandsgleichung, c_s^2, und die Scherviskosität unbeeinflusst. Daher sind die in der vorliegenden Arbeit untersuchten "fehlenden" Hagedornzustände für ein Verständnis der ablaufenden physikalischen Prozesse am LHC ebenso unerlässlich wie sie es für die am RHIC gewonnenen Resultate sind.

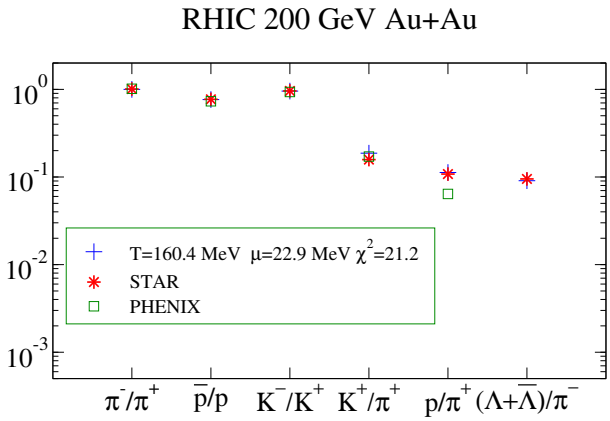

Figure 7.4: Thermische Fits für Au+Au Kollisionen am RHIC bei einer Schwerpunktsenergie von $\sqrt{s_{NN}} = 200$ GeV ohne Hagedornzustände.

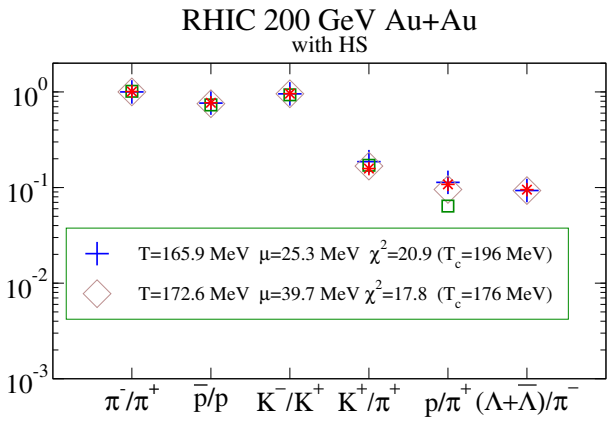

Figure 7.5: Thermische Fits für Au+Au Kollisionen am RHIC bei einer Schwerpunktsenergie von $\sqrt{s_{NN}} = 200$ GeV mit Hagedornzuständen.

Appendix A

Appendix: Hagedorn States in String Theory

The purpose of this appendix is to derive the number of partitions, $p(N)$, where $N \gg 1$. The end result should be

$$p_{24}(N) \approx \frac{1}{\sqrt{2}} N^{-27/4} \exp\left(4\pi\sqrt{N}\right). \tag{A.1}$$

In order to find the formula for the number of partitions of large integers we look to a quantum non-relativistic string, which has an infinite set of vibrating frequencies that are all multiples of the basic frequency ω_0. Thus, the quantum string is a collection of simple harmonic oscillators with the frequencies ω_0, $2\omega_0$, etc. The energy of a simple harmonic oscillator, assuming that the total number of excitations N is large, is

$$E = \omega_0 N \tag{A.2}$$

N is a large fixed positive integer. The number of states with the eigenvalue $\hat{N}$ ($\hat{N} = \sum_{l=1}^{\infty} l a_l^\dagger a_l$ where a_l and $a_l^\dagger$ annihilation and creation operators, respectively) equal to N is known as $p(N)$ or the number of partitions of N. $p(N)$ is determined by the number of different sets of positive integers that add to N. For example, the partitions of $N = 5$ are: $\{5\}$, $\{4,1\}$, $\{3,2\}$, $\{3,1,1\}$, $\{2,2,1\}$, $\{2,1,1,1\}$, and $\{1,1,1,1,1\}$, which means that $p(5) = 7$. A formula to describe $p(N)$ for all N is unknown but for large N, $\ln N$ can be described. Recalling the entropy in Eq. (1.22) and using Eq. (A.2), we find

$$S(E) = \ln p(N) = \ln p\left(\frac{E}{\hbar\omega_0}\right) \tag{A.3}$$

where $\Omega(E)$ is nothing other than $p(N)$. The entropy can be determined by calculating the partition function Z for the quantum non-relativistic string, which can then be used to calculate the free energy F. The free energy, F, can be determined through

$$F = E - TS, \tag{A.4}$$

which leads to

$$dF = -SdT - pdV. \tag{A.5}$$

Additionally, the free energy can be calculated from the partition function

$$F = -T \ln Z. \tag{A.6}$$

The free energy then allows us to calculate the temperature, entropy and pressure (using $S = (E + P)/T$ the energy could also be calculated)

$$T = \left(\frac{\partial S}{\partial E}\right)^{-1} \qquad S = -\left(\frac{\partial F}{\partial T}\right)_V, \qquad p = \left(\frac{\partial F}{\partial V}\right)_T. \tag{A.7}$$

It is only possible to explicitly determine F at high temperatures and from there $S(E)$ is found.

The partition function of a quantum non-relativistic string is

$$\begin{aligned} Z &= \sum_\alpha \exp\left(-\frac{E_\alpha}{T}\right) = \sum_{n_1,n_2,n_3,\ldots} \exp\left[-\frac{\omega_0}{T}(n_1 + 2n_2 + 3n_3 + ...)\right] \\ &= \sum_{n_1} \exp\left[-\frac{\omega_0}{T} n_1\right] \cdot \sum_{n_2} \exp\left[-\frac{\omega_0}{T} 2n_2\right] \\ &= \prod_{l=1}^{\infty} \sum_{n_l=0}^{\infty} \exp\left(-\frac{\omega_0 l n_l}{T}\right). \end{aligned} \tag{A.8}$$

However, Eq. (A.8) contains a geometric series, which can be rewritten as

$$Z = \prod_{l=1}^{\infty} \left[1 - \exp\left(-\frac{\omega_0 l}{T}\right)\right]^{-1}. \tag{A.9}$$

Substituting Eq. (A.9) into Eq. (A.6), we find the free energy

$$Z = T \sum_{n_l=0}^{\infty} \ln\left[1 - \exp\left(-\frac{\omega_0 l}{T}\right)\right]. \tag{A.10}$$

If we look only at high temperatures, such that $\frac{\omega_0 l}{T} \ll 1$, the difference between the terms in the sum shrink such a way that we can approximate the sum by an integral

$$F = T \int_{l=1}^{\infty} \ln\left[1 - \exp\left(-\frac{\omega_0 l}{T}\right)\right] dx. \tag{A.11}$$

and choosing l=1 plays (as compared to another small number) no role. We can then integrate over 'x' instead where

$$x = \frac{\omega_0}{T} \tag{A.12}$$

so that

$$F \approx \frac{T^2}{\omega_0} \int_0^{\infty} dx \ln(1 - e^{-x}) \tag{A.13}$$

and then use the expansion

$$\ln(1 - y) = -\left(y + \frac{1}{2}y^2 + \frac{1}{3}y^3 + ...\right), \tag{A.14}$$

which is valid as long as $0 \leq y < 1$. It follows then that

$$\begin{aligned} F &\approx \frac{T^2}{\omega_0}\int_0^\infty dx\left(e^{-x}+\frac{1}{2}e^{-2x}+\frac{1}{3}e^{-3x}+...\right) \\ &\approx \frac{T^2}{\omega_0}\left[1+\frac{1}{2^2}+\frac{1}{3^3}+...\right]. \end{aligned} \tag{A.15}$$

The sum can be expressed as a zeta function

$$\zeta(2) = 1+\frac{1}{2^2}+\frac{1}{3^3}+... = \frac{\pi^2}{6}, \tag{A.16}$$

which can be substituted into Eq. (A.15)

$$F \approx -\frac{T^2\pi^2}{\omega_0 6} = -\frac{\pi^2}{\omega_0 6\beta^2}. \tag{A.17}$$

From the free energy we can calculate the energy

$$E = \frac{\partial \ln Z}{\partial \beta} = -\frac{\pi^2 T^2}{6\omega_0} \tag{A.18}$$

and the entropy

$$S = -\frac{\partial F}{\partial T} = \frac{\pi^2 T}{3\omega_0}, \tag{A.19}$$

which leads to

$$S(E) = \pi\sqrt{\frac{2}{3}\frac{E}{\omega_0}} \tag{A.20}$$

and substituting in Eq. (A.2)

$$S(E) = 2\pi\sqrt{\frac{N}{6}}. \tag{A.21}$$

Then using Eq. (A.3),

$$\ln p(N) \approx 2\pi\sqrt{\frac{N}{6}}, \tag{A.22}$$

which is the first term in the Hardy-Ramanujan asymptotic expansion of $p(N)$ [67]

$$p(N) \approx \frac{1}{4N\sqrt{3}}\exp\left(2\pi\sqrt{\frac{N}{6}}\right). \tag{A.23}$$

Assuming that a quantum string can vibrate in b transverse directions, we have b harmonic oscillators for each frequency $l\omega_0$. Thus, we have the partition function Z_b with the occupation

numbers $n_k^{(q)}$ where $k = 1, 2, ..., \infty$ and $q = 1, 2, ..., b$ such that (in natural units $\hbar = k_B = 1$)

$$\begin{aligned} Z_b &= \sum_{n_k^{(1)},...,n_k^{(b)}} \exp\left[-\frac{\omega_0}{T}\sum_{t=0}^{\infty}\sum_{q=1}^{b} ln_l^{(q)}\right] \\ &= \sum_{n_k^{(1)}} \exp\left[-\frac{\omega_0}{T}\sum_{t=0}^{\infty} ln_l^{(1)}\right] ... \sum_{n_k^{(b)}} \exp\left[-\frac{\omega_0}{T}\sum_{t=0}^{\infty} ln_l^{(b)}\right] \\ &= (Z)^b. \end{aligned} \tag{A.24}$$

The free energy F_b is then

$$F_b = -T \ln Z_b = -Tb \ln Z = bF, \tag{A.25}$$

which implies that the entropy is

$$S_b = bS \tag{A.26}$$

and the energy is

$$E_b = bE = \omega_0 N \tag{A.27}$$

where $N = \sum_{l,q} ln_l^{(q)}$, because they are both simply derivatives of the free energy and b being a constant can be pulled out of the derivative. From Eq. (A.21) we see that the entropy becomes

$$S_b = 2\pi\sqrt{\frac{Nb}{6}}. \tag{A.28}$$

Recalling Eq. (A.3),

$$\ln p_b(N) \approx 2\pi\sqrt{\frac{Nb}{6}} \tag{A.29}$$

Here we consider only bosonic strings, which have $b = 24$ transverse light-cone directions

$$p_{24}(N) \approx \frac{1}{\sqrt{2}} N^{-27/4} \exp\left(4\pi\sqrt{N}\right), \tag{A.30}$$

which allows us to arrive at our desired $p_{24}(N)$.

Appendix B

Derivation of Volume Corrections

The volume corrections given in Chapter 2 in Eq. (2.3) are derived in this appendix for $\mu_b = 0$. The derivation of which is originally shown in [70] (see also [71]).

Initially we start with the partition function of a non-interacting point particle where the particles are treated relativistically but with Boltzman statistics

$$Z_{pt}(\beta, V) = \sum_{N=0}^{\infty} \frac{1}{N!} \prod_{i=1}^{N} \int \frac{d^3p}{(2\pi)^3} dm_i \rho(m_i) V^N e^{-\beta\epsilon_i} \tag{B.1}$$

where $\rho(m_i)$ is the mass spectrum, $\beta = 1/T$, and $\epsilon_i = \left(p^2 + m_i^2\right)^{1/2}$.

Then the point particle thermodynamic quantities can be found

$$\begin{aligned}
P_{pt}(\beta) &= \frac{\ln Z_{pt}(\beta, V)}{\beta V} \\
&= \frac{1}{\beta} \int \frac{d^3p}{(2\pi)^3} dm_i \rho(m_i) e^{-\beta\epsilon} \\
n_{pt}(\beta) &= \beta P_{pt}(\beta) \\
&= \int \frac{d^3p}{(2\pi)^3} dm_i \rho(m_i) e^{-\beta\epsilon} \\
\epsilon_{pt}(\beta) &= -\frac{dP_{pt}(\beta)}{d\beta} \\
&= \int \frac{d^3p}{(2\pi)^3} dm_i \rho(m_i) \epsilon e^{-\beta\epsilon} \\
S_{pt}(\beta) &= \frac{P_{pt}(\beta) + \epsilon_{pt}(\beta)}{\beta} \\
&= \int \frac{d^3p}{(2\pi)^3} dm_i \rho(m_i) \left[1 + \beta\epsilon\right] e^{-\beta\epsilon}
\end{aligned} \tag{B.2}$$

.

According to the MIT bag model, hadrons have a mass dependent volume, $V = m/(4B)$

where B is the bag constant. If we replace the volume in Eq. (B.1) by

$$V \to V - \sum_{j=1}^{\infty} \frac{\epsilon_j}{4B}, \tag{B.3}$$

then the available volume that the hadrons are allowed to move in is diminished by the volume size of the hadrons themselves. The energy is used instead of the mass due to relativity. Eq. (B.1) then becomes

$$Z_{pt}(\beta, V) = \sum_{N=0}^{\infty} \frac{1}{N!} \prod_{i=1}^{N} \int \frac{d^3p}{(2\pi)^3} dm_i \rho(m_i) \left[V - \sum_{j=1}^{\infty} \frac{\epsilon_j}{4B} \right]^N e^{-\beta\epsilon_i}. \tag{B.4}$$

To simply future calculates, we let $V_0 = \sum_{j=1}^{\infty} \frac{\epsilon_j}{4B}$. In order to further solve Eq. (B.4), we use the Laplace transform

$$\hat{Z}(\beta, \zeta) = \int_0^{\infty} dV Z(\beta, V) e^{-\zeta V}. \tag{B.5}$$

Substituting in Eq. (B.4) into Eq. (B.5),

$$\hat{Z}(\beta, \zeta) = \sum_{N=0}^{\infty} \frac{1}{N!} \prod_{i=1}^{N} \int \frac{d^3p}{(2\pi)^3} dm_i \rho(m_i) e^{-\beta\epsilon_i} \int_{V_0}^{\infty} dV \left[V - V_0 \right]^N e^{-\zeta V}. \tag{B.6}$$

Then integral over the volume can be solved such that

$$\int_{V_0}^{\infty} dV \left[V - V_0 \right]^N e^{-\zeta V} = \frac{e^{-\zeta V_0}}{\zeta^{N+1}} \Gamma(1+N) = \frac{e^{-\zeta V_0}}{\zeta^{N+1}} N!, \tag{B.7}$$

which can be substituted into Eq. (B.6)

$$\hat{Z}(\beta, \zeta) = \sum_{N=0}^{\infty} \prod_{i=1}^{N} \int \frac{d^3p}{(2\pi)^3} dm_i \rho(m_i) e^{-\beta\epsilon_i} \frac{e^{-\zeta V_0}}{\zeta^{N+1}}. \tag{B.8}$$

Substituting in V_0,

$$\hat{Z}(\beta, \zeta) = \frac{1}{\zeta} \sum_{N=0}^{\infty} \left[\frac{1}{\zeta} \int \frac{d^3p}{(2\pi)^3} dm \rho(m) e^{-\epsilon\left(\beta + \frac{\zeta}{4B}\right)} \right]^N. \tag{B.9}$$

Using the indentity,

$$\sum_{N=0}^{\infty} x^N = \frac{1}{1-x}, \tag{B.10}$$

we can rearrange Eq. (B.9)

$$\hat{Z}(\beta, \zeta) = \left[\zeta - \int \frac{d^3p}{(2\pi)^3} dm \rho(m) e^{-\epsilon\left(\beta + \frac{\zeta}{4B}\right)} \right]^{-1}. \tag{B.11}$$

However, we can define

$$\beta^* = \beta + \frac{\zeta}{4B} \tag{B.12}$$

and substitute it into Eq. (B.11)

$$\begin{aligned} \hat{Z}\left(\beta^*, \zeta\right) &= \left[\zeta - \int \frac{d^3p}{(2\pi)^3} dm \rho(m) e^{-\epsilon\beta^*}\right]^{-1} \\ &= \left[\zeta - F(\beta*, \zeta)\right]^{-1}. \end{aligned} \tag{B.13}$$

Then Eq. (B.13) has a pole of ζ^* at $\zeta = F(\beta*, \zeta)$, which is the pressure in the thermodynamic limit i.e.

$$\zeta^* = \beta P_{cor}(\beta) = \int \frac{d^3p}{(2\pi)^3} dm \rho(m) e^{-\epsilon\beta^*}. \tag{B.14}$$

For the point particle (using Eq. (B.2)),

$$\begin{aligned} \beta^* P_{pt}(\beta^*) &= \int \frac{d^3p}{(2\pi)^3} dm_i \rho(m_i) e^{-\beta^*\epsilon} \\ &= \beta P_{cor}(\beta) \end{aligned} \tag{B.15}$$

or in other words

$$\begin{aligned} \beta &= \beta^* - \frac{\beta^* P_{pt}(\beta^*)}{4B} = \frac{\beta^* P_{pt}(\beta^*)}{P_{cor}(\beta)} \\ P_{cor}(T) &= \frac{P_{pt}(T^*)}{1 - \frac{P_{pt}(T^*)}{4B}}, \end{aligned} \tag{B.16}$$

which also leads to

$$T = \frac{T^*}{1 - \frac{P_{pt}(T^*)}{4B}}. \tag{B.17}$$

Using $P_{cor}(T)$ and T the rest of the thermodynamic quantities can be calculated as see in Eq. (2.3).

Appendix C

Master Equations

C.1 Markov Process

A Markov process is a process in which the probability of a transition at time t_{n-1} to time t_n from a point y_{n-1} to y_n is dependent only at the value of y at point t_{n-1} and not on y at any time before $t < t_{n-1}$. The condition probability is $P_{1|1}(y_2, t_2|y_1, t_1)$, which is defined using the following relation

$$P_2(y_1, t_1; y_2, t_2) = P_{1|1}(y_2, t_2|y_1, t_1) P_1(y_1, t_1). \tag{C.1}$$

Basically, Eq. (C.1) describes the probability of finding both y_1 at t_1 and y_2 at t_2, which is found by multiplying the probability $(P_1(y_1, t_1))$ of finding y_1 at t_1 with the probability $(P_{1|1}(y_2, t_2|y_1, t_1))$ of finding y_2 at t_2 given that y_1 is at t_1. Moreover, the conditional probability must also satisfy the following

- $P_{1|1} \geq 0$
- $\int P_{1|1}(y_2, t_2|y_1, t_1)\, dy_2 = 1$
- $P_1(y_2, t_2) = \int P_{1|1}(y_2, t_2|y_1, t_1) P_1(y_1, t_1)\, dy_1$

Using the 3^{rd} relation it means that integrating Eq. (C.1) over y_1 yields

$$\int P_2(y_1, t_1; y_2, t_2)\, dy_1 = P_1(y_2, t_2). \tag{C.2}$$

Therefore, a Markov process would then be defined by Eq. (C.1)

$$P_{1|n-1}(y_n, t_n|y_{n-1}, t_{n-1}; ...; y_1, t_1) = P_{1|1}(y_n, t_n|y_{n-1}, t_{n-1}) \tag{C.3}$$

where $t_1 < t_2 < ... < t_n$ because all early times and positions before t_{n-1} are irrelevant. For $n \geq 3$ in a Markov process all the probabilities can be rewritten in terms of P_1 and $P_{1|1}$. Looking specifically at $n = 3$,

$$\begin{aligned} P_3(y_1, t_1; y_2, t_2; y_3, t_3) &= P_{1|2}(y_3, t_3|y_1, t_1; y_2, t_2) P_2(y_1, t_1; y_2, t_2) \\ &= P_{1|1}(y_3, t_3|y_2, t_2) P_{1|1}(y_2, t_2|y_1, t_1) P_1(y_1, t_1). \end{aligned} \tag{C.4}$$

Then integrating Eq. (C.4) over y_2, the left side of the equation becomes

$$\begin{aligned}\int P_3\left(y_1,t_1;y_2,t_2;y_3,t_3\right)dy_2 &= P_2\left(y_1,t_1;y_3,t_3\right)\\ &= P_{1|1}\left(y_3,t_3|y_1,t_1\right)P_1\left(y_1,t_1\right)\end{aligned} \tag{C.5}$$

and the right side of the equation in Eq. (C.4) becomes

$$P_1\left(y_1,t_1\right)\int P_{1|1}\left(y_3,t_3|y_2,t_2\right)P_{1|1}\left(y_2,t_2|y_1,t_1\right)dy_2. \tag{C.6}$$

We can then divide both Eq. (C.5) and Eq. (C.6) by $P_1\left(y_1,t_1\right)$ and equate them, which allows us to arrive at the Chapman-Kolmogorov equation

$$P_{1|1}\left(y_3,t_3|y_1,t_1\right)=\int P_{1|1}\left(y_3,t_3|y_2,t_2\right)P_{1|1}\left(y_2,t_2|y_1,t_1\right)dy_2, \tag{C.7}$$

which implies that a process starting at t_1 with the value y_1 reaches y_3 at time t_3 via any possible values for y_2 at the time t_2.

C.2 Deriving Master Equations

The Chapman-Kolmogorv uses a special notation for the transition probability:

$$P_{1|1}\left(y_2,t_2|y_1,t_1\right) = T_\tau\left(y_2|y_1\right) \tag{C.8}$$

$$T_{\tau+\tau'}\left(y_3|y_1\right) = \int T_{\tau'}\left(y_3|y_2\right)T_\tau\left(y_2|y_1\right) \tag{C.9}$$

We can then expand the transition probability using a Taylor series over zero

$$T_{\tau'}\left(y_3|y_2\right)=\delta(y_3-y_2)+\tau' W\left(y_3|y_2\right)+\mathcal{O}\left(\tau'^2\right) \tag{C.10}$$

where

$$W\left(y_3|y_2\right)=\frac{dT_\tau\left(y_3|y_2\right)}{dt}|_{\tau'=0}. \tag{C.11}$$

The delta function in Eq. (C.10) is the probability to stay at the same state after time zero equals one whereas the probability to change state after time zero equals zero.

Due to the second property above that the transition probability must be normalized, the integral over y_3 must be equal to one. Therefore, a correction term is added

$$T_{\tau'}\left(y_3|y_2\right)=\left(1-\alpha_0\tau'\right)\delta(y_3-y_2)+\tau' W\left(y_3|y_2\right)+\mathcal{O}\left(\tau'^2\right) \tag{C.12}$$

where the $-\alpha_0\tau'$ term takes into account the possibility for no transitio to take place and must then equal

$$\alpha_0\left(y_2\right)=\int W\left(y_3|y_2\right)dy_3. \tag{C.13}$$

Substituting Eq. (C.12) into Eq. (C.9),

$$\begin{aligned} T_{\tau+\tau'}(y_3|y_1) &= \int T_{\tau'}(y_3|y_2)\, T_\tau(y_2|y_1)\, dy_2 \\ &= \int \left[(1-\alpha_0\tau')\,\delta(y_3-y_2) + \tau' W(y_3|y_2)\right] T_\tau(y_2|y_1)\, dy_2 \\ &= \int T_\tau(y_2|y_1)\,\delta(y_3-y_2)dy_2 - \tau' \int \alpha_0 T_\tau(y_2|y_1)\,\delta(y_3-y_2)dy_2 \\ &+ \tau' \int W(y_3|y_2)\, T_\tau(y_2|y_1)\, dy_2 \\ &= T_\tau(y_3|y_2) + \tau' \int \left[W(y_3|y_2)\, T_\tau(y_2|y_1) - W(y_2|y_3)\, T_\tau(y_3|y_1)\right] dy_2 \\ \frac{T_{\tau+\tau'}(y_3|y_1) - T_\tau(y_3|y_1)}{\tau'} &= \int \left[W(y_3|y_2)\, T_\tau(y_2|y_1) - W(y_2|y_3)\, T_\tau(y_3|y_1)\right] dy_2. \end{aligned} \tag{C.14}$$

Taking the limit of $\tau' \to 0$, we arrive at the master equation

$$\frac{\delta T_\tau(y_3|y_1)}{\delta\tau} = \int \left[W(y_3|y_2)\, T_\tau(y_2|y_1) - W(y_2|y_3)\, T_\tau(y_3|y_1)\right] dy_2. \tag{C.15}$$

Master equations, otherwise known as rate equations, are a set of first-order differential equations. We can then relabel the indicies in Eq. (C.15)

$$\frac{\delta P(y,t)}{\delta t} = \int \left[W(y|y')\, P(y',t) - W(y'|y)\, P(y,t)\right] dy'. \tag{C.16}$$

Additionally, if all y's are discrete

$$\frac{\delta p_n(t)}{\delta t} = \sum_{n'} \left[W_{nn'} p'_n(t) - W_{n'n} p_n(t)\right] dy'. \tag{C.17}$$

The first term in Eq. (C.17) is the gain term from other $n' \to n$ states, while the second term is the loss term from $n \to n'$ states. Thus, Eq. (C.17) has the form

$$\dot{n} = \text{“}gain\text{”} + \text{“}loss\text{”} \tag{C.18}$$

where we can observe the change in the number of n over time.

C.3 Detailed Balance

There could be multiple gain and/or loss terms depending on the reactions the master equations describe. For instance, for the decay $k \leftrightarrow i + j$ where k, i, and j are all either particles or resonances,

$$\dot{N}_k = -\Gamma_k N_k + \langle \sigma_{ij} v_{ij} \rangle N_i N_j \tag{C.19}$$

where Γ is the decay width, which is the inverse of the mean lifetime for a particle and,therefore, the probability for the k particle to decay is contaiend within Γ, $\langle \sigma_{ij} v_{ij} \rangle$ is the thermally averaged total cross-section for the i and j particles, and N is the total number of particles (we use n to

describe the density of particles and N is the total number). but at equilibrium rate equations reach a fixed point such that $\dot{N}_k = 0$,

$$\begin{aligned} \Gamma_k N_k^{eq} &= \langle \sigma_{ij} v_{ij} \rangle N_i^{eq} N_j^{eq} \\ \langle \sigma_{ij} v_{ij} \rangle &= \frac{N_k^{eq}}{N_i^{eq} N_j^{eq}} \Gamma_k \end{aligned} \tag{C.20}$$

where the prefactor in front of Γ_k ensure detailed balance. Therefore, Eq. (C.19) becomes

$$\dot{N}_k = -\Gamma_k \left[N_k + \frac{N_k^{eq}}{N_i^{eq} N_j^{eq}} N_i N_j \right] \tag{C.21}$$

or in the $\lambda = N/N^{eq}$ form

$$\dot{\lambda}_k = -\Gamma_k \left[\lambda_k + \lambda_i \lambda_j \right]. \tag{C.22}$$

Appendix D

Appendix: Analytical Solutions

In order to make an estimate for the chemical equilibration time we first look at what happens to the rate equations at a constant temperature. Moreover, we consider only the dynamics between the Hagedorn states and the pions, i.e., $HS \leftrightarrow n\pi$,

$$\begin{aligned} \dot{N}_i &= \Gamma_i \left[N_i^{eq} \sum_{n=2} B_{i,n} \left(\frac{N_\pi}{N_\pi^{eq}} \right)^n - N_i \right] \\ \dot{N}_\pi &= \sum_i \Gamma_i \left[N_i \langle n \rangle - N_i^{eq} \sum_{n=2} B_{i,n} n \left(\frac{N_\pi}{N_\pi^{eq}} \right)^n \right], \end{aligned} \tag{D.1}$$

which is repeated here from Eq. (3.1) for convenience. Using this simplified set of rate equations we are then able to find an analytical solution at high temperatures. Additionally, it provides us with a better understanding of the underlying mechanics that drive the hadrons into chemical equilibrium.

D.0.1 Pions in Equilibrium

The simplest case is when the pions are held constant at α. Substituting in α for λ_π, the rate equation for the Hagedorn resonances becomes

$$\dot{\lambda}_i = \Gamma_i \left[\langle \alpha^n \rangle - \lambda_i \right] \tag{D.2}$$

where $\langle \alpha^n \rangle = \sum_{n=2} B_{i,n} \alpha^n$,which we can solve analytically

$$\lambda_i = \langle \alpha^n \rangle + \left(\beta_i + \langle \alpha^n \rangle \right) e^{-\frac{t}{\tau_i}} \tag{D.3}$$

where β_i is the initial value for the i^{th} resonance. Clearly, the pion rate equation is equal to zero because the pions are held constant. The chemical equilibration time is then the inverse of the decay width so

$$\tau_i = \frac{1}{\Gamma_i}. \tag{D.4}$$

Taking $\alpha = 1$ and $\beta_i = 0$, which implies that the pions are held constant at equilibrium, we

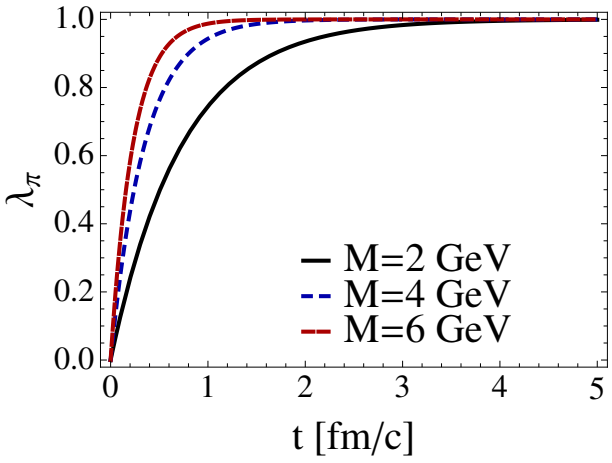

Figure D.1: Fugacity of the Hagedorn resonances for various masses. No temperature is given because the time scale is independent of the temperature; it just depends on the decay width as seen in Eq. (D.4).

can plot our numerical results as shown in Fig. D.1. Additionally, the equilibrium times of the Hagedorn states are shown in Fig. 3.1.

There is no temperature dependence in Eq. (D.3). The resulting equation is only dependent on the intial conditions (α and β_i) and on the decay widths of the Hagedorn states. However, when the pions are not held constant, the rate equations are then dependent on the temperature as seen in the next section. Because the chemical freezeout time is the inverse of the decay width, the heavier Hagedorn states equilibrate the quickest.

D.0.2 Hagedorn States in Equilibrium

When the resonances are held constant at β_i and the pions are allowed to freely equilibrate, we can once again solve Eq. (3.1) analytically. Using this assumption, the rate equation for the pions becomes

$$\dot{\lambda}_\pi = \sum_i^\infty \Gamma_i \frac{N_i^{eq}}{N_\pi^{eq}} \left[\beta_i \langle n \rangle - \sum_{n=2} B_{i,n} n \lambda_\pi^n \right]. \tag{D.5}$$

However, Eq. (D.5) is not as easy to solve analytically as Eq. (D.2) due to the sum over the branching ratios. Instead, we must first consider the initial value of λ_π. If $\alpha \approx 0$ then

$$\dot{\lambda}_\pi = \sum_i^\infty \Gamma_i \frac{N_i^{eq}}{N_\pi^{eq}} \beta_i \langle n \rangle, \tag{D.6}$$

which can easily be integrated

$$\lambda_\pi = \left(\frac{t}{\tau_\pi^0} + \alpha \right) \tag{D.7}$$

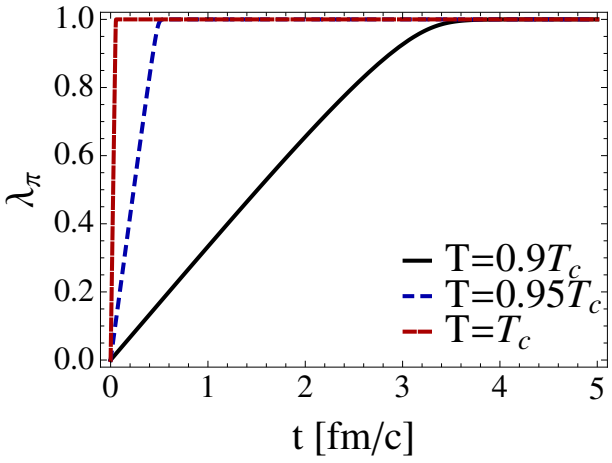

Figure D.2: Results for fugacity of the pions when the Hagedorn resonances are held in equilibrium.

where the equilibration time is defined as

$$\tau_\pi^0 = \frac{N_\pi^{eq}}{\sum_i \Gamma_i N_i^{eq} \langle n \rangle \beta_i} \, . \tag{D.8}$$

Unlike in the case where the pions were held in chemical equilibrium, Eqs. (D.7,3.3) are dependent on the temperature due to N_π^{eq} and N_i^{eq} being in the chemical freezeout time. As before there is a dependence on the initial conditions and the decay widths. Moreover, there is a dependence on the branching ratios, which appears in $\langle n \rangle$, and on the initial conditions from β_i.

As the pions near chemical equilibrium, our approximation of $\lambda_\pi \approx 0$ no longer holds and we instead assume $\lambda_\pi \approx 1$. Returning to Eq. (D.5), we can substitute in $\lambda_\pi = 1 - \epsilon$ and use the approximation $(1-\epsilon)^n = 1 - n\epsilon$

$$\dot{\epsilon} \;\; = \;\; -\sum \Gamma_i \frac{N_i^{eq}}{N_\pi^{eq}} \left((\beta_i - 1)\langle n \rangle + \langle n^2 \rangle \epsilon \right) \, . \tag{D.9}$$

After integration we use $\epsilon(t_0) = 1 - \eta$ where η is a point when the pions are near equilibrium and t_0 is the time when the pions reach η. We then take η as a free paramenter and choose a value that best fits the data. We obtain

$$\lambda_\pi = \left(1 + \gamma - (1 + \gamma - \eta) \, e^{-\frac{t - t_0}{\tau_\pi}} \right) \tag{D.10}$$

where $\gamma = \frac{\sum_i \Gamma_i N_i^{eq} (\beta_i - 1) \langle n \rangle}{\sum_i \Gamma_i N_i^{eq} \langle n^2 \rangle}$ and our equilibration time is defined as

$$\tau_\pi = \frac{N_\pi^{eq}}{\sum_i \Gamma_i N_i^{eq} \langle n^2 \rangle} \, . \tag{D.11}$$

Thus, we see linear growth when there are no initial pions. However, as they approach chemical equilibrium they undergo an exponential growth. A comparison betwen both τ_π^0 and τ_π is later shown in Fig. 3.1. Again, we see a dependence on the temperature, the decay widths, and branching ratios. However, here there is no dependence on the initial conditions.

D.1 All Particles Out of Equilibrium

If our initial conditions are such that both the pions and Hagedorn states begin far out of chemical equilibrium, we can find an analytical solution by subdividing the analysis into three distinct stages. Initially, during stage 1 the pions are underpopulated such that we can say that they approximately begin at $\alpha \approx 0$ (we can also start the pions above zero and the approximation works well). Because the pions reach chemical equilibrium much quicker than the Hagedorn states due to all the Hagedorn states decaying quickly into pions, then we can make the approximation that the Hagedorn states are held at their initial value of β_i. One can see this from the difference in the time scales from Tab. 3.1 where $\tau_i > \tau_\pi^0$ and $\tau_i > \tau_\pi$. Since $\alpha \approx 0$ we let $\lambda_\pi^n \approx 0$, then substituting this into Eq. (3.1) we obtain

$$\begin{aligned} \dot{\lambda}_\pi &= \sum \Gamma_i \frac{N_i^{eq}}{N_\pi^{eq}} \beta_i \langle n_i \rangle, \\ \lambda_\pi &= \left(\frac{t}{\tau_\pi^0} + \alpha \right) , \end{aligned} \tag{D.12}$$

which is the fugacity of the pions in stage 1 and gives $\tau_\pi^0 \equiv \frac{N_\pi^{eq}}{\sum_i \Gamma_i N_i^{eq} \langle n_i \rangle \beta_i}$. Again using the approximation $\alpha \approx 0$ and substituting Eq. (D.12) into the Hagedorn state rate equation in Eq. (3.1), with the solution

$$\begin{aligned} \dot{\lambda}_i &= \Gamma_i \left[\left(\frac{t}{\tau_\pi^0} \right)^{\langle n_i \rangle} - \lambda_i \right], \\ \lambda_i &= \left[1 - \langle n_i \rangle \left(\frac{-t}{\tau_i} \right)^{-\langle n_i \rangle} e^{-\left(\frac{t}{\tau_i}\right)} \int_0^{-\frac{t}{\tau_i}} x^{\langle n_i \rangle - 1} e^{-x} dx \right] \\ &\quad \cdot \left(\frac{t}{\tau_\pi^0} \right)^{\langle n_i \rangle} + \beta_i e^{-\left(\frac{t}{\tau_i}\right)}. \end{aligned} \tag{D.13}$$

Substituting $x = \frac{t}{\tau_i}\xi$ into the integral in Eq. (D.13), expanding the exponential inside the integral so $e^y = \sum_{j=0}^{\infty} \frac{y^j}{j!}$, and integrating over ξ, provides us with the fugacity of the Hagedorn states in stage 1

$$\begin{aligned} \lambda_i &= \left(\frac{t}{\tau_\pi^0} \right)^{\langle n_i \rangle} \left[1 - e^{-\left(\frac{t}{\tau_i}\right)} \sum_{j=0}^{\infty} \frac{\langle n_i \rangle}{j! (\langle n_i \rangle + j)} \left(\frac{t}{\tau_i} \right)^j \right] \\ &\quad + \beta_i e^{-\left(\frac{t}{\tau_i}\right)} . \end{aligned} \tag{D.14}$$

Therefore, Eq. (D.12) and Eq. (D.14) describe the behaviour of the pions and Hagedorn states during the initial stage of the evolution towards chemical equilibrium. They are then compared to the numerical results in Fig. D.3.

As the pions near equilibrium our approximation of $\lambda_\pi \approx 0$ no longer holds and we switch to stage 2 where we assume $\lambda_\pi \approx 1$ at time t_1. Here t_1 is a time when the pions are almost in chemical equilibrium, which is normally taken when the pions reach about $\sim 95\%$ of their chemical equilibrium value. Returning to the pion equation in Eq. (3.1), we can substitute in $\lambda_\pi = 1 - \epsilon$ and use the approximation $(1-\epsilon)^n \approx 1 - n\epsilon$

$$\dot{\epsilon} \;=\; -\sum \Gamma_i \frac{N_i^{eq}}{N_\pi^{eq}} \left((\beta_i - 1)\langle n_i \rangle + \langle n_i^2 \rangle \epsilon \right) \; . \tag{D.15}$$

Additionally, we substituted in β_i for λ_i as an approximation since the Hagedorn states do not change significantly in Stage 1 (the majority of the evolution is done by the pions). Recall that $\beta_i = \lambda_i(t=0)$ and it is a constant. In its present form, Eq. (D.15) can be integrated. We also define $\epsilon(t_1) = 1 - \eta$ where η is close to 1 (η is the measurement of how close the pions are to their equilibrium value when we switch from Stage 1 to Stage 2). Then, after integration

$$\lambda_\pi = \left(1 + \gamma - (1 + \gamma - \eta)\, e^{-\frac{t-t_1}{\tau_\pi}} \right) \tag{D.16}$$

where $\gamma = \frac{\sum_i \Gamma_i N_i^{eq} (\beta_i - 1)\langle n_i \rangle}{\sum_i \Gamma_i N_i^{eq} \langle n_i^2 \rangle}$ and $\tau_\pi \equiv \frac{N_\pi^{eq}}{\sum_i \Gamma_i N_i^{eq} \langle n_i^2 \rangle}$. Analogously to stage 1, we substitute the pion equation, i.e., Eq. (D.16) into the Hagedorn resonance equation in Eq. (3.1) and integrate

$$\begin{aligned} \lambda_i \;&=\; \Big[d e^{-\frac{t-t_1}{\tau_i}} + 1 + \langle n_i \rangle \gamma \\ &-\; \left(\frac{\tau_\pi}{\tau_\pi - \tau_i} \right) \langle n_i \rangle \, (1 + \gamma - \eta)\, e^{-\frac{t-t_1}{\tau_\pi}} \Big] \end{aligned} \tag{D.17}$$

where $d = \omega_i - 1 + \langle n_i \rangle \gamma + \left(\frac{\tau_\pi}{\tau_\pi - \tau_i} \right) \langle n_i \rangle \, (1 + \gamma - \eta)$ and $\lambda_i(t_1) = \omega_i$. Thus, our equations for the evolution of the pions and Hagedorn states are Eq. (D.16) and Eq. (D.17), respectively. As with stage 1, the evolution equation for the Hagedorn states is dictated by that of the pions.

Stage 3 i.e. quasi-equilibrium begins once the pions and at least one species of Hagedorn resonances (τ_{7GeV} is the shortest chemical equilibration time) has surpassed its equilibration time (τ_π and τ_i, respectively). To understand quasi-equilibrium we must use the effective pion number

$$\tilde{N}_\pi = N_\pi + \sum_i N_i \langle n_i \rangle \; , \tag{D.18}$$

because we need a variable that can observe the effects of both the pions and resonances. The effective pion number essentially includes the number of effective pions that each Hagedorn state could decay into. Thus, we start by taking the derivative of Eq. (D.18) in terms of its fugacity

$$\begin{aligned} \dot{\tilde{\lambda}}_\pi \;&=\; \frac{1}{\tilde{N}_\pi^{eq}} \left[N_\pi^{eq} \dot{\lambda}_\pi + \sum_i N_i^{eq} \dot{\lambda}_i \langle n_i \rangle \right] \\ &=\; \frac{\sum_i \Gamma_i N_i^{eq}}{\tilde{N}_\pi^{eq}} \left[\langle n_i \rangle \sum_n B_{i,n} \lambda_\pi^n - \sum_n B_{i,n} n \lambda_\pi^n \right] \; . \end{aligned} \tag{D.19}$$

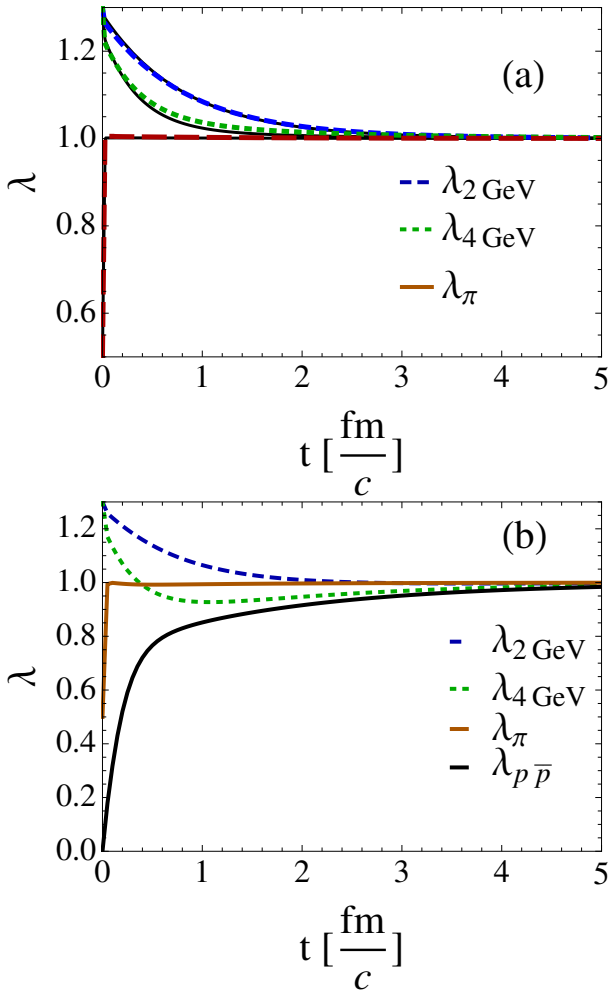

Figure D.3: (a) Numerical and analytical results for the fugacity of pions and Hagedorn states where $\eta = 0.9$ at $T = 175$ MeV for $T_H = 176$ MeV when $\beta_i = 1.1$ and $\alpha = 0.9$ and (b) the numerical results for the same initial conditions including $p\bar{p}$ pairs with $\phi = 0$.

Once again we make the substitution $\lambda_\pi = 1 - \epsilon$ so that

$$\dot{\tilde{\epsilon}} \;=\; -\frac{1}{\tilde{N}_\pi^{eq}} \sum_i \Gamma_i N_i^{eq} \sigma_i^2 \epsilon \; . \tag{D.20}$$

where $\sigma_i^2 = \langle n_i^2 \rangle - \langle n_i \rangle^2$ in the Gaussian distribution of our branching ratios. To relate ϵ and $\tilde{\epsilon}$ we return to Eq. (D.18) and separate λ_i into a sum over the resonances in quasi-equilibrium and one over the "freely" equilibrating resonances

$$\tilde{\lambda}_\pi = \frac{1}{\tilde{N}_\pi^{eq}} \left[N_\pi^{eq} \lambda_\pi + \sum_{QE} N_i^{eq} \langle n_i \rangle \lambda_i + \sum_{free} N_i^{eq} \langle n_i \rangle \lambda_i \right] . \tag{D.21}$$

Since the pions reach quasi-equilibrium first, i.e., $\tau_\pi < \tau_i$ near T_c, we set the π rate equation in Eq. (3.1) equal to zero, which gives $\lambda_i \approx \frac{1}{\langle n_i \rangle} \sum_n B_{i,n} n \lambda_\pi^n$, so

$$\begin{aligned} \tilde{\lambda}_\pi \;&\approx\; 1 - \frac{\left(N_\pi^{eq} + \sum_{QE} N_i^{eq} \langle n_i^2 \rangle \right) \epsilon}{\tilde{N}_\pi^{eq}} \\ &-\; \frac{\sum_{free} \langle n_i \rangle (N_i^{eq} - N_i^{eq} \lambda_i)}{\tilde{N}_\pi^{eq}} \; . \end{aligned} \tag{D.22}$$

Eq. (D.22) then has the form $\tilde{\lambda}_\pi \approx 1 - \tilde{\epsilon}$ where

$$\tilde{\epsilon} = \frac{\left(N_\pi^{eq} + \sum_{QE} N_i^{eq} \langle n_i^2 \rangle \right) \epsilon}{\tilde{N}_\pi^{eq}} + \frac{\sum_{free} \langle n_i \rangle (N_i^{eq} - N_i^{eq} \lambda_i)}{\tilde{N}_\pi^{eq}} . \tag{D.23}$$

We can then solve for ϵ in Eq. (D.23) and substitute ϵ into Eq. (D.20), which in turn can be integrated. This leads us to the solution

$$\begin{aligned} \tilde{\epsilon} \;&=\; \epsilon_j e^{-\frac{t-\tau_j}{\tau_\pi^{QE}}} + \sum_{free} \langle n_i \rangle N_i^{eq} - \frac{\sum_i \Gamma_i N_i^{eq} \sigma_i^2}{\tilde{N}_\pi^{eq} \sum_{QE} N_i \langle n_i^2 \rangle} \\ &\cdot\; \sum_{free} N_i^{eq} \langle n_i \rangle e^{-\frac{t-\tau_j}{\tau_\pi^{QE}}} \int_0^t e^{\frac{x-\tau_j}{\tau_\pi^{QE}}} \lambda_i(x) dx \; . \end{aligned} \tag{D.24}$$

where j stands for the latest resonance to reach chemical equilibrium at that point in time and

$$\tau_\pi^{QE} \equiv \frac{N_\pi^{eq}}{\sum_i \Gamma_i N_i^{eq} \sigma_i^2} + \frac{\sum_{QE} N_i^{eq} \langle n_i^2 \rangle}{\sum_i \Gamma_i N_i^{eq} \sigma_i^2} \tag{D.25}$$

is the quasi-equilibrium time. Clearly, once all the Hagedorn states have reached chemical equilibrium than j symbolizes the resonance of $M = 2$ GeV, since it is the slowest Hagedorn state to equilibrate. The sums over "free" is the sum over the Hagedorn states that have not yet surpassed their respective chemical equilibrium time, τ_i. Once τ_{2GeV} is reached those sums equal zero. Therefore, after τ_{2GeV} all that remains is

$$\tilde{\epsilon} = \epsilon_{2GeV} e^{-\frac{t-\tau_{2GeV}}{\tau_\pi^{QE}}} \tag{D.26}$$

where τ_π^{QE} is shown in Tab. 3.1. Finally, we rewrite Eq. (D.26) in terms of the pion evolution equation

$$\lambda_\pi = 1 - (1-\kappa)e^{-\frac{t-\tau_{2GeV}}{\tau_\pi^{QE}}} \tag{D.27}$$

where $\kappa = \lambda_\pi(\tau_{2GeV})$.

Because the resonance equation depends on the population of the pions we substitute Eq. (D.27) into the Hagedorn resonance rate equation in Eq. (3.1), assuming the pions are near equilibrium (i.e., we use the approximation $\lambda = 1 - \epsilon$ and $(1-\epsilon)^n \approx 1 - n\epsilon$)

$$\begin{aligned} \lambda_i &= \left(\theta_i - 1 + \frac{\tau_\pi^{QE}}{\tau_\pi^{QE} - \tau_i}\langle n_i\rangle(1-\kappa)\right) e^{-\frac{t-\tau_{2GeV}}{\tau_i}} \\ &+ 1 - \frac{\tau_\pi^{QE}}{\tau_\pi^{QE} - \tau_i}\langle n_i\rangle(1-\kappa)e^{-\frac{t-\tau_j}{\tau_\pi^{QE}}} . \end{aligned} \tag{D.28}$$

where $\theta_i = \lambda_i(\tau_{2GeV})$. Thus, for stage 3 the population equations for the pions and the Hagedorn states are Eq. (D.27) and Eq. (D.28) so long as $t \geq \tau_{2GeV}$.

Fig. D.3 reveals a remarkable close fit with our numerical results for $T = 175$ MeV i.e. $T < T_H$. Thus, the quasi-chemical equilibrium time, τ^{QE}, depends only on Γ_i, $\langle n_i\rangle$, σ_i^2, and N^{eq}, which is temperature dependent, but not on our initial conditions. As mentioned in the text, though, τ^{QE} includes many non-linear affects that only occur close to the chemical equilibrium. Thus, the more appropriate time scale is τ_π^0 in order to describe the dynamics.

We also see from Fig. D.3 that when $p\bar{p}$ pairs are included that the pions and Hagedorn resonances equilibrate in roughly the same amount of time, which implies that our analytical solution can still be approximately applied when $p\bar{p}$ pairs are present.

Appendix E

Zero-momentum Euclidean Correlator

In this appendix we will be proving that the following statement

$$\begin{aligned} G^E(0,\mathbf{0}) &= \int d^4x \, \langle \theta^\mu_\mu(\tau,\mathbf{x}) \theta^\nu_\mu(0,\mathbf{0}) \rangle \\ &= (T\partial_T - 4)\,(\epsilon - 3p)\,. \end{aligned} \tag{E.1}$$

at a finite temperature. We consider only one quark flavor that has the mass m_0. The derivation of this is shown in [119] for finite T and μ_b. However, since we consider $\mu_b = 0$ the following derivation will only contain a finite temperature.

In the imaginary time approach the partition function is

$$Z = \int \mathcal{D}\bar{A}\mathcal{D}q\mathcal{D}\bar{q} \exp\left\{ \int_0^{1/T} d\tau d^3x \left[-\frac{1}{4g_0^2} \bar{F}^{\mu\nu}_a \bar{F}^a_{\mu\nu} + \bar{q}(i\partial - \tfrac{1}{2}\bar{A}_a \, \lambda^a - m_0)q \right] \right\} \tag{E.2}$$

where λ^a denote the generators fo color $SU(3)$ and the gluon fields and field strength tensors are scaled by the bare coupling constant g_0 such that $\bar{A}^\mu_a = g_0 A^\mu_a$ and $\bar{F}^a_{\mu\nu} = g_0 F^a_{\mu\nu}$ At first let us assume that the quark mass is zero ($m_0 = 0$). The grand potential of the systems is

$$\Omega = -T \ln Z$$

. Substituting in Eq. (E.2),

$$\frac{\partial}{\partial(-1/g_0^2)} \frac{\Omega}{V} = -\frac{g_0^2}{4} \left\langle F^{\mu\nu}_a(0,\boldsymbol{\mu}0) F^a_{\mu\nu}(0,\boldsymbol{\mu}0) \right\rangle \tag{E.3}$$

where the angle brackets denote the thermal average.

Alternatively, Ω can also be derived using an explicit form of Ω/V determined on the basis of dimensional analysis. The theory has a mass scal M at which the subtractions are performed, therefore, the results can be written in terms of a nonperturbative dimensional parameter

$$\Lambda = M \exp\left\{ \int_{\alpha_s(M)}^{\infty} \frac{d\alpha_s}{\beta_s(\alpha_s)} \right\} \,, \tag{E.4}$$

where $\alpha_s = g_0^2/4\pi$ and β_s is the Gell-Mann-Low function: $Md\alpha_s/dM = \beta_s$. We can then write

$$\frac{\Omega}{V} = \Lambda^4 f\left(\frac{T}{\Lambda}\right) , \tag{E.5}$$

where f is some function that is not dependent on g_0. Thus, taking the derivative of Eq. (E.5) in respect to $-1/g_0^2$

$$\frac{\partial}{\partial(-1/g_0^2)}\frac{\Omega}{V} = -\frac{4\pi\alpha_s^2}{\beta_s(\alpha_s)}\left(4 - T\frac{\partial}{\partial T}\right)\frac{\Omega}{V} . \tag{E.6}$$

Recalling Eq. (E.3),

$$-\frac{4\pi\alpha_s^2}{\beta_s(\alpha_s)}\left(4 - T\frac{\partial}{\partial T}\right)\frac{\Omega}{V} = -\frac{g_0^2}{4}\left\langle F_a^{\mu\nu}(0,\boldsymbol{\mu}0)F_{\mu\nu}^a(0,\boldsymbol{\mu}0)\right\rangle , \tag{E.7}$$

which leads to

$$\left(4 - T\frac{\partial}{\partial T}\right)\frac{\Omega}{V} = \frac{\beta_s(\alpha_s)}{4\alpha_s}\left\langle F_a^{\mu\nu}(0,\boldsymbol{\mu}0)F_{\mu\nu}^a(0,\boldsymbol{\mu}0)\right\rangle = \left\langle\theta_\mu^\mu(0,\boldsymbol{\mu}0)\right\rangle = \mathcal{E} - 3P . \tag{E.8}$$

where we have used the standard QCD result for the trace of the energy-momentum tensor density, θ_μ^μ.

Leads to

$$\begin{aligned}(-1)^n\left(4 - T\frac{\partial}{\partial T}\right)^{n+1}\frac{\Omega}{V} &= \left(T\frac{\partial}{\partial T} - 4\right)^n\left\langle\theta_\mu^\mu\right\rangle \\ &= \int d^4x_n\cdots\int d^4x_1\left\langle\theta_\mu^\mu(\tau_n,\mathbf{x}_n)\cdots\theta_\mu^\mu(\tau_1,\mathbf{x}_1)\theta_\mu^\mu(0,\mathbf{0})\right\rangle_c .\end{aligned} \tag{E.9}$$

and, therefore, when $n = 1$

$$\int d^4x\,\langle\theta_\mu^\mu(\tau,\mathbf{x})\theta_\mu^\nu(0,\mathbf{0})\rangle = \left(T\frac{\partial}{\partial T} - 4\right)(\epsilon - 3p) , \tag{E.10}$$

which is the property that we wanted to prove in Eq. (4.12).

Bibliography

[1] D. J. Gross and F. Wilczek, Phys. Rev. Lett. **30**, 1343 (1973); H. D. Politzer, Phys. Rev. Lett. **30**, 1346 (1973).

[2] E. V. Shuryak, Sov.Phys.JETP 47:212-219,1978, Zh.Eksp.Teor.Fiz.74:408-420,1978; Phys. Lett. B 78, 150 (1978); Phys.Rept.61:71-158,1980; O. K. Kalashnikov and V. V. Klimov, Phys. Lett. B 88, 328 (1979); J. I. Kapusta, Nucl. Phys. B 148 (1979) 461; D. J. Gross, R. D. Pisarski and L. G. Yaffe, Rev. Mod. Phys. **53**, 43 (1981). References for the first chapter about strangeness enhancement?

[3] M. Tegmark, M. Zaldarriaga and A. J. S. Hamilton, Phys. Rev. D **63**, 043007 (2001) [arXiv:astro-ph/0008167].

[4] CERN symposium, Feb. 10, 2000. See, e.g, CERN Courier **40** (May 2000) 13; B. Schwarzschild, Phys. Today **53** (May 2000) 20.

[5] J. Adams *et al.* [STAR Collaboration], Nucl. Phys. A **757**, 102 (2005); B. B. Back *et al.* [PHOBOS Collaboration], Nucl. Phys. A **757**, 28 (2005); I. Arsene *et al.* [BRAHMS Collaboration], Nucl. Phys. A **757**, 1 (2005); K. Adcox *et al.* [PHENIX Collaboration], Nucl. Phys. A **757**, 184 (2005).

[6] N. Armesto *et al.*, J. Phys. G **35**, 054001 (2008) [arXiv:0711.0974 [hep-ph]].

[7] B. B. Back *et al.* [PHOBOS Collaboration], Phys. Rev. Lett. **88**, 022302 (2002) [arXiv:nucl-ex/0108009].

[8] M. Cheng *et al.*, Phys. Rev. D **77**, 014511 (2008).

[9] Y. Aoki, Z. Fodor, S. D. Katz and K. K. Szabo, JHEP **0601**, 089 (2006) [arXiv:hep-lat/0510084].

[10] D. H. Rischke, Prog. Part. Nucl. Phys. **52**, 197 (2004) [arXiv:nucl-th/0305030].

[11] T. Matsui and H. Satz, Phys. Lett. B **178**, 416 (1986).

[12] J. Adams *et al.* [STAR Collaboration], Phys. Rev. Lett. **91**, 072304 (2003) [arXiv:nucl-ex/0306024].

[13] T. Isobe, arXiv:nucl-ex/0510085; M. Shimomura [PHENIX Collaboration], Nucl. Phys. A **774**, 457 (2006) [arXiv:nucl-ex/0510023].

[14] M. Gyulassy, P. Levai and I. Vitev, Nucl. Phys. B **594**, 371 (2001) [arXiv:nucl-th/0006010].

[15] S. Wicks, W. Horowitz, M. Djordjevic and M. Gyulassy, Nucl. Phys. A **784**, 426 (2007) [arXiv:nucl-th/0512076].

[16] J. D. Bjorken, Phys. Rev. D **27**, 140 (1983).

[17] M. Gyulassy and L. McLerran, Nucl. Phys. A **750**, 30 (2005) [arXiv:nucl-th/0405013].

[18] J. Bielcik [STAR Collaboration], Nucl. Phys. A **774**, 697 (2006) [arXiv:nucl-ex/0511005]. X. Dong, AIP Conf. Proc. **828**, 24 (2006) [Nucl. Phys. A **774**, 343 (2006)] [arXiv:nucl-ex/0509038].

[19] A. Adare *et al.* [PHENIX Collaboration], Phys. Rev. Lett. **98**, 172301 (2007) [arXiv:nucl-ex/0611018].

[20] M. Djordjevic and M. Gyulassy, Nucl. Phys. A **733**, 265 (2004) [arXiv:nucl-th/0310076].

[21] M. Djordjevic, M. Gyulassy, R. Vogt and S. Wicks, Phys. Lett. B **632**, 81 (2006) [arXiv:nucl-th/0507019].

[22] D. Molnar and M. Gyulassy, Nucl. Phys. A **697**, 495 (2002) [Erratum-ibid. A **703**, 893 (2002)] [arXiv:nucl-th/0104073].

[23] Z. Xu, C. Greiner and H. Stocker, Phys. Rev. Lett. **101**, 082302 (2008) [arXiv:0711.0961 [nucl-th]].

[24] L. D. McLerran and R. Venugopalan, Phys. Rev. D **49** (1994) 2233.

[25] L. D. McLerran and R. Venugopalan, Phys. Rev. D **49** (1994) 3352.

[26] D. Kharzeev, E. Levin and M. Nardi, Nucl. Phys. A **730** (2004) 448 [Erratum-ibid. A **743** (2004) 329].

[27] H. J. Drescher, A. Dumitru, A. Hayashigaki and Y. Nara, Phys. Rev. C **74** (2006) 044905.

[28] P. F. Kolb, U. W. Heinz, P. Huovinen, K. J. Eskola and K. Tuominen, Nucl. Phys. A **696** (2001) 197.

[29] M. Luzum and P. Romatschke, Phys. Rev. C **78**, 034915 (2008) [Erratum-ibid. C **79**, 039903 (2009)] [arXiv:0804.4015 [nucl-th]].

[30] J. Noronha-Hostler, J. Noronha and C. Greiner, Phys. Rev. Lett. **103**, 172302 (2009) [arXiv:0811.1571 [nucl-th]].

[31] G. S. Denicol, T. Kodama, T. Koide and Ph. Mota, Phys. Rev. C **80**, 064901 (2009) [arXiv:0903.3595 [hep-ph]].

[32] P. Huovinen and P. Petreczky, arXiv:0912.2541 [hep-ph].

[33] B. Alver *et al.* [PHOBOS Collaboration], arXiv:nucl-ex/0702036.

[34] J. Adams *et al.* [STAR Collaboration], Phys. Rev. Lett. **92**, 062301 (2004) [arXiv:nucl-ex/0310029].

[35] P. Koch, B. Muller and J. Rafelski, Phys. Rept. **142**, 167 (1986).

[36] R. Rapp and E. V. Shuryak, Phys. Rev. Lett. **86** (2001) 2980.

[37] C. Greiner, AIP Conf. Proc. **644**, 337 (2003); Heavy Ion Phys. **14**, 149 (2001); C. Greiner and S. Leupold, J. Phys. G **27**, L95 (2001).

[38] P. Braun-Munzinger *et al.* Phys. Lett. B **344** (1995) 43; Phys. Lett. B **365** (1996) 1; P. Braun-Munzinger, I. Heppe and J. Stachel, Phys. Lett. B **465** (1999) 15.

[39] J. I. Kapusta and I. Shovkovy, Phys. Rev. C **68** (2003) 014901; J. I. Kapusta, J. Phys. G **30** (2004) S351;

[40] P. Huovinen and J. I. Kapusta, Phys. Rev. C **69** (2004) 014902.

[41] P. Braun-Munzinger, J. Stachel and C. Wetterich, Phys. Lett. B **596** (2004) 61.

[42] R. Stock, Phys. Lett. B **456** (1999) 277; arXiv:nucl-th/0703050.

[43] U. Heinz and G. Kestin, arXiv:nucl-th/0612105.

[44] C. Greiner *et al.* J. Phys. G **31**, S725 (2005).

[45] P. Braun-Munzinger, K. Redlich and J. Stachel, arXiv:nucl-th/0304013; P. Braun-Munzinger, J. Stachel, J. P. Wessels and N. Xu, Phys. Lett. B **344**, 43 (1995);Phys. Lett. B **365**, 1 (1996); J. Cleymans, D. Elliott, A. Keranen and E. Suhonen, Phys. Rev. C **57**, 3319 (1998); J. Cleymans, H. Oeschler and K. Redlich, Phys. Rev. C **59**, 1663 (1999); R. Averbeck, R. Holzmann, V. Metag and R. S. Simon, Phys. Rev. C **67**, 024903 (2003); P. Braun-Munzinger, I. Heppe and J. Stachel, Phys. Lett. B **465**, 15 (1999). J. Cleymans, H. Satz, E. Suhonen and D. W. von Oertzen, Phys. Lett. B **242**, 111 (1990); J. Cleymans and H. Satz, Z. Phys. C **57**, 135 (1993); F. Becattini, M. Gazdzicki and J. Sollfrank, Eur. Phys. J. C **5**, 143 (1998); F. Becattini, J. Cleymans, A. Keranen, E. Suhonen and K. Redlich, Phys. Rev. C **64**, 024901 (2001).

[46] P. Braun-Munzinger, D. Magestro, K. Redlich and J. Stachel, Phys. Lett. B **518**, 41 (2001); W. Florkowski, W. Broniowski and M. Michalec, Acta Phys. Polon. B **33**, 761 (2002); W. Broniowski and W. Florkowski, Phys. Rev. C **65**, 064905 (2002); M. Kaneta and N. Xu, arXiv:nucl-th/0405068; J. Adams *et al.* [STAR Collaboration], Nucl. Phys. A **757**, 102 (2005).

[47] T. E. O. Ericson, M. Jacob, H. Satz and J. Rafelski, *Prepared for NATO Advanced Study Workshop on Hot Hadronic Matter: Theory and Experiment, Divonne-les-Bains, France, 27 Jun - 1 Jul 1994.*

[48] R. Hagedorn, Nuovo Cim. Suppl. **6** (1968) 311.

[49] W. Broniowski, W. Florkowski and L. Y. Glozman, Phys. Rev. D **70**, 117503 (2004) [arXiv:hep-ph/0407290].

[50] K. A. Bugaev, V. K. Petrov and G. M. Zinovjev, arXiv:0801.4869 [hep-ph]; K. A. Bugaev, V. K. Petrov and G. M. Zinovjev, arXiv:0812.2189 [nucl-th].

[51] L. G. Moretto, L. Phair, K. A. Bugaev and J. B. Elliott, PoS C **POD2006** (2006) 037; L. G. Moretto, K. A. Bugaev, J. B. Elliott and L. Phair, arXiv:nucl-th/0601010; arXiv:hep-ph/0511180.

[52] I. Zakout and C. Greiner, Phys. Rev. C **78**, 034916 (2008) [arXiv:0709.0144 [nucl-th]].

[53] I. Zakout, C. Greiner and J. Schaffner-Bielich, Nucl. Phys. A **781**, 150 (2007) [arXiv:nucl-th/0605052].

[54] R. Hagedorn, *Prepared for NATO Advanced Study Workshop on Hot Hadronic Matter: Theory and Experiment, Divonne-les-Bains, France, 27 Jun - 1 Jul 1994*, 13.

[55] J. Noronha-Hostler, C. Greiner and I. A. Shovkovy, Phys. Rev. Lett. **100**, 252301 (2008) [arXiv:0711.0930 [nucl-th]].

[56] J. Noronha-Hostler, M. Beitel, C. Greiner and I. Shovkovy, To be Published in Phys. Rev. C, arXiv:0909.2908 [nucl-th].

[57] J. Noronha-Hostler, C. Greiner and I. Shovkovy, Eur. Phys. J. ST **155**, 61 (2008).

[58] J. Noronha-Hostler, C. Greiner and I. A. Shovkovy, arXiv:nucl-th/0703079.

[59] J. Noronha-Hostler, C. Greiner and I. Shovkovy, arXiv:1001.2948 [nucl-th].

[60] J. Noronha-Hostler, J. Noronha, H. Ahmad, I. Shovkovy and C. Greiner, Nucl. Phys. A **830**, 745C (2009) [arXiv:0907.4963 [nucl-th]].

[61] P. Kovtun, D. T. Son and A. O. Starinets, Phys. Rev. Lett. **94**, 111601 (2005).

[62] D. Kharzeev and K. Tuchin, arXiv:0705.4280 [hep-ph].

[63] J. Noronha-Hostler, H. Ahmad, J. Noronha and C. Greiner, To be Published in Phys. Rev. C, arXiv:0906.3960 [nucl-th].

[64] J. Noronha-Hostler, J. Noronha and C. Greiner, To be Published in Phys. Rev. C, arXiv:1001.2610 [nucl-th].

[65] S. Eidelman *et al.* Phys. Lett. B **592** (2004) 1.

[66] T. D. Cohen, arXiv:0901.0494 [hep-th].

[67] B. Zwiebach, *A First Course in String Theory*, Cambridge University Press, 2004.

[68] A. Bazavov *et al.*, arXiv:0903.4379 [hep-lat].

[69] S. Chatterjee, R. M. Godbole, S. Gupta, arXiv:0906.2523 [hep-ph].

[70] J. I. Kapusta and K. A. Olive, Nucl. Phys. A **408**, 478 (1983).

[71] D. H. Rischke, M. I. Gorenstein, H. Stoecker and W. Greiner, Z. Phys. C **51**, 485 (1991).

[72] C. Spieles, H. Stoecker and C. Greiner, Eur. Phys. J. C **2**, 351 (1998).

[73] S. A. Bass *et al.*, Prog. Part. Nucl. Phys. **41**, 255 (1998) [Prog. Part. Nucl. Phys. **41**, 225 (1998)] [arXiv:nucl-th/9803035]; M. Bleicher *et al.*, J. Phys. G **25**, 1859 (1999) [arXiv:hep-ph/9909407].

[74] S. Pal and P. Danielewicz, Phys. Lett. B **627**, 55 (2005).

[75] F. M. Liu, K. Werner and J. Aichelin, Phys. Rev. C **68** (2003) 024905; F. M. Liu, et. al., J. Phys. G **30** (2004) S589; Phys. Rev. C **69** (2004) 054002.

[76] F. Becattini and L. Ferroni, Eur. Phys. J. C **38**, 225 (2004)

[77] I. Senda, Phys. Lett. B **263**, 270 (1991); F. Lizzi and I. Senda, Nucl. Phys. B **359**, 441 (1991); F. Lizzi and I. Senda, Phys. Lett. B **244**, 27 (1990).

[78] I. G. Bearden *et al.* [BRAHMS Collaboration], Phys. Rev. Lett. **94** (2005) 162301.

[79] C. Greiner, C. Gong and B. Muller, Phys. Lett. B **316**, 226 (1993).

[80] J. Letessier and J. Rafelski, Cambridge Monogr.Part.Phys.Nucl.Phys.Cosmol.18:1-397 (2002).

[81] M. Beitel,Diplomarbeit (2009).

[82] U. W. Heinz and P. F. Kolb, Nucl. Phys. A **702**, 269 (2002); D. Teaney, J. Lauret and E. V. Shuryak, arXiv:nucl-th/0110037; D. Teaney, Phys. Rev. C **68**, 034913 (2003); A. Adare *et al.* [PHENIX Collaboration], Phys. Rev. Lett. **98**, 172301 (2007); T. Hirano and M. Gyulassy, Nucl. Phys. A **769**, 71 (2006); M. Asakawa, S. A. Bass and B. Muller, Phys. Rev. Lett. **96**, 252301 (2006); P. Romatschke and U. Romatschke, Phys. Rev. Lett. **99**, 172301 (2007); Z. Xu, C. Greiner and H. Stocker, Phys. Rev. Lett. **101**, 082302 (2008); H. Song and U. W. Heinz, Phys. Lett. B **658**, 279 (2008).

[83] G. Policastro, D. T. Son and A. O. Starinets, Phys. Rev. Lett. **87**, 081601 (2001).

[84] J. M. Maldacena, Adv. Theor. Math. Phys. **2**, 231 (1998) [Int. J. Theor. Phys. **38**, 1113 (1999)].

[85] T. D. Cohen, Phys. Rev. Lett. **99**, 021602 (2007); D. T. Son, Phys. Rev. Lett. **100**, 029101 (2008); T. D. Cohen, Phys. Rev. Lett. **100**, 029102 (2008); A. Dobado, F. J. Llanes-Estrada and J. M. T. Rincon, AIP Conf. Proc. **1031**, 221 (2008).

[86] A. Dobado and F. J. Llanes-Estrada, Eur. Phys. J. C **51**, 913 (2007).

[87] H. B. Meyer, Phys. Rev. D **76**, 101701 (2007).

[88] Z. Xu and C. Greiner, Phys. Rev. C **71**, 064901 (2005); **76**, 024911 (2007).

[89] Z. Xu and C. Greiner, Phys. Rev. Lett. **100**, 172301 (2008).

[90] T. Hirano and M. Gyulassy, Nucl. Phys. A **769**, 71 (2006) [arXiv:nucl-th/0506049]; L. P. Csernai, J. I. Kapusta and L. D. McLerran, Phys. Rev. Lett. **97**, 152303 (2006).

[91] M. Prakash, M. Prakash, R. Venugopalan, and G. Welke, Phys. Rep. **227**, 321 (1993); see also S. Gavin, Nucl. Phys. A **435**, 826 (1985).

[92] P. Arnold, G. D. Moore and L. G. Yaffe, JHEP **0305**, 051 (2003).

[93] Y. Hidaka and R. D. Pisarski, Phys. Rev. D **78**, 071501 (2008).

[94] A. Muronga, Phys. Rev. C **69**, 044901 (2004).

[95] K. Itakura, O. Morimatsu and H. Otomo, Phys. Rev. D **77**, 014014 (2008).

[96] M. I. Gorenstein, M. Hauer and O. N. Moroz, Phys. Rev. C **77**, 024911 (2008).

[97] A. Muronga, Phys. Rev. C **69**, 044901 (2004); D. Fernandez-Fraile and A. G. Nicola, Int. J. Mod. Phys. E **16**, 3010 (2007); J. W. Chen, Y. H. Li, Y. F. Liu and E. Nakano, Phys. Rev. D **76**, 114011 (2007); J. W. Chen and E. Nakano, Phys. Lett. B **647**, 371 (2007); A. Dobado, F. J. Llanes-Estrada and J. M. Torres-Rincon, arXiv:0803.3275 [hep-ph]; N. Demir and S. A. Bass, arXiv:0812.2422 [nucl-th].

[98] K. Huang and S. Weinberg, Phys. Rev. Lett. **25**, 895 (1970); C. J. Hamer and S. C. Frautschi, Phys. Rev. D **4**, 2125 (1971); W. Nahm, Nucl. Phys. B **45**, 525 (1972); A. Chodos, R. L. Jaffe, K. Johnson, and V. F. Weisskopf, Phys. Rev. D **9**, 3471 (1974); J. I. Kapusta, Phys. Rev. D **23**, 2444 (1981); Nucl. Phys. B **196**, 1 (1982).

[99] G. Welke, R. Venugopalan, and M. Prakash, Phys. Lett. B **245**, 137 (1990).

[100] R. Venugopalan and M. Prakash, Nucl. Phys. A **546**, 718 (1992).

[101] R. Hagedorn and J. Rafelski, Phys. Lett. B **97**, 136 (1980).

[102] S. Pratt, Phys. Rev. C **49**, 2722 (1994); D. H. Rischke and M. Gyulassy, Nucl. Phys. A **608**, 479 (1996).

[103] F. Reif, *Fundamentals of Statistical and Thermal Physics* (McGraw-Hill, Singapore, 1965).

[104] H. B. Meyer, Phys. Rev. Lett. **100**, 162001 (2008).

[105] F. Karsch, D. Kharzeev and K. Tuchin, Phys. Lett. B **663**, 217 (2008).

[106] A. Hosoya and K. Kajantie, Nucl. Phys. B **250**, 666 (1985); P. Danielewicz and M. Gyulassy, Phys. Rev. D **31**, 53 (1985); S. Jeon, Phys. Rev. D **52**, 3591 (1995).

[107] G. Torrieri, B. Tomasik and I. Mishustin, Phys. Rev. C **77**, 034903 (2008); G. Torrieri and I. Mishustin, Phys. Rev. C **78**, 021901 (2008); R. J. Fries, B. Muller and A. Schafer, Phys. Rev. C **78**, 034913 (2008).

[108] P. J. Ellis, J. I. Kapusta and H. B. Tang, Phys. Lett. B **443**, 63 (1998); I. A. Shushpanov, J. I. Kapusta and P. J. Ellis, Phys. Rev. C **59**, 2931 (1999).

[109] S. S. Gubser, A. Nellore, S. S. Pufu and F. D. Rocha, Phys. Rev. Lett. **101**, 131601 (2008); G. D. Moore and O. Saremi, JHEP **0809**, 015 (2008); H. B. Meyer, arXiv:0805.4567 [hep-lat]; C. Sasaki and K. Redlich, arXiv:0806.4745 [hep-ph]; K. Huebner, F. Karsch and C. Pica, arXiv:0808.1127 [hep-lat].

[110] N. Demir and S. A. Bass, Phys. Rev. Lett. **102**, 172302 (2009) [arXiv:0812.2422 [nucl-th]].

[111] S. Pal, arXiv:1001.1585 [nucl-th].

[112] B. Schenke and C. Greiner, J. Phys. G **30**, 597 (2004).

[113] A. Andronic, P. Braun-Munzinger and J. Stachel, Nucl. Phys. A **772**, 167 (2006) [arXiv:nucl-th/0511071].

[114] J. Manninen and F. Becattini, Phys. Rev. C **78**, 054901 (2008) [arXiv:0806.4100 [nucl-th]].

[115] J. Cleymans, R. Sahoo, D. K. Srivastava and S. Wheaton, Eur. Phys. J. ST **155**, 13 (2008).

[116] P. Braun-Munzinger and J. Stachel, Nucl. Phys. A **638**, 3 (1998); J. Cleymans and K. Redlich, Phys. Rev. Lett. **81**, 5284 (1998);Phys. Rev. C **60**, 054908 (1999); J. Cleymans, J. Phys. G **35**, 044017 (2008); J. Cleymans, R. Sahoo, D. P. Mahapatra, D. K. Srivastava and S. Wheaton, Phys. Lett. B **660**, 172 (2008); J. Cleymans, H. Oeschler, K. Redlich and S. Wheaton, J. Phys. G **32**, S165 (2006).

[117] O. Y. Barannikova [STAR Collaboration], arXiv:nucl-ex/0403014.

[118] S. S. Adler *et al.* [PHENIX Collaboration], Phys. Rev. C **69**, 034909 (2004).

[119] I. A. Shushpanov, J. I. Kapusta and P. J. Ellis, Phys. Rev. C **59**, 2931 (1999) [arXiv:nucl-th/9901033].

[120] A. Majumder, B. Muller and X. N. Wang, Phys. Rev. Lett. **99**, 192301 (2007) [arXiv:hep-ph/0703082].

Acknowledgements

I would first like to thank Carsten Greiner for being a wonderful advisor who was patient with me over the years and was always there to answer my questions. I would also like thank him for initially setting me on the right track with his suggestion to look into Hagedorn states. Carsten's group, both the students and postdocs, also deserve thanks for interesting discussions and talks. I am also grateful to Prof. Walter Greiner who invited me to Frankfurt way back when I was still an undergraduate and convinced me to continue to return to Frankfurt thereafter. As a second advisor, Igor Shovkovy was very insightful, helpful and also a good friend. He had a very good eye for details, which helped immensely in our papers together.

Other professors from Frankfurt have earned a heartfelt thanks from me: Horst Stoecker for asking thought provoking questions and also providing many laughs, Dirk Rischke for many wonderful lectures, and Marcus Bleicher for nice discussions about transport models. While in Frankfurt I also enjoyed classes and discussions with Christoph Blume, Elena Bratkovskaya, Igor Mishustin, and many others. Henner Busching helped me with everything about the Helmholtz Research School. The physics professors at Berea College deserve many thanks for providing me with a strong physics background, so thank you Amer Lahamer, Kingshuk Majumdar, and Smith T. Powell. I would also like to thank Dr. Reinhardt for always having answers to my questions and the right physics book at the right time.

During my time as a graduate student I was supported financially by FIAS. Additionally, Helmholtz was kind enough to provide me with extra travel support and more recently I have been supported by the LOEWE program launched by the State of Hesse.

Rolf Hagedorn is receiving all my thanks for him up in heaven for his wonderful idea, which has had many far reaching consequences that I was privileged to explore as I am sure many others will also do in the future.

Miklos Gyulassy can't be thanked enough for all the infinite number of questions about my work and also for providing me support while in New York at Columbia University. I always had a spot to write this thesis at. Moreover, Miklos and his wife Gyorgi opened their home to us. Gyorgy helped us by watching Chloe at times so I'd have a few more minutes to write, and giving me wise motherly advice for which I am infinitely thankful for.

All the secretaries at Frankfurt needed to be thanked for helping me deal with all the complications of being an international graduate student. Thank you Denise Meixler, Daniele Radulescu, Veronika Palade, Gabi Meyer, Walburga Bergmann, and Frau Knoll. The former physics secretary at Columbia University, Lalla Grimes, also deserves my thanks for helping me during my time at Columbia.

I would personally like to thank Johann Rafelski for providing me with a copy of the book

Hot Hadronic Matter: Theory and Experiment. It was an absolute joy to read and provided me with good material for this thesis. I would also like to thank Steffen Bass for insightful questions and discussions about hadronic transport models.

I would like to thank Giorgio Torrieri for providing a living proof of the second law of thermodynamics: the entropy always increases because it is trying to follow him. Thank you Veronica Dexheimer for being both a roommate and a good friend and giving me an ear to talk to while Jorge was in NY. I would also like to thank my other friends and colleagues who have supported me over the years: Barbara Betz, Sophie Nahrwold, Basil Sa'd, Tatia Engelmore, Mauricio Martinez, Gabriel Denicol, Prof. Takeshi Kodama, Maxim Beitel, Hasnaat Ahmad, Mike Strickland, Luan Cheng, Debarati Chatterjee, Ben Koch, Michael Hauer, Anna Mason, Alexandra Martin and all the others friends at CtK, Nan Su, Stephane Hauessler, Hossein Malekzadeh, Jan Steinheimer, Adrian Dumitru, Jamal Jalilian-Marian, Will Horowitz, Simon Wicks, Thomas and Tina Cornellius, Bjoern Schenke, Oliver Fochler, Irina Sagert, Sascha Voegel, Jess Smochek, Jolene Wee, and Jess Marketta. I would also like to thank John Locke, Benjamin Linus, Harry Potter, Michael Scott, Sookie Stackhouse, Bill Compton, Denny Crane, Alan Shore, and Terry Prattchett for giving me inspiration. A special thanks goes to Christine Nattrass for lending me a laptop when mine decided to break. I would also like to thank Marisa and Ellie, Tina and Donal, and Carolin and Maya for playing with Chloe and sympathizing with my lack of sleep.

A special thanks goes to Lufthansa and US Airways for jetting me back and forth from Frankfurt to NY and for never losing my luggage on those many trips (I cannot say the same about the infamous Alitalia!). I would also like to thank the Physical Review referees and editors for publishing all my papers without complaining too much.

Thanks go out to my entire family for their love and support over the years. They have always encouraged me in all my endeavors and never thought it was crazy that I was running off to become a theoretical physicist. Thank you mom, dad, Liane, Mollie, Amanda, Mike, Doug, Beth, Becky, Jeremiah, and Grandma Holliday. Grandma and Grandpa Hostler and Grandma and Grandpa Thomas will always be kept in loving memory. Kami Sanderlin has also been such a good friend to me over the years that she really must be counted as one of my family. Thank you for listening.

None of this would have been possible with out my husband, best friend, confidant, love of my life, and personal theoretical physicist, Jorge Noronha. His passion for physics has been an inspiration for me over the years and his questions have pushed me to understand my own work much more deeply. He has been with me every step of the way and for that I am eternally thankful. My daughter, Chloe Noronha-Hostler, receives my thank for all the hugs, kisses, and cuddles that I have gotten in the past year. She was also kind enough to nap on occasion so that I had a chance to write this thesis.

Jacquelyn Noronha-Hostler

CONTACT INFORMATION

Jacquelyn Noronha-Hostler
400 W 119th St
Apt 10A
New York, NY USA

Phone: (914)355-1516
Fax: +49 (069) 798-47611

E-mail:
hostler@th.physik.uni-frankfurt.de

PERSONAL

Citizenship: USA
Birthday: 26.06.1982
City of Birth: San Diego, CA USA Relationship Status: married
Gender: female

EDUCATION

Johann Wolfgang Goethe-Universität, Frankfurt am Main, Deutschland

Ph.D, Frankfurt International Graduate School for Science

- Thesis: Properties of Hadronic Matter Close to the Critical Temperature
- Advisor: Professor Carsten Greiner
- Research Area: Heavy Ion Collisions
- Expected Graduation Date: October 2010
- Member of Helmholtz Research School
- Guest Student at Columbia University, New York, NY (2008,2009)

Berea College, Berea, Kentucky USA

B.A., Double Major Physics and Mathematics, May 2004

- *Magna cum Laude* (GPA 3.82)
- Minor: German
- Dean's List (six times)
- Foreign Exchange Student at Goethe Universität (Summer 2002, Spring/Summer 2003)

Lincoln Senior High School, Sioux Falls, South Dakota USA

HS Diploma, **September 1996- May 2000**

- GPA 3.9
- 4 years Debate Club (Student Congress National Finalist 1999)
- National Honor Society Member
- Regent's Scholar
- Presidential Scholar

ACADEMIC EXPERIENCE

Research

Columbia University, New York, NY USA
Part Time Employment **10/08-12/08, 10/09-12/09**

- Radiative Energy Loss at High Opacity using the GLV Formalsism

Frankfurt International Graduate School for Science (FIGSS), Frankfurt am Main, Germany
Doctorate **September 2004-present**

- Strangeness Enhancement, Master Equations, Statistical Models, Heavy Ion Collisions, Transport Coefficients, Coupled Non-linear Differential Equations (Analytical and Numerical Approaches)

Berea College, Berea, KY USA
Bachelor Student **September 2000 - May 2004**

- Physics Senior Thesis: White Dwarfs
- Mathematics Senior Thesis: Quantum Computing
- Worked as an assistant in a Planetarium

Tutoring

Institut für Theoretische Physik **September 2004 - present**

- Held tutorial groups (in German and English) in Classical Mechanics 1 & 2, Electrodynamics, Quantum Mechanics, and Thermodynamics

Berea College **September 2001 - September 2004**

- Corrected homework and held office hours in Introduction to Astronomy, General/Intermediate Physics, Quantum Mechanics, and Mathematical Methods in Physics.
- Assisted and occasionally held the lab seminars in Introduction to Astronomy and General/Intermediate Physics.

Publications

J. Noronha-Hostler, C. Greiner and I. A. Shovkovy, Proceedings of 45th International Winter Meeting on Nuclear Physics, Bormio, Italy, 2007. **arXiv:nucl-th/0703079**
J. Noronha-Hostler, C. Greiner and I. Shovkovy, Eur. Phys. J. ST **155**, 61 (2008).
J. Noronha-Hostler, C. Greiner and I. A. Shovkovy, Phys. Rev. Lett. **100**, 252301 (2008).
J. Noronha-Hostler, C. Greiner and I. A. Shovkovy, Proceedings of 24th Winter Workshop on Nuclear Dynamics, South Padre Island, Texas, 2008.
J. Noronha-Hostler, J. Noronha, and C. Greiner, Phys. Rev. Lett. **103**,172302 (2009)
J. Noronha-Hostler, J. Noronha, H. Ahmad, I. Shovkovy, C. Greiner, Nucl. Phys. A **830**, 745c-748c (2009)
J. Noronha-Hostler, H. Ahmad, J. Noronha, C. Greiner, To be published in Phys. Rev. C, **arXiv:0906.3960 [nucl-th]**
J. Noronha-Hostler, M. Beitel, C. Greiner, I. Shovkovy, To be published in Phys. Rev. C, **arXiv:0909.2908 [nucl-th]**
J. Noronha-Hostler, J. Noronha, C. Greiner, To be published in J. Phys. G, **arXiv:1001.2610 [nucl-th]**
J. Noronha-Hostler, Carsten Greiner, Igor Shovkovy, To be published in J. Phys. G, **arXiv:1001.2610 [nucl-th]**

Talks and Posters

45th International Winter Meeting on Nuclear Physics, Bormio, Italy, Talk, 14-21 Jan 2007.
http://wspig2.physik.uni-giessen.de:8000/bormio2007/talks/2_MondayAfternoon/
Quark Matter 2008, Poster, Feb 4-10, 2008.
24th Winter Workshop on Nuclear Dynamics, South Padre Island, Texas, Talk, 5-12 April 2008. **http://rhic.physics.wayne.edu/ bellwied/wwnd08/hostler-wwnd08.pdf**
Yale-Columbia Day, Talk, May 2008.
The statistical model of hadron formation and the nature of the QCD hadronization process, ECT*, Talk, Sept 1-5 2008.
http://www.ect.it/Meetings/ConfsWksAndCollMeetings/ConfWksDocument/2008/talks/1_5_Sept/Nohona.pdf
Quark Matter 2009, Knoxville, TN, USA April 2009. **http://qm09.phys.utk.edu/indico/getFile.py/access?contribId=645&sessionId=19&resId=0&materialId=slides&confId=1**
Strange Quark Matter 2009, Buzios, Brazil, Sept 2009.
http://omnis.if.ufrj.br/ sqm09/

Work Experience

Argonne National Laboratory, Argonne, IL USA
Internship (High Energy Physics Division) **June 2004 to August 2004**

- Worked on spin physics for STAR
- Computer programming in Root

Awards and Grants

- NSF Travel Grant, Kemer, Turkey Sept. 2003
- FIGSS, October 2005-present
- Institut für Theoretische Physik, September 2004-September 2005
- Benjamin A. Gilman International Scholarship, Summer Semester 2003
- DAAD Short Term Study Abroad, Summer 2002
- Senior Mathematics Award, Berea College, 2004
- Waldemar Noll Scholarship in Physics, Berea College, 2004
- Berea College Study Abroad Program, Summer Semester 2003
- Berea College Study Abroad Scholarship for German Minors, Summer 2002
- Berea College Study Internship Scholarship for German Minors, Summer Semester 2003
- NAIA Academic All-American (Women's Soccer), 2001,2002
- NAIA Academic All-Conference (Women's Soccer), 2001,2002
- Pi Mu Epsilon Member, 2003-2004
- Phi Kappa Phi Member, 2002-2004
- Mortar Board Member, 2002-2004

Organizations

- Student Government Association (SGA) Senator, Berea College **Fall 2000**
- German Club, Berea College **2000-2003**
- Physics Club, Berea College **2000-2004**
  - Secretary (2002-2003)
  - President (2003-2004)

Computer Skills

Experience in numerical analysis and general programming
Program Languages: C, C++, Root, Fortran
Programs: LaTeX, Maple, Matlab, Mathematica, Microsoft Office, Open Office
Operating Systems: Microsoft Windows Vista/XP/2000 and Linux

Languages

English (native speaker)
German (fluent): Passed informal DSH on 06.09.2005 (University level proficiency test), taught classes and worked in German for 4 years
Portuguese (intermediate to advanced): 2 classes, spoken at home